ABSTRACT

Title of dissertation: **SPECTROSCOPIC STUDY OF DIFFUSION IN A GLASSY POLYMER**

Juchen Guo, Doctor of Philosophy, 2007

Dissertation directed by: Professor Timothy A. Barbari
Department of Chemical and Biomolecular Engineering

Understanding the diffusion of small molecules in glassy polymer films is very important to applications where selectivity is important, including membrane separations, barrier materials, the controlled-release of pharmaceuticals, and chemical sensors. The non-equilibrium nature of glassy polymers results in sorption and diffusion behavior that can be considerably more complicated than that observed in rubbery polymers. Time-resolved, Fourier transform infrared attenuated total reflectance (FTIR-ATR) spectroscopy has been used increasingly to study diffusion in polymers and has proven to be very accurate and reliable. FTIR-ATR spectroscopy is capable of identifying changes in the local environment for both the penetrant and the polymer, resulting in information at the molecular level during the transport process.

In this study, FTIR-ATR spectroscopy was used to study the diffusion of a small molecule, acetonitrile, in a glassy polymer, cellulose acetate (CA) from the vapor phase. By monitoring the IR absorbances of the nitrile group in acetonitrile and the carbonyl group in cellulose acetate, the kinetics of sorption/desorption and the rates of penetrant-induced swelling/deswelling, respectively, were studied. An additional physical mechanism, resulting in a time delay prior to the appearance of a Fickian-like concentration profile, was uncovered with this technique. A dual mode transport model with local equilibrium relaxation was proposed and successfully used to capture this phenomenon, revealing that a finite hole-filling rate in the dual mode framework is necessary to fully describe transport in glassy polymers. A modified dual mode transport model, taking into account penetrant-induced plasticization in addition to local equilibrium relaxation, was also used and compared to the original version. Differences in the two models were most apparent when describing desorption and were ascribed to differences in the redistribution of molecules between the two modes at the start of the desorption process. Swelling and deswelling rates in the acetonitrile/CA system were predicted using the dual mode model, with and without the modification. Predictions were excellent for swelling, but the inability to predict deswelling was attributed to limitations inherent in the two models.

This work revealed that local equilibrium must be relaxed to fully describe diffusion in glassy polymers. The model developed here should find use in sensor applications of FTIR-ATR spectroscopy, where transient behavior is the key to performance.

SPECTROSCOPIC STUDY OF DIFFUSION IN A GLASSY POLYMER

by

Juchen Guo

Dissertation Submitted to the Faculty of the Graduate School of the
University of Maryland, College Park In partial fulfillment
of the requirements for the degree of
Doctor of Philosophy
2007

Advisory Committee:

Professor F. Joseph Schork, Chair
Professor Raymond A. Adomaitis
Professor Timothy A. Barbari
Professor Robert M. Briber
Professor Srinivasa R. Raghavan

Dedicated to my parents, Guo Shanyong and Chen Xuena,

who love me much more than I can pay them back.

ACKNOWLEDGEMENTS

I am truly grateful to my advisor, Dr. Timothy Barbari, who advised, mentored and supported me during my PhD study. From 2001 to 2006, I learned from him not only how to be a good researcher, but also how to succeed in life. Without his generosity and support, I could not have achieved what I have done. Thanks for everything from the bottom of my heart.

In addition, I would like to thank my dear colleagues and friends, Chong Yung, Jianfeng Du, Yuesheng Ye and Quanzeng Wang, who supported and helped me in many ways throughout my study. Also, I am very thankful to my lifelong friends Zhen, Yuejiao, Lizhi, Ji, Jing, Rui and Jingying. They share in my happiness and sorrow, and their friendships are invaluable treasures to me.

However, none of this would have been possible if it were not for my Mom and Dad. It is their endless love and faith that has supported me to come this far. There are no words that can describe how much I love you two. I hope that what I accomplished makes you happy and proud. My sister, Juqian, my brother-in-law, Fan and my lovely niece Sophie, I love you all very much. I will never forget the joy you brought to me. Without your love, I would not have been able to persevere throughout the past six years.

Table of Contents

List of Tables

List of Figures

Chapter 1

Introduction

1.1 Diffusion in Polymers

1.1.1 Characteristics of Fickian Diffusion

During penetrant sorption into a polymer film, the mass of penetrant, M_t, changes with time. If the penetrant concentration profile, as a function of position and time, is known, M_t can be obtained by integrating the profile over the film thickness and multiplying by the film area, ignoring edge effects (thickness much smaller than the other two dimensions). The governing equation for determining the concentration profile in the film is the one-dimensional species continuity equation. In the absence of chemical reaction, the resulting equation describing diffusion is given by:

$$\frac{\partial C}{\partial t} = -\frac{\partial N}{\partial z} = \frac{\partial}{\partial z}\left(D \frac{\partial C}{\partial z} \right) \tag{1.1}$$

where C is the concentration, N is the mass (or molar) flux, and D is the diffusion coefficient of the penetrant. Equation (1.1) assumes that the constitutive equation relating flux and concentration is given by Fick's law; the flux is proportional to the negative of the concentration gradient.

The solution to this differential equation depends on the initial and boundary conditions for a particular application or experimental arrangement. Solutions are available for a number of situations. Crank and Park[1] summarized the important features of Fickian sorption:

1. The mass uptake, M_t/M_∞, is linear with $t^{1/2}/L$ at short times, where M_∞ is the amount of penetrant sorbed at equilibrium, and *L* is the thickness of the dry film.
2. Above the linear portion, M_t/M_∞ is concave to the $t^{1/2}/L$ axis.
3. Under the same initial and boundary conditions, sorption curves for polymer films of different thickness are the same.

These three criteria are independent of the form of *D* as a function of concentration. Thus, whether or not a given system exhibits Fickian behavior can be determined experimentally by checking the fulfillment of these three criteria.

1.1.2 Characteristics of Non-Fickian Diffusion

Below the glass transition temperature, due to the non-equilibrium nature of glassy polymers, the diffusion behavior can depart from the Fickian criteria. Generally, such behavior in glassy polymers is said to exhibit 'anomalous' or 'non-Fickian' behavior. There is an extreme non-Fickian case known as Case II diffusion.[2-5] It is characterized by the following observations:

1. As penetrant diffuses in the polymer, a sharp advancing front separates a glassy core from a swelling, rubbery shell.
2. The penetrant concentration is uniform behind the advancing front.
3. The mass uptake, M_t/M_∞, is directly proportional to time initially, rather than the square root of time.
4. The sharp diffusion front advances with constant velocity.

Case II diffusion of a penetrant is believed to only occur in glassy polymers because it results from the internal stress caused by the swelling of a system in a state of mechanical non-equilibrium. Diffusion in a glassy polymer can often exhibit more complicated behavior than the two above limiting cases, Fickian and Case II diffusion. If the initial amount of penetrant sorbed at time *t* is denoted by Kt^n, with *K* and *n* as constants, then Fickian systems are characterized by $n = \frac{1}{2}$ and Case II systems are characterized by $n = 1$, with most other non-Fickian systems lying between Fickian and Case II such that *n* takes an intermediate value between $\frac{1}{2}$ and 1. These anomalous diffusion behaviors can be considered as a combination of Fickian and Case II diffusion. The following anomalous sorption behaviors have been reported: [6]

1. Pseudo-Fickian behavior in which the sorption curve plotted vs. $t^{1/2}$ shows an anomalously small initial linear region or resembles a Fickian curve, but departs from film thickness scaling.
2. Sigmoidal behavior of the sorption curve that is encountered when M_t / M_∞ is plotted against $t^{1/2}$.
3. Two-stage sorption: after an initial rapid uptake, the sorption curve as a function of $t^{1/2}$ approaches a quasi-equilibrium followed by a slow approach to a final true equilibrium.
4. Time dependent surface concentration.

In previous studies, superposition of Fickian and Case II diffusion was observed in some penetrant-glassy polymer systems, such as methanol mixed with acetone in highly cross-linked polystyrene,[3] methylene chloride mixed with benzene, pure trichloroethylene and pure methyl ethyl ketone in epoxy polymers,[7-9] and methyl acetate in poly (methyl methacrylate).[10]

Several models have been proposed in the literature to describe the non-Fickian diffusion behavior observed in glassy polymers.[11-16] One example of a generalized diffusion equation was derived to describe a combination of Fickian and Case II mechanisms by Frisch, Wang and Kwei:[15-16]

$$\frac{\partial C}{\partial t} = \frac{\partial}{\partial z}\left[D\frac{\partial C}{\partial z} - vC \right] \tag{1.2}$$

where D is the diffusion coefficient and v is the velocity of the Case II diffusion front. The parameter, v, also has been interpreted as a stress coefficient.

1.1.3 Free Volume Theory for Diffusion Above the Glass Transition

The first effort to theoretically describe diffusion in rubbery polymers was based on free volume theory, popularized by Barrer[17]. The free volume theory of diffusion in amorphous polymers is based on the lattice vacancy or defect theories of diffusion in rigid crystals. The theory employs the conceptual model of discrete cavities which may be either mobile or fixed within and throughout an ordered matrix. A molecule of penetrant can move only when there is a space available to receive it. The activation barrier in diffusion is the energy necessary to form a cavity of proper

dimensions. Several versions of free volume and related theories are outlined as follows: [1]

1. An analysis of polymer segmental mobility was given by Bueche (1953) using the theory of fluctuations. In his theory, it was stipulated that a polymer segment would be able to move when a certain group of segments has its volume enlarged as a result of volume fluctuation.
2. Barrer's zone theory (1957) gives a general expression for the diffusion coefficient: $$D = \frac{\nu}{2} d^2 \sum_{f=1}^{f_{\max}} \rho_f \left\{ \left(\frac{E}{RT} \right)^{f-1} \left[\frac{1}{(f-1)!} \right]^{-1} \right\} \exp\left(-\frac{E}{RT} \right) \quad (1.3)$$

   where ν is the thermal vibration frequency of the penetrant molecule, d is the jump distance, f is the number of degrees of freedom involved in a particular movement, f_{max} is the value of f for which the expression in the square bracket has a maximum, E is the total energy of 1 mole of the activated zones under consideration, and ρ_f is the probability that the f degrees of freedom will co-operate in a diffusion step.
3. Brandt (1959) formulated a molecular model for estimation of the activation energy and compared the predictions of the model to experimental results. In his treatment, the total energy of the activated zone is shown to be strongly dependent on the number of degrees of freedom. The total energy is expressed as: $$E = E_i + E_b + E_{th} \quad (1.4)$$

   where E_i is the intermolecular term due to repulsion, which the chains experience from their neighbors on making room for the penetrant molecule,

E_b is the intra-molecular term arising from the bending of two neighboring chains, and E_{th} is the thermal energy.

4. Cohen and Turnbull (1959) considered transport in a liquid of hard spheres. Molecules reside in cages bound by their neighbors. Occasionally a fluctuation in density opens up a cavity within the cage large enough to permit a considerable displacement of the molecule contained by it. Successful diffusive transport occurs if another molecule jumps into the cavity before the first one can return to its original position. They expressed the diffusion coefficient as: $D = ga^* u \exp(-\gamma \upsilon^* / \upsilon_f)$ (1.5)

   where g is a geometric factor, a^* approximately equals the molecular diameter, u is the gas kinetic velocity, υ^* is the critical volume just large enough to permit another molecule to jump in after the displacement, the average free volume $\upsilon_f = V_f / N$, V_f is the total free volume, N is the number of molecules, and γ is a numerical factor introduced to correct for overlap of free volume.

5. By analogy with the Cohen-Turnbull free volume treatment mentioned above, Fujita (1961) [18] proposed an expression for the thermodynamic diffusion coefficient: $D_T = A_d \exp(-B_d / \upsilon_f) = A_d \exp(-B_D \overline{V}_h^* / \upsilon_f)$ (1.6)

   where the proportionality factor A_d is considered to be dependent primarily upon the size and shape of the penetrant molecule and hence may be independent of temperature and penetrant concentration. B_d is the minimum hole size required for a given penetrant molecule to permit a displacement. B_D

is a proportionality constant and $\overline{V}_h^*$ represents the volume of one mole of cavities of the minimum size required to permit a diffusion jump. Also, υ_f is the fractional free volume of the polymer-penetrant system. (Here, it is the average free volume per unit volume, different from its definition in the Cohen-Turnbull formulation, which is the average free volume per molecule.)

6. The most notable modification of Fujita's free volume theory was proposed by Vrentas and Duda (1977): [19,20] (a) They introduced an energy factor included in A_d, on the consideration that energy E_J per mole is needed for the penetrant molecule to jump into the opened cavity; (b) replacement of $\overline{V}_f$ (free volume per mole) in the Fujita treatment by υ_f in Equation (1.6), meaning that B_D includes the molar volume of the corresponding polymer segment involved in the diffusion jump; (c) if the occupied volume is identified with the volume at $T = 0K$, then only part of the free volume will be fluctuating ("hole volume") and should be included in Equation (1.6). The resulting expression for D_T, given in terms of specific volumes $\hat{V}$ and mass fractions ω, is

$$D_T = A_{d0} \exp\left(\frac{E_J}{RT}\right) \exp\left[\gamma_{o\upsilon}\left(\omega_A + \frac{\omega_P M_A}{M_{PJ}}\right)\frac{\hat{V}_h^*}{\hat{V}_{fh}}\right] \qquad (1.7)$$

where M_A and M_{PJ} denote the molecular weights of penetrant and polymer segment, respectively. $\gamma_{o\upsilon}$ is a factor between 0.5 and 1, introduced to allow for the fact that the same free volume is available to more than one segment. $\hat{V}_h^*$ is the minimum local hole free volume per gram of polymer required for

displacement of a jumping unit and $\hat{V}_{fh}$ is the average hole free volume per gram of polymer.

7. Pace and Datyner (1979) proposed a diffusion theory incorporating features of both the molecular model by DiBenedetto and Paul (1964, 1965) and that by Brandt. They assume that the penetrant molecule can move through the matrix of an amorphous polymer in two distinct ways: (a) along the axis of a "tube" formed by four adjacent parallel chains, and (b) perpendicular to this axis, when two polymer chains separate sufficiently to permit passage of the molecule. Processes (a) and (b) are assumed to occur effectively in series, not in parallel. The observed activation energy for diffusion should thus be that of process (b), which is rate-limiting.

Meares (1958) has shown that the free volume approach provides an additional understanding of segmental motions and the phenomenon of diffusion in polymers. He assumed a direct proportionality between D and the segmental mobility and applied Bueche's theory (1953) for the dependence of the latter quantity on the free volume. Frisch and Rogers (1965) called attention to the relationship of diffusivity to viscosity. Fujita et al. (1960) considered the case of substantial concentration of plasticizing penetrant.

1.1.4 Dual Mode Model for Diffusion Below the Glass Transition

Meares (1954) [21] is attributed with developing the concept that an additional sorption mechanism may be implicated in the diffusion behavior of small molecules in amorphous polymers below the glass transition. His investigations indicated that

glassy polymers contain a distribution of microvoids frozen into the structure as the polymer is cooled through its glass transition temperature. Free segmental rotations of the polymer chains are restricted in the glassy state, resulting in fixed microvoids or "holes" throughout the polymer. These microvoids in the glassy polymer network were thought to immobilize a portion of the penetrant molecules by entrapment or by binding at high energy sites. Subsequent research by Michaels, Vieth and co-workers[22-25] demonstrated that the sorption isotherms of gas molecules in glassy polymers are generally concave to the pressure axis. Such observation is now widely known as dual mode sorption character. The dual mode sorption model describes the sorption mechanism in terms of one population of ordinarily dissolved penetrant molecules within the polymer matrix that is described by Henry's law, and a second population of penetrant molecules considered to occupy unrelaxed free volume within the polymer that is described by a Langmuir isotherm. The dual mode sorption model then gives the total concentration, C, of sorbed penetrant:

$$C = C_D + C_H = k_D p + C_H' \frac{bp}{1+bp} \tag{1.8}$$

where k_D is the Henry's law constant, p is the penetrant pressure in the gas or vapor phase, C_H' is the Langmuir capacity constant, and b is the Langmuir affinity constant.

Vieth and Sladek (1965) [25] described the transient sorption of penetrant in a polymer film when dual mode sorption occurs. The basic assumptions applied to the transport model are: [26]

1. The two modes of sorption, Henry's law and Langmuir, occur simultaneously.

2. Local equilibrium between the two modes is maintained throughout the polymer film.
3. The population sorbed in the Langmuir mode is completely immobilized.
4. Diffusion occurs only in the Henry's mode.
5. The true diffusion coefficient is a constant, independent of concentration or position in the film.

The possibility that the penetrant population sorbed in the Langmuir mode may not be completely immobilized was noted by Paul (1969) [27] and Petropoulos (1970). [28] Petropoulos eliminated the complete immobilization assumption and suggested a general transport process achieved by separation of the effects for each of the two modes, assuming that the chemical potential gradient is the driving force for diffusion. Paul and Koros (1976) [29,30] extended Petropoulos' earlier analysis by using concentration as the driving force for diffusion. The resulting model is known as the dual mobility or partial immobilization model. They suggested that the Langmuir population is not completely immobilized but has a partial mobility. Tshudy and von Frankenberg (1973) [31] considered an invariant set of immobilizing sites distributed throughout the medium, each site capable of immobilizing one penetrant molecule.

$$\text{hole} + \text{penetrant molecule} \underset{k_f}{\overset{k_r}{\rightleftharpoons}} \text{hole-molecule complex}$$

where k_f is the rate constant for hole-filling, and k_r is the rate constant for hole-emptying. This approach places the dual mode model within a reaction framework, with identical results when local equilibrium is assumed.

Although the dual mode sorption model can usually describe gas or vapor sorption behavior in glassy polymers, modifications are necessary to interpret phenomena such as conditioning effects, sorption-desorption hysteresis and unusual isotherms for some gases and vapors. Mauze and Stern (1982 and 1983) [32,33] modified the dual mode sorption to account for the plasticizing effect of sorbed penetrant molecules. For systems in which the polymers were plasticized, they assumed the concentration of ordinarily dissolved molecules (Henry's law population) was a much stronger function of penetrant concentration than in the common dual mode sorption model. Kamiya (1986) [34] extended this modified model, taking into account the plasticization effect on the Langmuir population residing in the pre-existing free volume ("holes"). The details of Kamiya's model will be discussed in one of the later chapters.

1.2 Motivation

Understanding diffusion of small molecules in polymers is very important to many applications, including membrane separations, selective barrier materials, the controlled-release of pharmaceuticals, and the optimal design of fuel cell membranes, packaging materials, coatings and chemical sensors. Glassy polymers are used in many of the applications mentioned above where selectivity is important (separations and sensors, in particular). Below the glass transition temperature, molecular motion

in the polymer chains is hindered and the diffusion process is much more complicated than that above the glass transition temperature. The non-equilibrium nature of glassy polymers results in sorption and diffusion behavior that can be considerably different than that seen for rubbery polymers, even when the diffusion mechanism is inherently Fickian in nature. Despite the tremendous work that has been done in studying diffusion in glassy polymers, as briefly reviewed above, a number of observations unique to glassy polymers, suggesting a lack of full knowledge of diffusion in glassy polymers, has motivated this work:

1. Solvent removal often takes longer than one might predict from simple Fickian diffusion with reasonable values of the diffusion coefficient.
2. A spike of organic contaminant in steady-state membrane gas separations can take longer than expected to flush out of the system.
3. Polymers used to concentrate a particular species in chemical sensors based on evanescent field spectroscopy can exhibit a time delay prior to detection.

Hence, it is very important to improve our understanding of diffusion in glassy polymers, which could then lead to new and expanded applications, particularly when transient diffusion dictates polymer function.

1.3 A Brief Review of Previous Work Utilizing FTIR-ATR Spectroscopy

To analyze molecular diffusion in glassy polymer systems, an experimental technique that can probe the diffusion process in molecular detail is vital. The most common experimental techniques used for the measurement of the diffusion coefficient include the permeation or diffusion cell and gravimetric sorption. [35] Other techniques that

have been used less frequently for examining diffusion in polymers are laser interferomerty, [36-39] ellipsometry, [40-43] capillary column inverse gas chromatography, [44-48] NMR spectroscopy, [49] and Rutherford backscattering spectroscopy. [50-55] Over the past three decades, time-resolved Fourier transform infrared attenuated total reflectance (FTIR-ATR) spectroscopy has been used increasingly to study molecular diffusion in polymers. [56-117] This technique has several advantages over the traditional methods such as gas permeation, gravimetric sorption, liquid sorption and the side-by-side diffusion cell. For liquid penetrants, FTIR-ATR spectroscopy is a non-invasive, *in situ* method, so the polymer sample does not need to be removed from the penetrant environment to measure the amount of penetrant sorption, leading to more reliable data. Moreover, unlike conventional methods measuring total mass or total concentration of a penetrant, FTIR-ATR spectroscopy is capable of identifying penetrant-penetrant and penetrant-polymer interactions, which leads to more detailed diffusion information at the molecular level. In addition, this technique is also simple to use and inexpensive compared to other new techniques, such as NMR imaging.

Beginning in the late 1970's and early 1980's, time-resolved FTIR-ATR spectroscopy emerged to study the diffusion of small molecules in polymers for a variety of applications, such as sorption of organics in polymer membranes, drying of paints and films, drug delivery, transport across ion-exchange membranes, and movement of toxic chemicals in barrier polymers. Some of the early pioneering work utilizing the ATR technique was done by Trifonov *et al*. [56] and Lavrent'ev, Popov *et al*., [57-63] who demonstrated that ATR spectroscopy was a powerful alternative technique to study

liquid sorption in polymers and proposed quantitative methods to determinate the diffusion coefficient. Their early work was followed by Brandt and coworkers. [64-67] Both groups produced similar results and also compared their results to those obtained from conventional sorption techniques with reasonable agreement. However, because of a lack of accuracy in detection and peak resolution at the time, the application of ATR spectroscopy was limited.

With the introduction of Fourier transform infrared spectrometers in the 1980's, more diffusion studies have taken place. Xu and Balik [68,69] studied the diffusion of calcium carbonate in a latex paint film. They related the intensity of the evanescent field to a simple Fickian equation to determine the diffusion coefficient. Xu and Balik [70] also studied the diffusion of water in these films, and concluded that the diffusion behavior is non-Fickian. This was one of the first studies that foreshadowed the ability of FTIR-ATR spectroscopy to probe changes in the local environment of both the penetrant and polymer at the molecular level during the sorption process.

There are two research groups, in particular, that have focused on utilizing FTIR-ATR technique to study the diffusion in polymers. The recent work of these two groups, Barbari and coworkers and Yarwood and coworkers, is reviewed here. Studies conducted by Barbari's group investigated the effect of solute-polymer interactions during the diffusion process, particularly self-associating penetrants, specific solute-polymer binding, and multicomponent diffusion with solute-solute interactions. Fieldson and Barbari [71-73] looked at a variety of systems, such as

diffusion of water in polyacrylonitrile, acetone in polypropylene, methanol in both polystyrene and poly(methyl methacrylate), and a binary mixture of MEK/ethanol in polypropylene. These studies were the first to derive the full ATR diffusion equation based on Fickian diffusion. Since these early studies, the majority of their work has focused on using this equation as the standard for measuring diffusion coefficients with FTIR-ATR spectroscopy. Hong and Barbari [74-76] studied MEK and MEK/toluene mixture diffusion in polyisobutylene. Their work demonstrated that time-resolved FTIR-ATR spectroscopy could be a powerful technique for measuring multicomponent diffusion in polymers. Elabd and Barbari [77-82] investigated solute-solute interactions in multicomponent diffusion and solute-polymer binding. They studied systems of MEK in vinyl alcohol/vinyl butyral copolymers, acetonitrile and deuterated hexane in H_{12}MDI polyurethane isomers, and MEK/butanol mixtures in polyisobutylene.

Yarwood's group [83-98] primarily focused on the diffusion of water in polymers, such as sulfonated poly(ether sulfone), poly(ethylene terephthalate), and poly(vinyl chloride), and paint. They provided the most comprehensive body of work for diffusion of water in polymers, both informative and quantitative. In addition to studies on the diffusion of water in polymers, Yarwood and coworkers also examined the diffusion of methanol in poly(ethylene terephthalate), electrolyte solutions and heavy water in SPEES/PES copolymer, silane coupling agents in poly(vinyl chloride) and acetone/water mixtures in poly(vinyl alcohol).

Other studies of interest include those of McLoughlin and coworkers. [99-102] Their investigations focused on polymer-coated sensors for environmental pollution detection. They studied diffusion from the vapor phase of chloroform, bromoform, chlorodibromomethane and dibromodichloromethane in polyisobutylene and ethylene-propylene copolymers. They also studied diffusion of a wide variety of organic species from aqueous solutions into perfluorinated polymer films. Fried and Li [103] studied the diffusion of carbon dioxide in cellulose acetate and polymethyl methacrylate. Schlotter and Furlan [104] studied the diffusion of additives in polyolefins and the effects of changing the branch content of the polymer on the diffusion coefficient. Van Alsten and Coburn [105] studied structure effects on the transport of water in polyimides. Farinas *et al*. [106] studied urea in a silicone polymer. Kasarian *et al*. [107] studied carbon dioxide in polydimethylsiloxane. Baschetti *et al*. [108] studied the dilation of polycarbonate, poly(vinyl acetate) and poly(ether urethane) induced by sorption of acetonitrile. Mizaikoff *et al*. [109,110] used FTIR-ATR spectroscopy to monitor chlorohydrocarbons in polymers from a marine environment. Moon *et al*.[111] extended FTIR-ATR to fuel cell membranes. Gupper *et al*. [112] used FTIR to study solvent-induced crystallization in polymers. Li and Wu [113] studied diffusion of glycol in an epoxy membrane. Musto *et al.* [114] used time-resolved FTIR to study the diffusion of water and water/ammonia mixtures in organic-inorganic hybrid polymers. Cotugno *et al*. [115] studied the diffusion of water vapor in an epoxy with a high cross-link density. Bodzenta *et al*. [116] investigated drug diffusion into collodion membranes using FTIR-ATR spectroscopy. Salgin and coworkers [117]

studied the effect of ionic environment on the diffusion of serine alkaline protease enzyme in polyethersulfone.

These studies have demonstrated the ability of FTIR-ATR spectroscopy to examine a wide range of different penetrant-polymer systems. Although FTIR-ATR spectroscopy has gained respect as an alternative measurement technique for diffusion in polymers, the strengths of this technique are still not fully exploited. Furthermore, although Case II behavior has been observed with FTIR-ATR [72] and sensor applications have employed a glassy polymer on an ATR crystal, [100,102] diffusion in glassy polymers has not been studied extensively with the FTIR-ATR technique. This work extends FTIR-ATR spectroscopy to glassy polymers in order to determine whether or not the technique adds additional insight into the diffusion process with this class of materials.

1.4 Infrared Spectroscopy

1.4.1 Molecular Interactions with Electromagnetic Radiation

Infrared radiation is defined as light with wavenumbers (reciprocal of wavelength) between 400 cm^{-1} and 4000 cm^{-1}. Infrared spectroscopy is based on the interaction of electromagnetic radiation with molecular bonds. The easiest way to consider molecular vibrations is to imagine the atoms in a molecule as balls, and the chemical bonds connecting them as mass-less springs. The vibration frequency υ_0 of the harmonic in terms of classical mechanics is given by

$$\upsilon_0 = \frac{1}{2\pi}\sqrt{\frac{k}{m}} \tag{1.9}$$

where k is the force constant of the spring, and m is the reduced mass:

$$m = \frac{m_1 m_2}{m_1 + m_2} \tag{1.10}$$

In Equation (1.10), m_1 and m_2 are the masses of the two atoms involved in the bond. In infrared spectroscopy, it is common to use the wavenumber ($\tilde{\nu}$) instead of frequency, because it is linearly related to the energy of radiation, and is given by

$$\tilde{\nu} = \frac{1}{\lambda} = \frac{\upsilon}{c} \tag{1.11}$$

where λ is the wavelength, υ is the frequency of the radiation and c is the velocity of light in vacuum ($2.997925 \times 10^8\ m/s$).

From Equation (1.9), two molecular properties, the force constant of the chemical bond and the reduced mass of the atoms, determine the frequency (wavenumber in IR spectroscopy) at which a bond will absorb infrared radiation. As a result, the IR radiation absorption for a molecular bond is very selective. Each individual functional group absorbs IR radiation at a unique wavenumber. This consistent behavior of chemical bonds is what IR spectroscopy exploits in order to reveal the molecular structure of a chemical compound. [118]

1.4.2 Attenuated Total Reflection (ATR)

When light travels from a dense medium into a rare one, three different situations can occur depending on the relationship between the angles of incident light, α, and the critical angle, which is defined as:

$$\theta_c = \sin^{-1}\left(\frac{n_1}{n_2}\right) \tag{1.12}$$

where n_1 and n_2 represent the refractive indices in the dense and rare media, respectively.

a. If $\alpha < \theta_c$, most of the incident light will reflect into the rare medium and the angle of refraction, β, will be larger than the angle of incidence.
b. If $\alpha = \theta_c$, the refracted light will move along the interface. The angle of refraction equals 90˚.
c. If $\alpha > \theta_c$, the incident light will be totally reflected back into the dense medium at the interface. This phenomenon is referred to as attenuated total reflection (ATR), also known as total internal reflection. The word attenuated in ATR refers to the process in which the rare medium absorbs light at the dense-rare interface. [119]

These three situations are shown in Figure 1.1.

When internal reflection occurs, an evanescent wave propagates into the rare medium at the interface (Figure 1.2). The formation of the wave is due to the electromagnetic field produced by the superposition of incident and reflective radiation in the dense medium. The strength of the electric field, as well as the amplitude of the evanescent

wave, decreases exponentially with respect to distance from the interface into the rare medium. The strength can be expressed by the following equation:

$$E = E_0 \exp(-\gamma z) \tag{1.13}$$

where z is the depth into the rare medium from the interface, E and E_0 are the electric field strengths at position z and the interface, respectively, and γ is the evanescent wave decay coefficient. [120]

$$\gamma = \frac{2\pi n_1 \left(\sin^2 \alpha - \left(n_2 / n_1\right)^2\right)^{1/2}}{\lambda} \tag{1.14}$$

where λ is the wavelength of the incident radiation.

The depth of penetration, d_p, is defined as the depth where the intensity of the evanescent wave decays to $1/e$ of the original intensity at the interface. It can be expressed by the following equation:

$$\gamma = 1/d_p \tag{1.15}$$

The depth of penetration is important in ATR spectroscopy because it is approximately the sampling depth, which is important in determining the region over which absorbance occurs.

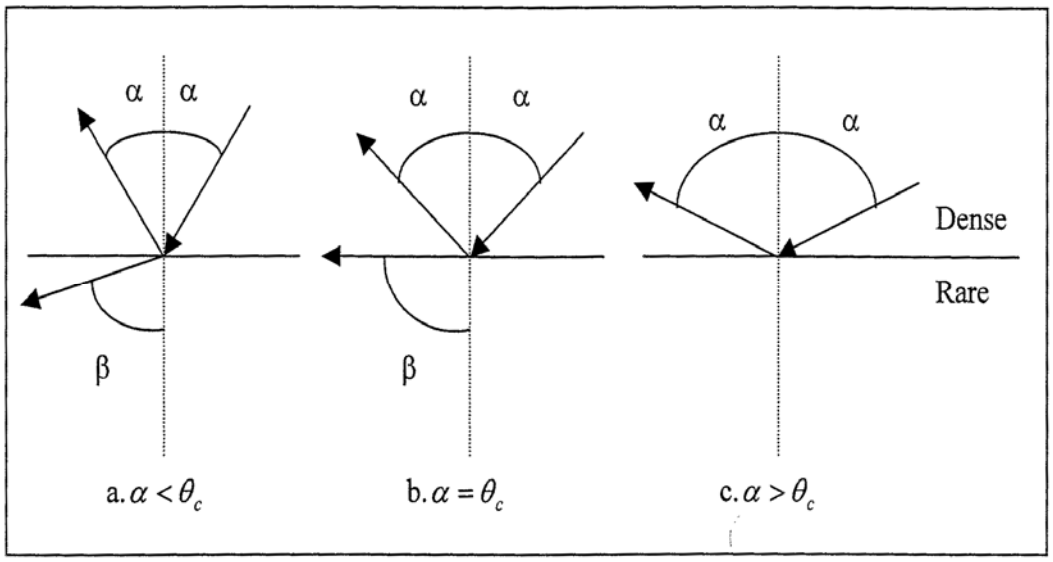

Figure 1.1 Reflection/refraction diagram [77]

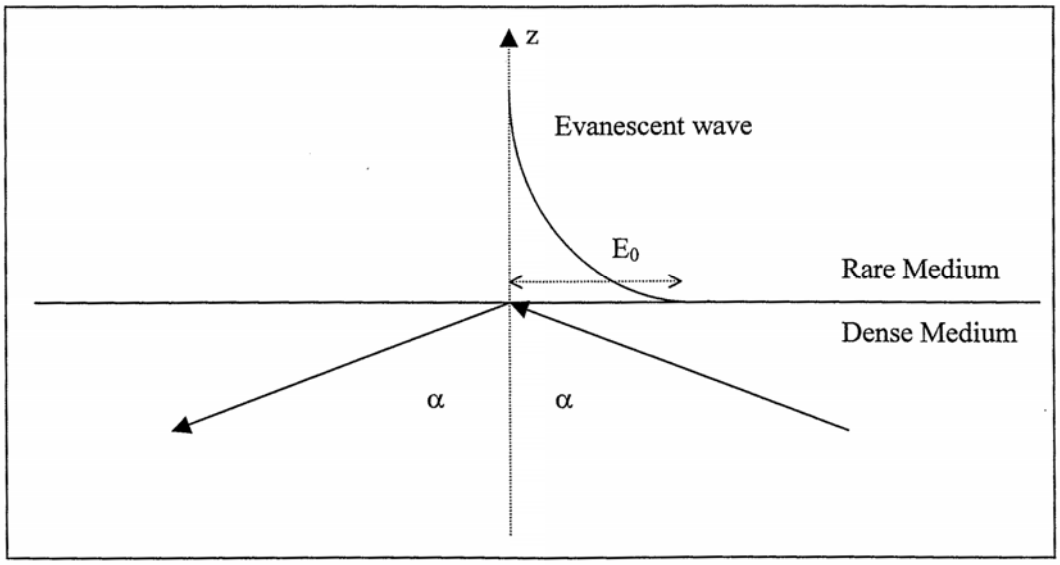

Figure 1.2 Diagram of evanescent wave when total reflection occurs at the interface between dense and rare media. [121]

1.4.3 Quantitative Analysis

When operated properly, IR spectroscopy can provide quantitative information, such as the concentration (or relative concentration) of diffusing molecules, as well as qualitative information, such as molecular structure and interactions. The relationship between absorbance and concentration (the Beer-Lambert law) is derived from the following expression:

$$dI = -\varepsilon C I dz \tag{1.16}$$

where I is the intensity of the radiation absorbed by a particular molecular group at position z, ε is the molar extinction coefficient, and C is the concentration of the absorbing group. Integrating Equation (1.16) over a length scale, L, gives

$$I = I_0 \exp\left(\int_0^L -\varepsilon C dz\right) \tag{1.17}$$

The absorbance is defined as the difference between the logarithmic intensity before and after entering the sample:

$$A = \ln I_0 - \ln I = -\ln\left(\frac{I}{I_0}\right) \tag{1.18}$$

Assuming that the system is dilute or the radiation is weakly absorbed, Equation (1.18) can be simplified to:

$$\frac{I}{I_0} = e^{-A} \approx 1 - A \tag{1.19}$$

or in differential form:

$$dI = -I_0 dA \tag{1.20}$$

Combining Equation (1.20) with Equation (1.16), the ATR absorbance is expressed as a function of penetrant concentration and position in the rare medium:

$$A = \int_0^L \varepsilon \frac{I}{I_0} C dz \tag{1.21}$$

The intensity of IR energy can be related to the field strength E by:

$$I = E^2 \tag{1.22}$$

Combining Equations (1.13), (1.21) and (1.22), the fundamental relationship between absorbance and concentration for FTIR-ATR spectroscopy is obtained:

$$A = \int_0^L \varepsilon C \exp(-2\gamma z) dz \tag{1.23}$$

For multiple reflections, as used in this study, Equation (1.23) becomes:

$$A = m \int_0^L \varepsilon C \exp(-2\gamma z) dz \tag{1.24}$$

The number of reflections, m, is defined by the following equation:

$$m = \frac{L_E \cot \alpha}{2T} \tag{1.25}$$

where L_E and T are the length and thickness of the dense medium, respectively. α is the incidence angle of the IR beam.

If a time-evolving penetrant concentration profile is substituted for C in Equation (1.24), the corresponding absorbance profile can be obtained. Since the absorbance data can be monitored directly by the FTIR-ATR technique, the diffusion processes of the penetrant can be followed.

1.5 Experimental

1.5.1 Materials and Sample Preparation

The diffusion of acetonitrile in cellulose acetate was chosen as the system to be investigated in this study. Acetonitrile (CH_3CN) and cellulose acetate (39.8 wt. % acetyl content, average Mn *ca* 30,000, structure shown in Figure 1.3) were purchased from Sigma-Aldrich, and used as received.

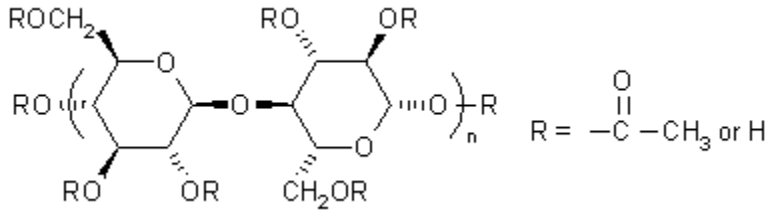

Figure 1.3 Structure of Cellulose Acetate

Cellulose acetate (CA) was chosen as the polymer for two main reasons:

1. Cellulose acetate is a well-studied and well-used glassy polymer for membrane gas separation.
2. Cellulose acetate films adhere very well to the ATR crystal.

Acetonitrile was chosen as the penetrant for two main reasons:

1. Acetonitrile is a good solvent, in the liquid phase for cellulose acetate, so it dilates the polymer film from the vapor phase, such that polymer dilation can be studied.

2. The nitrile absorbance peak from acetonitrile is located far from the carbonyl peak in cellulose acetate in the IR spectra, such that the nitrile peak can be easily distinguished and studied.

The CA films were prepared by a solvent casting method. CA solutions were made in acetone (purchased from J. T. Baker, 99.5%, used as received) with a CA concentration of 3.9 wt %. The solution was cast onto the appropriate substrate, either an ATR crystal or a glass cover slip depending on whether a spectroscopic or gravimetric experiment, respectively, was to be conducted. The substrate was placed in a leveled chamber saturated with acetone. The chamber was sealed at the top by two sheets of FISHERBrand® plastic wrap (to control the acetone evaporation rate), and placed in a laboratory hood for 24 hours at room temperature. After this initial evaporation step, the substrate was taken out of the chamber and placed in a vacuum oven, pre-heated to 70ºC, for another 24 hours. The substrate was then taken out of the oven and immediately placed in a fume hood at room temperature to cool. The dried film on the ATR crystal was found to contain no residual acetone by analysis of the polymer spectrum. Film thickness was measured using a micrometer with $\pm 2.5 \mu m$ precision.

1.5.2 Experimental Procedure

The sorption and diffusion of acetonitrile from the vapor phase in CA was studied by both gravimetric and spectroscopic techniques. Both types of experiments were conducted with the apparatus shown in Figure 1.4. The vapor generating system, enclosed by the heavy dark line in Figure 1.4, is connected independently to a quartz

spring microbalance (Ruska Instrument Corporation, spring constant is $0.0201\,g/cm$) and an ATR cell, allowing experiments to be conducted either simultaneously or separately. The vapor pressure of the penetrant is controlled by the heating element inside the insulated chamber, while a temperature-controlled water bath regulates the experimental temperature by circulating water through the glass jacket around the quartz spring and through the ATR cell.

Sorption and diffusion measurements were made as a function of activity. The activity was calculated from the ratio of the system pressure (P_M) to the saturated vapor pressure (P_{sat}) of the acetonitrile at the system temperature:

$$a = \frac{P_M}{P_{sat}} \tag{1.26}$$

The system pressure of the penetrant was measured with a pressure gauge (MKS instruments Inc.). The system pressure was controlled with the valve between the vapor source and the reservoir. Prior to each experiment, vacuum is applied to the vapor generation system with the acetonitrile reservoir valve closed. After the system is evacuated, the reservoir valve is opened and the system is filled with acetonitrile vapor. When the pressure reading reaches the desired value, the vapor source valve is closed. Once the pressure and temperature inside the vapor generation system reach equilibrium, a valve separating the system from either the ATR cell or the quartz spring is opened. The total amount of acetonitrile in the vapor system is much larger than the amount sorbed by the polymer at equilibrium. As a result, the system can be treated as an infinite reservoir of penetrant and the concentration of acetonitrile at the

polymer film surface can be assumed constant [118]. The temperature of the ATR cell and gravimetric sorption column was kept at 25ºC using a water bath for all experiments.

The Antoine equation was used to determine the saturated vapor pressure for acetonitrile. The parameters are listed in Table 1.1 for the following equation with P_{sat} [=] *bar* and T [=] K.

$$\ln P_{sat} = A - \frac{B}{T + C} \tag{1.27}$$

Table 1.1 Antoine parameters for acetonitrile [122]

A	B	C
16.2874	2945.47	-49.15

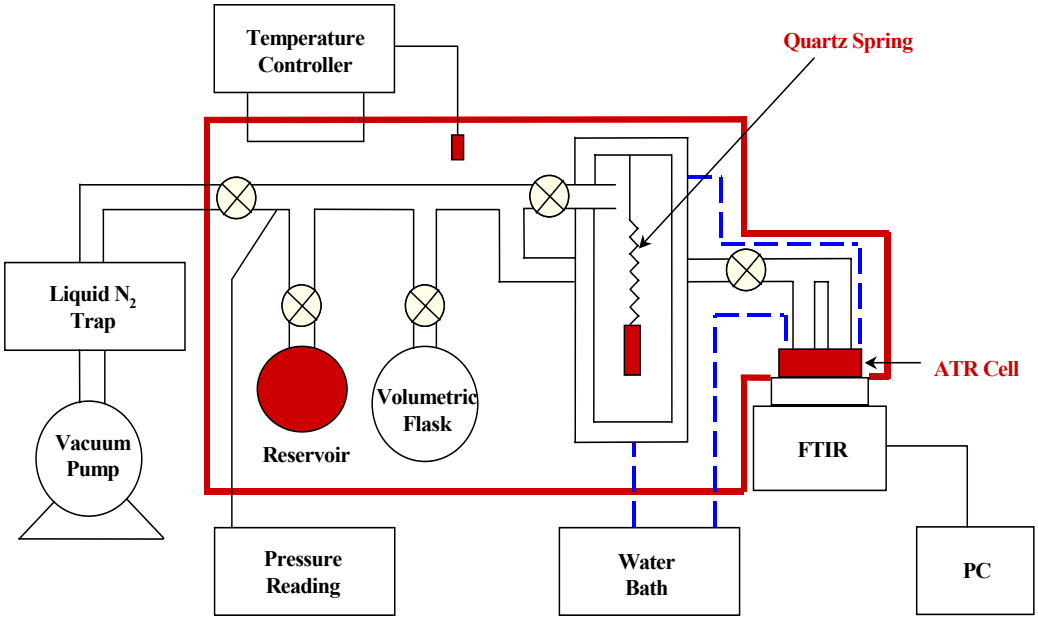

Figure 1.4 Diagram of the combined vapor generating system, FTIR-ATR spectrometer, and gravimetric sorption apparatus. [77]

1.5.3 Gravimetric Experiments

To conduct the gravimetric experiments, the CA polymer films were prepared, as described above, on microscope glass cover slips (2 cm x 2 cm), removed carefully, and hung directly on the quartz spring. The mass uptake was determined from the spring extension, using a cathetometer, as a function of time. Hooke's law, with a pre-determined spring constant, *k* (listed above for this study), was used to calculate the total acetonitrile vapor mass uptake, m_s . Hooke's law must be modified to correct for buoyancy in order to obtain a precise value of the mass uptake. The corrected form is:

$$m_s = k(x - x_0) + \rho_g (V_{sample} + V_{spring}) \tag{1.28}$$

where *x* is the equilibrium spring extension [cm]; x_0 is the initial extension [cm]; ρ_g is the density of the acetonitrile vapor, calculated from the ideal gas law [g/cm^3]; and V_{sample} and V_{spring} are the volumes of the sample and spring, respectively [cm^3]. The accuracy of obtaining the density of vapor acetonitrile using the ideal gas law was tested by calculating values of the compressibility factor *Z* of acetonitrile at different activities using Pitzer's correlation. [123] In this study, the activity range is from 0.06 to 0.5, and the corresponding *Z* ranges from 0.9996 to 0.997, which is very close to 1. Hence, it is reasonable to use the ideal gas law to obtain the density of acetonitrile vapor.

1.5.4 FTIR-ATR Experiments

Infrared spectra for the diffusion experiments were obtained with a Mattson Research Series 1® FTIR spectrometer with a horizontal, temperature-controlled, ATR cell (shown in Figure 1.5) purchased from Graseby Specac, Inc. The ATR element crystal (Graseby Specac, Inc.) used in this study was a zinc selenide trapezoid (70 x 10 x 6 mm) with entry and exit faces beveled at a 45º angle of incidence for the IR beam and with a refractive index of 2.43. Experimental spectra are acquired when infrared radiation enters one side of the ATR crystal (clamped in the ATR cell), reflects multiple times down the length of the crystal, is attenuated by infrared absorption at the crystal-polymer interface, and is detected at the opposite side of the ATR crystal with a liquid nitrogen-cooled, mercury-cadmium-telluride (MCT) detector. A background spectrum of the pure polymer on the crystal was subtracted from all spectra obtained during the diffusion process. Detailed spectroscopic parameters are listed in Table 1.2.

Table 1.2 FTIR Spectroscopic Parameters

Parameter	Value
Resolution	4 cm^{-1}
Starting Wavenumber	600 cm^{-1}
Ending Wavenumber	4000 cm^{-1}
Sample Scans	32
Signal Gain	1
Forward Scan Velocity	0.6 cm/s
Reverse Scan velocity	1.3 cm/s
Sampling Time	0.46 minute

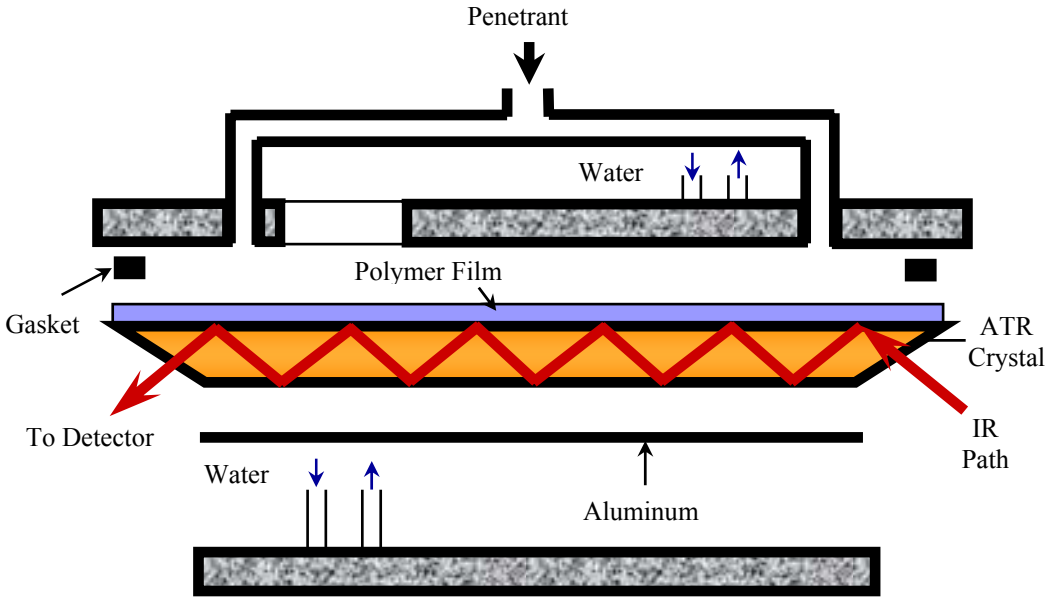

Figure 1.5 Schematic diagram of the ATR cell [77]

1.6 Overview

In Chapter 2, the gravimetric results will demonstrate that the diffusion of acetonitrile in cellulose acetate is Fickian. However, anomalous behavior is observed in FTIR-ATR absorbance experiments that cannot be captured by a simple Fickian model. It suggests that the true mechanism determining transport may be masked by the conventional gravimetric technique and revealed by the FTIR-ATR technique. A dual mode transport model is proposed and applied to interpret this experimental observation and it is determined that the local equilibrium assumption between Henry's law and Langmuir populations must be relaxed. Kinetic parameters, hole-filling and hole-emptying rate constants, must be taken into account to correctly describe the mechanism of vapor acetonitrile diffusion in cellulose acetate.

In Chapter 3, it will be shown that the dual mode transport model with finite kinetics breaks down for interpreting the FTIR-ATR data at high experimental activities. The magnitude of the diffusion coefficients from the gravimetric experiments at high activity suggests that penetrant molecules may be inducing a glass transition. A moving boundary model, combining simple Fickian diffusion in the rubbery state behind the boundary and dual mode transport model in the glassy state in advance of the boundary, is proposed in Chapter 3 to solve this problem.

Chapter 4 discusses the desorption behavior of acetonitrile from cellulose acetate back into the vapor phase. Desorption FTIR-ATR data were fitted using the dual mode transport model and model parameters obtained in Chapter 2. The results

suggest that the sorption dual mode parameters are not applicable to desorption. New desorption isotherms were measured, which demonstrate that the conditioning effect induced by penetrant sorption changes the distribution of dual mode populations upon desorption. New dual mode parameters for desorption were obtained from the desorption isotherms and used in the dual mode transport model to fit the desorption FTIR-ATR data successfully.

A modification of the dual mode sorption model, taking account of plasticization effects and first proposed by Kamiya *et al*., [153,154] is introduced in Chapter 5. This modified model was utilized to interpret the FTIR-ATR experimental data for sorption and desorption. The results are compared to those from the original dual mode transport model. The results provide another physical explanation for the observed transport behavior.

Chapter 6 covers the study of polymer dilation induced by the penetrant molecules. The FTIR-ATR dilation data were compared to the direct measurement made independently with a quartz spring, and the results were in very good agreement. It was demonstrated that the FTIR-ATR spectroscopy is a good technique to study the polymer dilation. Furthermore, utilizing the time resolved FTIR-ATR dilation data, the polymer swelling and deswelling mechanisms were interpreted using both classical dual mode sorption and the Kamiya sorption frameworks.

Conclusions, potential applications and future work are presented in Chapter 7.

Chapter 2

Dual Mode Sorption, Immobilization and the Relaxation of Local Equilibrium

2.1 Introduction

In this chapter, FTIR-ATR (Fourier Transform Infrared-Attenuated Total Reflectance) spectroscopy is combined with a conventional gravimetric sorption balance to examine the diffusion of acetonitrile from the vapor phase in glassy cellulose acetate (CA). From gravimetric experiments, the mass uptake is well described by a simple Fickian model. However, the experimental data from FTIR-ATR spectroscopy cannot be described within a simple Fickian framework. Effectively measuring the concentration at a solid boundary, the FTIR-ATR technique indicates that an additional physical phenomenon, resulting in a time delay, must be present. In order to explain the observed behavior, a transport model based on dual mode sorption and total immobilization of the hole population is employed with the assumption of local equilibrium relaxed. This model is able to capture the observed FTIR-ATR data and predict the gravimetric results.

2.2 Transport Model

2.2.1 Simple Fickian Model

For one-dimensional molecular diffusion in a polymer film with a thickness of 2*L* (-*L* to *L*) and a constant diffusion coefficient, the continuity equation of the diffusion species is described by the following expression:

$$\frac{\partial C}{\partial t} = D\frac{\partial^2 C}{\partial z^2} \tag{2.1}$$

where *C* is the penetrant concentration and *D* is the diffusion coefficient. With the initial condition:

$t = 0$ (*all z*) $\quad C = 0$

and the boundary conditions:

$z = L$ ($t > 0$) $\quad C = C_L$

$z = 0$ ($t > 0$) $\quad \frac{\partial C}{\partial z} = 0$

the following solution of Equation (2.1) is obtained: [2]

$$\frac{C}{C_L} = 1 - \frac{4}{\pi}\sum_{n=0}^{\infty}\frac{(-1)^n}{2n+1}\exp\left[\frac{-D(2n+1)^2\pi^2 t}{4L^2}\right]\cos\left[\frac{(2n+1)\pi z}{2L}\right] \tag{2.2}$$

In gravimetric sorption experiments, the mass uptake of sorbed penetrant is measured as a function of time. The ratio of mass uptake to its equilibrium value is obtained by integrating Equation (2.2) over the thickness of the film. The result of this integration is:

$$\frac{M_t}{M_\infty} = 1 - \sum_{n=0}^{\infty} \frac{8}{(2n+1)^2 \pi^2} \exp\left[\frac{-D(2n+1)^2 \pi^2 t}{4L^2}\right] \tag{2.3}$$

where M_t is the mass sorbed at time *t*, and M_∞ is the mass sorbed at equilibrium.

In FTIR-ATR diffusion experiments, a polymer film of thickness *L* is attached onto the surface of an ATR crystal and has one surface exposed to the penetrant. With assumptions of weak infrared absorption and constant polymer refractive index, an analogous expression to Equation (2.2) can be derived in term of absorbance: [71]

$$\frac{A_t}{A_{eq}} = 1 - \frac{8\gamma}{\pi\left[1 - \exp(-2\gamma L)\right]} \sum_{n=0}^{\infty} \left[\frac{\exp(g)\left[f \exp(-2\gamma L) + (-1)^n (2\gamma)\right]}{(2n+1)\left(4\gamma^2 + f^2\right)}\right] \tag{2.4}$$

where

$$g = \frac{-D(2n+1)^2 \pi^2 t}{4L^2},$$

$$f = \frac{(2n+1)\pi}{2L},$$

and

$$\gamma = \frac{2n_1 \pi \left(\sin^2 \alpha - (n_2/n_1)^2\right)^{1/2}}{\lambda}$$

γ is the evanescent field decay coefficient, n_1 and n_2 are the refractive indices of the ATR crystal and polymer, respectively, α is the incidence angle, and λ is the wavelength of absorbed light. The reciprocal of γ is often referred to as the depth of penetration, d_p, or the characteristic length scale over which absorbance occurs in FTIR-ATR spectroscopy. If $d_p \leq 0.1L$, then Equation (2.4) can be approximated by: [72]

$$\frac{A_t}{A_\infty} = \frac{C(z=0)}{C_L(z=0)} = 1 - \frac{4}{\pi}\sum_{n=0}^{\infty}\frac{(-1)^n}{2n+1}\exp\left[\frac{-D(2n+1)^2\pi^2 t}{4L^2}\right] \tag{2.5}$$

2.2.2 Development of Dual Mode Transport Model with Local Equilibrium

For small molecules at low concentrations in glassy polymers, the most widely accepted model for sorption and diffusion, the dual mode model, assumes that there are two populations of molecules in the polymer, those "dissolved" in the equilibrium portion of the matrix and those residing in the "holes" created by the additional free volume in the system. A key assumption in the application of this model to diffusion is that local equilibrium exists between the two populations. Physically, the two types of sorption mechanisms can be described as follows:

1. Ordinary dissolution in the continuous amorphous matrix. The concentration of this population, C_D, is related to pressure (or activity) by Henry's law, and
2. Sorption in a limited number of fixed preexisting micro-voids, or "holes", in the polymer. The concentration of this population, C_H, is related to pressure (or activity) by a Langmuir expression.

The dual mode sorption model then gives the total concentration, C_T, of sorbed penetrant:

$$C_T = C_D + C_H = k_D a + C_H^{'}\frac{ba}{1+ba} \tag{2.6}$$

where k_D is the Henry's law constant, a is the penetrant activity in the gas or vapor phase, $C_H^{'}$ is the Langmuir capacity constant, and b is the Langmuir affinity constant.

The diffusion of small molecules in glassy polymers at low concentrations is typically represented as Fickian and assumes that the two penetrant species are mobile, with a fraction of the langmuir population immobilized. According to this partial immobilization hypothesis, a fraction, *F*, of the Langmuir population, is mobile with the same diffusion coefficient as the "dissolved" population, represented by D_D.

Under these assumptions, the general dual mode transport model is: [124-125]

$$\frac{\partial C_D}{\partial t} = D_D \frac{\partial^2 C_D}{\partial Z^2} - k_f C_D (C_H^{'} - C_H) + k_r C_H \tag{2.7}$$

$$\frac{\partial C_H}{\partial t} = F D_D \frac{\partial^2 C_H}{\partial Z^2} + k_f C_D (C_H^{'} - C_H) - k_r C_H \tag{2.8}$$

where k_f is the rate constant for hole filling and k_r is the rate constant for hole emptying in the Langmuir framework presented in Equation (2.6). Alternatively, the product FD_D can be written as D_H, which is interpreted as a diffusion coefficient for molecules sorbed into the "holes", all of which are assumed to be mobile with a lower diffusivity. The initial and boundary conditions are:

$t = 0$ *(all z)* $\quad C_D = 0,\ C_H = 0$

$z = 0$ *(t > 0)* $\quad \frac{\partial C_D}{\partial z} = 0,\ \frac{\partial C_H}{\partial z} = 0$

$z = L$ *(t > 0)* $\quad C_D = C_{T_L} - C_H,\ C_H = C_H^{'} \frac{ba}{1+ba}$

where C_{T_L} is the total concentration at *z=L*.

Alternatively, a continuity equation can be written for the total amount of penetrant:

$$\frac{\partial C_T}{\partial t} = -\frac{\partial N_T}{\partial z} \tag{2.9}$$

where N_T is the total flux given by:

$$N_T = -D_D\left[\frac{\partial C_D}{\partial z} + F\frac{\partial C_H}{\partial z}\right] \tag{2.10}$$

which can be rearranged to:

$$N_T = -D_D\left[1 + F\frac{\partial C_H}{\partial C_D}\right]\frac{\partial C_D}{\partial z} \tag{2.11}$$

Assuming local equilibrium between the two populations,

$$k_f C_D\left(C_H^{'} - C_H\right) = k_r C_H \tag{2.12}$$

C_H can be written in terms of C_D

$$C_H = \frac{KC_D}{1+\alpha C_D} \tag{2.13}$$

where

$$K = \frac{C_H^{'} b}{k_D} = \frac{C_H^{'} k_f}{k_r}, \tag{2.14}$$

$$\alpha = \frac{b}{k_D} = \frac{k_f}{k_r}. \tag{2.15}$$

From the local equilibrium assumption, Equation (2.13), one can obtain:

$$\frac{dC_H}{dC_D} = \frac{K}{(1+\alpha C_D)^2} \tag{2.16}$$

Combining Equation (2.11) with (2.16) gives:

$$N_T = -D_D\left[1 + \frac{FK}{(1+\alpha C_D)^2}\right]\frac{\partial C_D}{\partial z} \tag{2.17}$$

Using Equation (2.17) in Equation (2.9) requires the following relationship:

$$\frac{\partial C_T}{\partial z} = \frac{\partial C_D}{\partial z} + \frac{\partial C_H}{\partial z} = \left[1 + \frac{dC_H}{dC_D}\right]\frac{\partial C_D}{\partial z} \tag{2.18}$$

Combining Equation (2.16) and (2.18) gives,

$$\frac{\partial C_T}{\partial z} = \left[1 + \frac{K}{(1+\alpha C_D)^2}\right]\frac{\partial C_D}{\partial z} \tag{2.19}$$

Combining Equations (2.17) and (2.19) gives,

$$N_T = -D_D\left[\frac{1 + \dfrac{FK}{(1+\alpha C_D)^2}}{1 + \dfrac{K}{(1+\alpha C_D)^2}}\frac{\partial C_T}{\partial z}\right] \tag{2.20}$$

Combining Equation (2.9) and (2.20), the continuity equation in terms of total concentration for the dual mode model under the local equilibrium assumption can be obtained:

$$\frac{\partial C_T}{\partial t} = D_D\frac{\partial}{\partial z}\left[\frac{1 + \dfrac{FK}{(1+\alpha C_D)^2}}{1 + \dfrac{K}{(1+\alpha C_D)^2}}\frac{\partial C_T}{\partial z}\right] \tag{2.21}$$

where

$$C_D = \frac{-(1+K) + \left[(1+K)^2 + 4\alpha C_T\right]^{\frac{1}{2}}}{2\alpha}$$

2.3 Results and Discussion

2.3.1 Converting Infrared Absorbance to Concentration

In order to convert FTIR-ATR absorbance (A_t) to concentration ($C_{z=0}$) for application in a transport model, a relationship between the two must be found. A series of FTIR-ATR and gravimetric experiments were done simultaneously to obtain the equilibrium integrated absorbance (cm^{-1}) and concentration ($\frac{g_{nitrile}}{g_{polymer}}$), respectively, at different activities. The functional group of interest in this study is the C≡N stretching mode associated with acetonitrile. This region was integrated using a numerical peak integration algorithm in WinFIRST® (Mattson Instruments, Inc.) over the wavenumber range of 2350 to 2200 cm^{-1}. At each activity, the experiment was carried out for 24 h to insure equilibrium sorption prior to increasing the pressure to increase the activity. The films were prepared so that the time scale for diffusion (L^2/D) would be the same for both techniques. A linear relationship ($C_{z=0} = \varepsilon A_t$) between ATR absorbance and concentration was obtained with $\varepsilon = 0.0873 \ \frac{g_{nitrile}}{g_{polymer} \cdot cm^{-1}}$ ($r^2 = 0.9959$), as shown in Figure 2.1.

2.3.2 Sorption Isotherm for Acetonitrile in Cellulose Acetate.

In a separate series of experiments with freshly-cast CA films, FTIR-ATR absorbance and mass uptake at equilibrium were obtained simultaneously as a function of activity. The absorbance data so obtained were converted to equilibrium concentrations using the value of ε reported above and plotted alongside the mass

uptake values in Figure 2.2. The dual mode sorption model, Equation (2.6) was used to fit to all of the data to obtain the dual mode sorption parameters:

$$k_D = 0.2815 \frac{g_{nitrile}}{g_{polymer}};$$

$$C'_H = 0.0300 \frac{g_{nitrile}}{g_{polymer}};$$

$$b = 38.1.$$

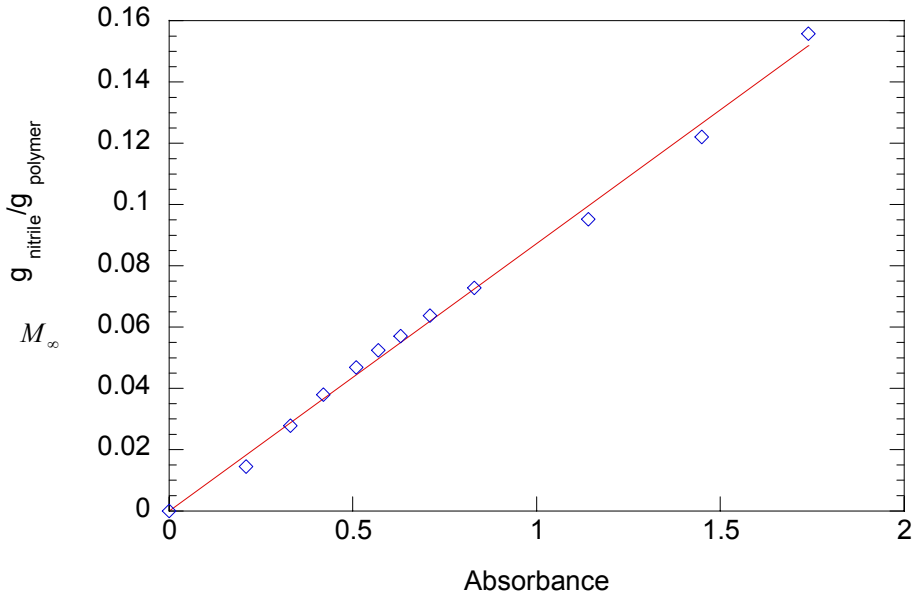

Figure 2.1 Linear relationship between acetonitrile concentration and ATR absorbance at equilibrium sorption (T=25˚C).

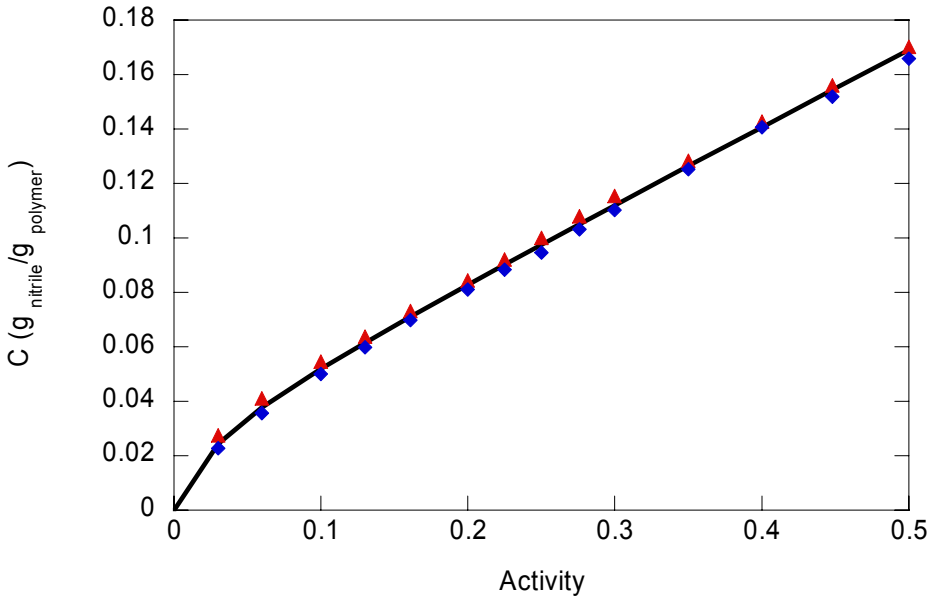

Figure 2.2 Equilibrium mass uptake versus activity at 25˚C and the dual mode sorption model fit of the data (solid line). Triangles are the direct mass uptake values and diamonds are those converted from FTIR-ATR absorbance data.

2.3.3 Simple Fickian Diffusion.

Gravimetric measurements of acetonitrile diffusion in CA at 25˚C were done at activities of 0.06, 0.1, 0.2, 0.3, 0.4 and 0.5 and the data were fit using Equation (2.3). Representative examples of the time-evolved mass uptake data and corresponding fits are shown in Figures 2.3 and 2.4 for activities 0.2 and 0.4, respectively. The linear dependence at short times between mass uptake and the square root of time clearly shows that the underlying physical mechanism for diffusion in the acetonitrile-CA system is Fickian. Experiments at each activity were done in triplicate. The mean values of the resulting diffusion coefficients are listed in Table 2.1, and plotted in Figure 2.5 as a function of activity. It interesting to note here that there appears to be a sharp increase in the magnitude of the diffusion coefficient at activity 0.3, which may be the result of plasticization and the traversing of a glass transition, even though the sorption isotherm is linear above this activity.

Similar experiments were performed with the spectroscopic technique as a function of activity at 25˚C. FTIR-ATR diffusion experiments were conducted at activities of 0.06, 0.1, 0.15, 0.2, 0.25, 0.3, 0.4 and 0.5. Infrared spectra at a few time points for acetonitrile diffusion in CA at activity 0.2 and a thickness L of 49.2 μm are shown in Figure 2.6. The integrated absorbances, normalized by the equilibrium absorbance, are plotted in Figure 2.7 for all time points. In Figure 2.7(a), Equation (2.5) is used to calculate the concentration at the interface as a function of time using the average diffusion coefficient obtained from gravimetric experiments at this activity,

D = 6.5 x 10^{-10} cm^2/s. The predicted values of concentration at the interface are consistently higher than the actual values measured by spectroscopy. In Figure 2.7(b), Equation (2.5) was used to obtain the best fit to the data, resulting in a diffusion coefficient of 5.7 x 10^{-10} cm^2/s; however, the fit is rather poor. It is clear that there is a time delay in the spectroscopic data that cannot be captured by a simple Fickian model.

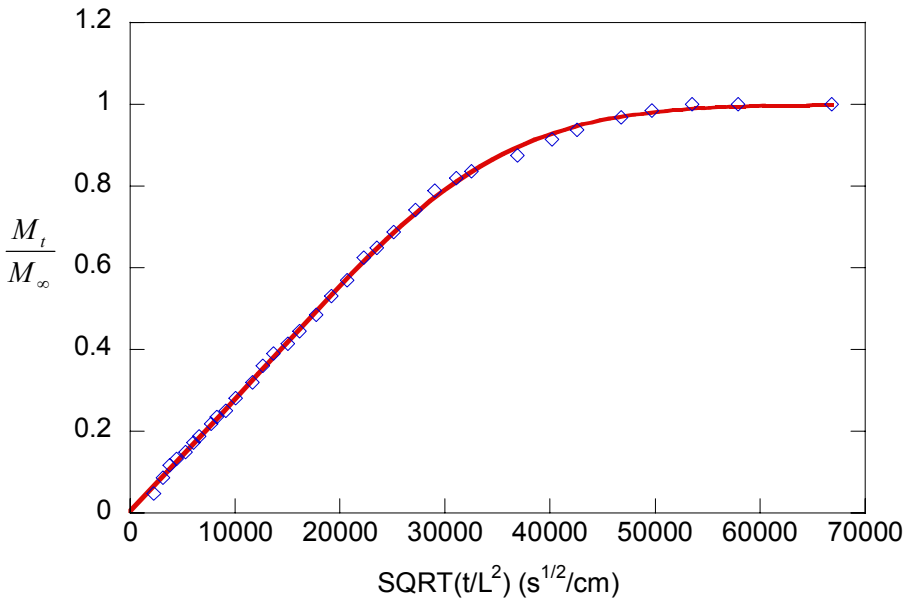

Figure 2.3 M_t/M_∞ vs. $\sqrt{t/L^2}$ and the fit using Eq. (2.3) at activity 0.2; L = 50.4 μm and T = 25˚C.

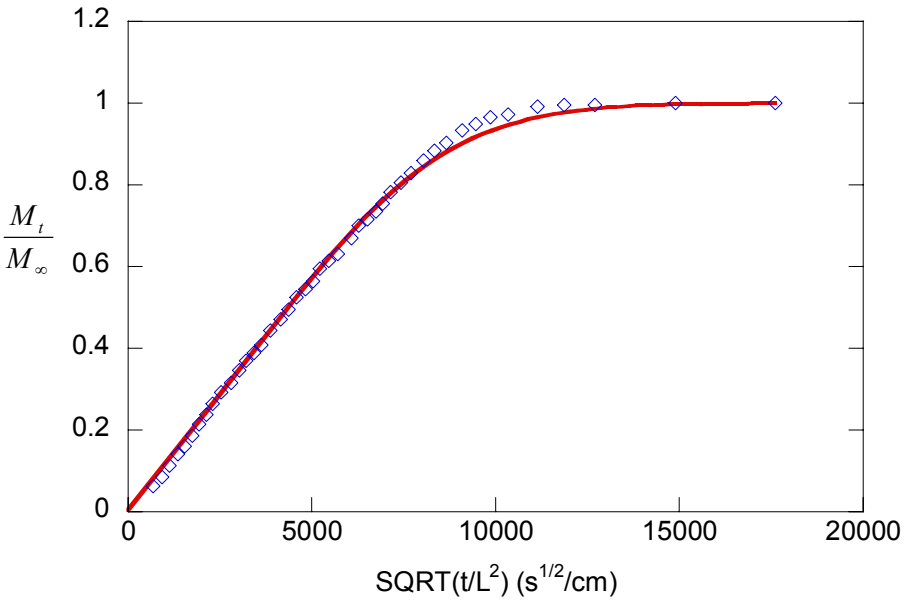

Figure 2.4 M_t/M_∞ vs. $\sqrt{t/L^2}$ and the fit using Eq. (2.3) at activity 0.4; L = 78.6 μm and T = 25˚C.

Table 2.1 Diffusion coefficients for acetonitrile in cellulose acetate at various activities from gravimetric measurements (T = 25˚).

Activity (N=3)	$D \times 10^{10}\ cm^2/s$
0.06	2.06 ± 0.26
0.10	3.20 ± 0.42
0.20	6.50 ± 0.40
0.30	9.90 ± 0.71
0.40	27.0 ± 1.60
0.50	50.5 ± 2.10

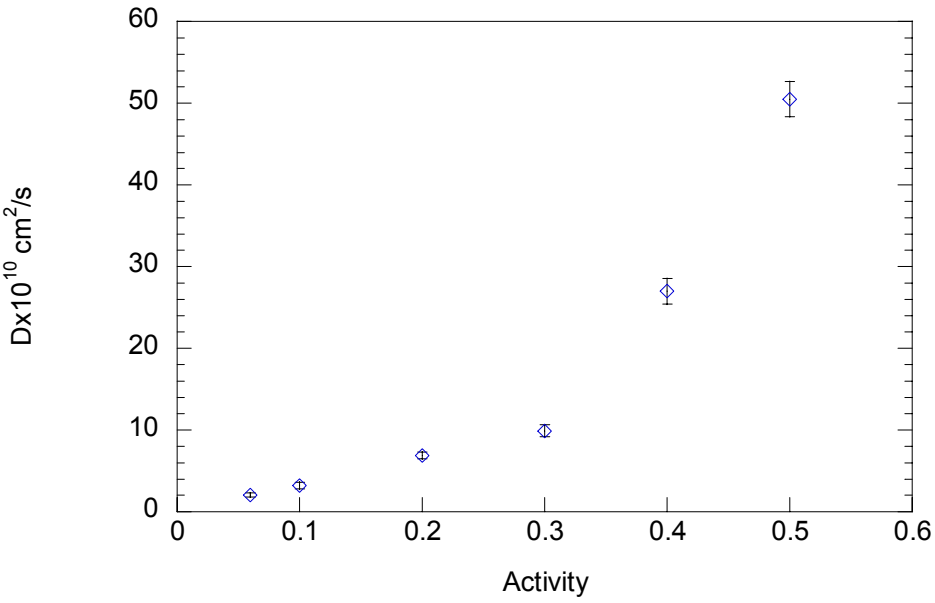

Figure 2.5 Diffusion coefficients for acetonitrile in CA obtained from gravimetric measurements as a function of activity at T = 25˚C.

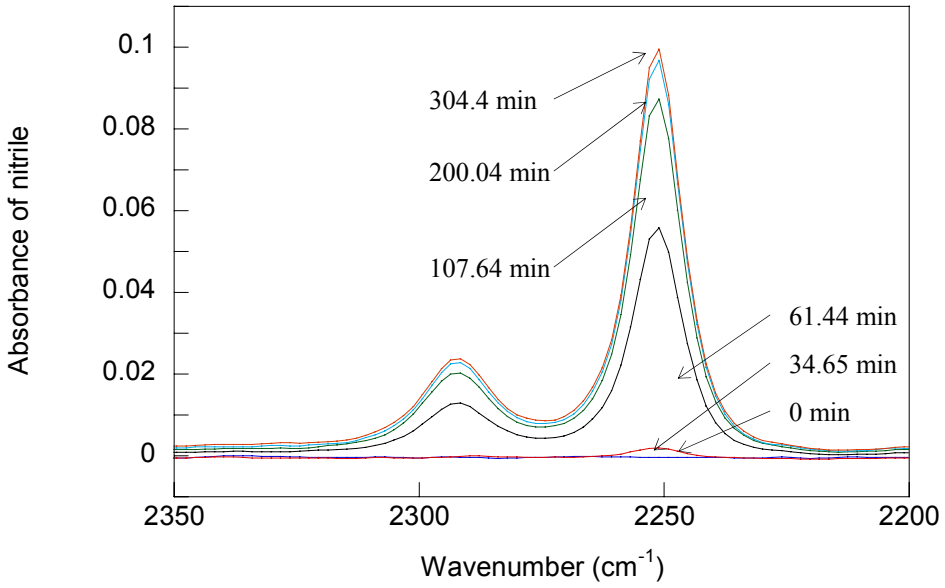

Figure 2.6 Time-resolved acetonitrile absorbance spectra in cellulose acetate at activity 0.2 and T = 25˚C.

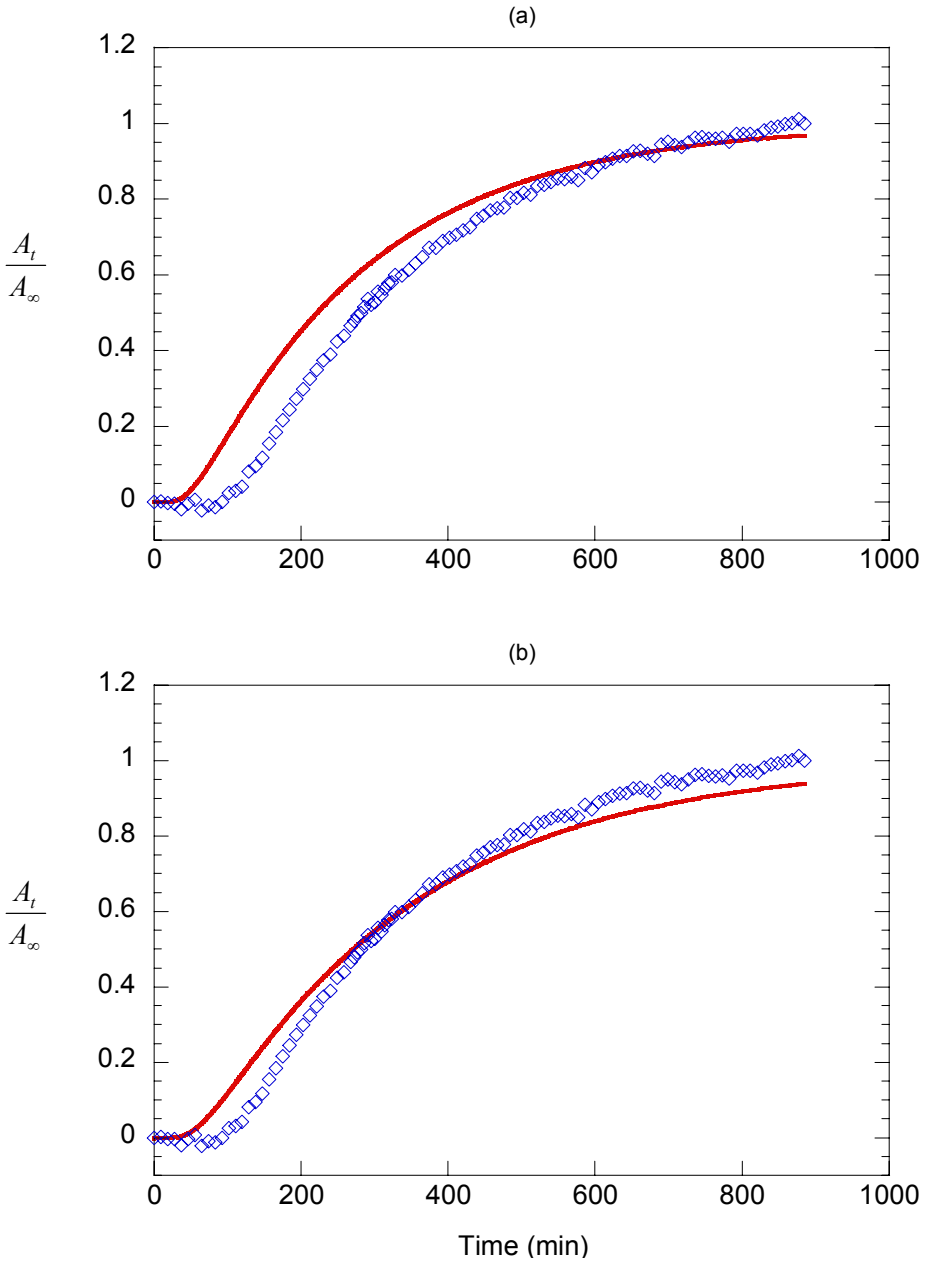

Figure 2.7 FTIR-ATR absorbance data of acetonitrile in CA at activity 0.2 and T = 25˚C with (a) the calculated absorbance curve using the simple Fickian model (Eq. 2.5) and the diffusion coefficient obtained from the gravimetric measurements, and (b) the best fit simple Fickian model (Eq. 2.5). L=49.2 μm.

2.3.4 Dual Mode with Local Equilibrium

One explanation for the observed lag in the concentration at the polymer-crystal interface is that immobilization of acetonitrile in "holes" removes a fraction of penetrant from the diffusion process, thereby lowering local gradients and decreasing the flux. Assuming local equilibrium between the two populations, the spectroscopic data for the same experiment at activity 0.2 were fit using Equation (2.21) in conjunction with a numerical simulation of the differential equation. If F, the fraction of the "hole" (Langmuir) population that is mobile, is taken to be zero, then this would remove the most penetrant molecules from the process. The best fit value of D_D for Equation (2.21) assuming $F = 0$ was 2.2 x 10^{-9} cm^2/s and the resulting fit is shown in Figure 2.8(a). As was the case for simple Fickian diffusion, the dual mode model with local equilibrium cannot capture the time delay in concentration at the polymer-crystal interface and cannot represent the data well. There appears to be another mechanism operative during diffusion in a glassy polymer that results in this behavior. The same phenomenon occurs at all activities, as will be shown below, and is reproducible at any given activity.

2.3.5 Dual Mode Relaxing Local Equilibrium

If the local equilibrium assumption is relaxed, the rates of hole-filling and hole-emptying, given in the generalized dual mode transport model of Equations (2.7) and (2.8), become finite and the hole filling/emptying mechanism can further slow the diffusion of the mobile species. A numerical method was used to solve these equations, which was then coupled to a fitting routine to determine the best fit values

for the relevant adjustable parameters in the model. Equations (2.7) and (2.8) were transformed into non-dimensional form as follows:

$$\frac{\partial \theta_D}{\partial \tau} = \frac{\partial^2 \theta_D}{\partial \xi^2} - \phi \theta_D \left(\theta'_H - \theta_H \right) + \theta_H \tag{2.22}$$

$$\frac{\partial \theta_H}{\partial \tau} = F \frac{\partial^2 \theta_H}{\partial \xi^2} + \phi \theta_D \left(\theta'_H - \theta_H \right) - \theta_H \tag{2.23}$$

where $\theta_D = \frac{C_D}{C_{TL}}$;

$\theta_H = \frac{C_H}{C_{TL}}$;

$\tau = tk_r$;

$\xi = \frac{z}{\sqrt{D_D / k_r}}$;

$\phi = \frac{k_f C_{TL}}{k_r} = \frac{bC_{TL}}{k_D}$;

$\theta'_H = \frac{C'_H}{C_{TL}}$.

The transformed initial and boundary conditions are

$\tau = 0$ (all ξ)	$\theta_D = 0$, $\theta_H = 0$
$\xi = 0$ ($\tau \geq 0$)	$\frac{\partial \theta_D}{\partial \xi} = 0$, $\frac{\partial \theta_H}{\partial \xi} = 0$
$\xi = \frac{L}{\sqrt{D_D / k_r}}$ ($\tau \geq 0$)	$\theta_D = 1 - \theta_H$, $\theta_H = \theta'_H \frac{ba}{1+ba}$

The ratio of the rate constants, k_f and k_r, was fixed at $135.3\frac{g_{polymer}}{g_{nitrile}}$, which is the ratio of b to k_D from the sorption isotherm. The value of $C_H^{'}$ was fixed from the isotherm at $0.0300\frac{g_{nitrile}}{g_{polymer}}$. The Henry's law population was assumed to be immobile (F = 0), because preliminary results using F as an adjustable parameter resulted in values near zero for the best fits. Hence, there are only two adjustable parameters in the non-dimensional dual mode transport model presented here, k_r in τ and $\frac{D_D}{k_r}$ in ξ.

The result using the dual mode transport model with local equilibrium relaxed for the 0.2 activity data is shown in Figure 2.8(b). The model captures the time delay and well represents all of the data, indicating that accounting for the finite rate at which the holes are filled and emptied better describes the sorption kinetics for acetonitrile in cellulose acetate. From triplicate experiments at activity 0.2, the mean values of D_D and k_r were determined to be (6.38±0.04) x 10^{-10} cm^2/s and (4.85±0.09) x 10^{-3} s^{-1}, respectively.

To test the robustness of the model and its physical interpretation, the rate constants for hole-filling and emptying were assumed to be independent of activity. Fixing the value of k_r at 4.85 x 10^{-3} s^{-1}, FTIR-ATR data for diffusion at all remaining activities were fit with D_D as the only adjustable parameter. Representative fits for each of these activities are shown in Figures 2.9 to 2.15 and the mean values of D_D are listed in Table 2.2. The values of D_D in Table 2.2 are plotted in Figure 2.16 to again show that there is a sudden increase in the value of the diffusion coefficient at activity 0.3,

consistent with the mass uptake results. At the higher activities, namely 0.4 and 0.5, the fit using the dual mode model with local equilibrium relaxation (Figures 2.14 and 2.15) is rather poor compared to those at or below activity 0.3. The inability to capture the behavior at higher activities may support the plasticization (or glass transition) hypothesis stated above. If a penetrant-induced glass transition occurs near activity 0.3, then the dual mode model presented here would have to be combined with a simple Fickian model for the rubbery region in a moving boundary problem. This problem is the focus of Chapter 3.

2.3.6 Prediction of Mass Uptake Using Dual Mode with Local Equilibrium Relaxation

As a further validation of the dual mode transport model with local equilibrium relaxation, mass uptake curves were predicted from the parameters obtained from the FTIR-ATR data. First, the total concentration profile was calculated numerically and then integrated over the film thickness to obtain the mass uptake. The calculated mass uptake, using the mean value of D_D listed in Table 2.2 and with k_r fixed at 4.85×10^{-3} s^{-1}, is plotted as a function of $\sqrt{t/L^2}$ alongside the actual mass uptake data at activities 0.1, 0.2 and 0.3, in Figures 2.17, 2.18 and 2.19, respectively. In these figures, the open diamonds are the mass uptake experimental data and the solid lines are the predictions from the dual mode transport model with local equilibrium relaxation. In general, there is good agreement between the predictions and the actual data.

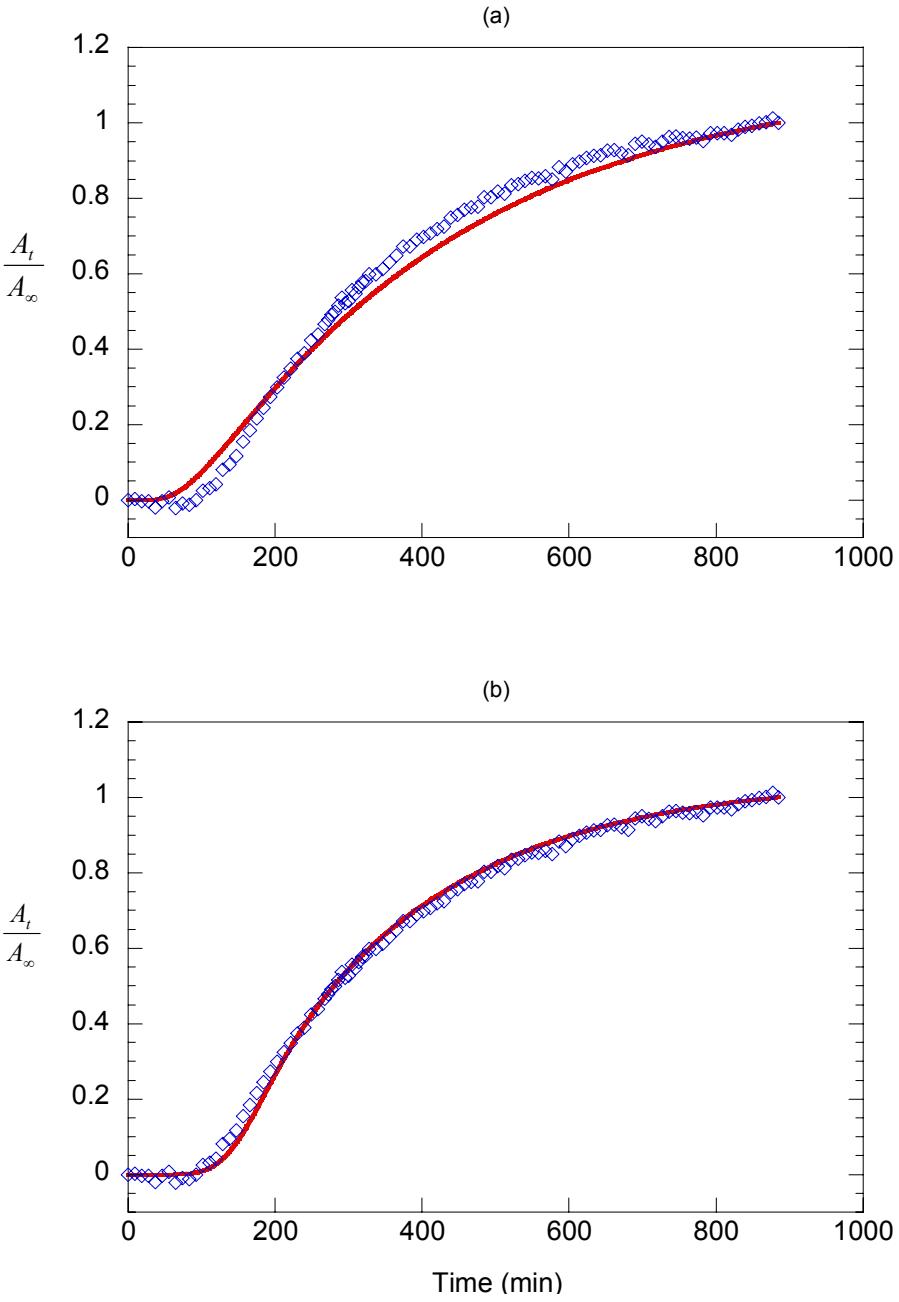

Figure 2.8 FTIR-ATR absorbance data of acetonitrile in CA at activity 0.2 and T=25˚C with (a) the best fit using the dual mode model under local equilibrium assumption, Eq. 2.21, and (b) the best fit using the dual mode model with the local equilibrium assumption relaxed. L=49.2 μm.

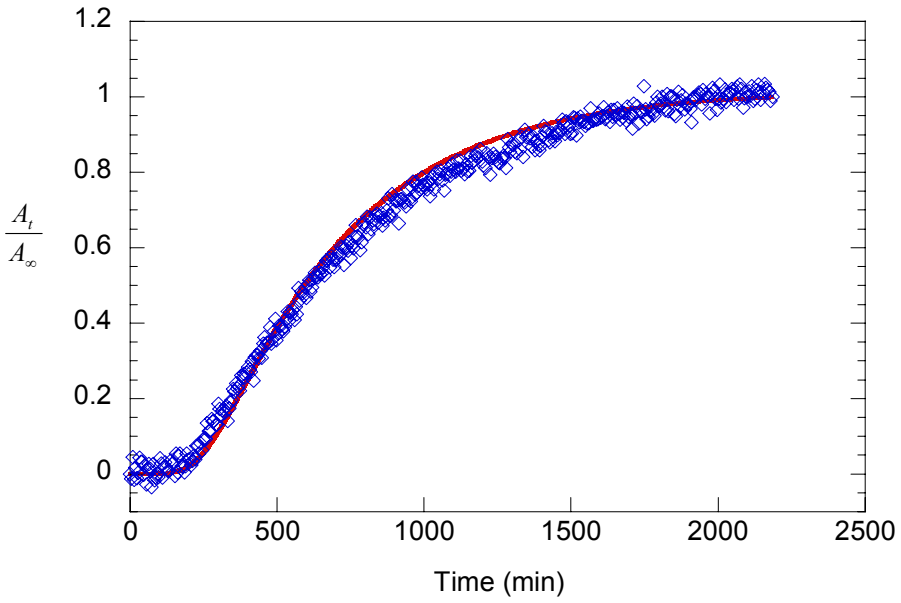

Figure 2.9 FTIR-ATR data for absorbance of acetonitrile in CA at activity 0.06 with the fit using the dual mode model with local equilibrium relaxation. T=25˚C and L=20.8 μm.

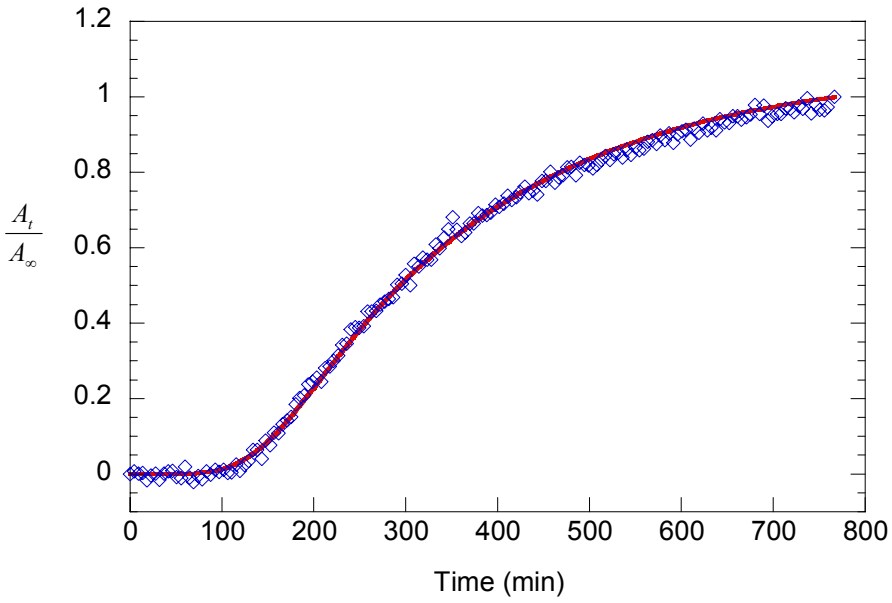

Figure 2.10 FTIR-ATR data for absorbance of acetonitrile in CA at activity 0.1 with the fit using the dual mode model with local equilibrium relaxation. T=25˚C and L=29.8 μm.

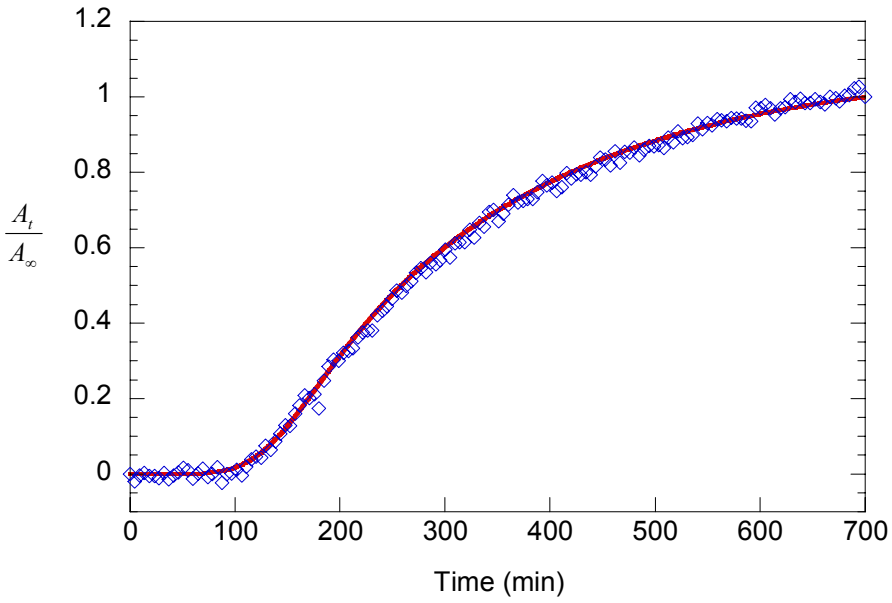

Figure 2.11 FTIR-ATR data for absorbance of acetonitrile in CA at activity 0.15 with the fit using the dual mode model with local equilibrium relaxation. T=25˚C and L=38.4 μm.

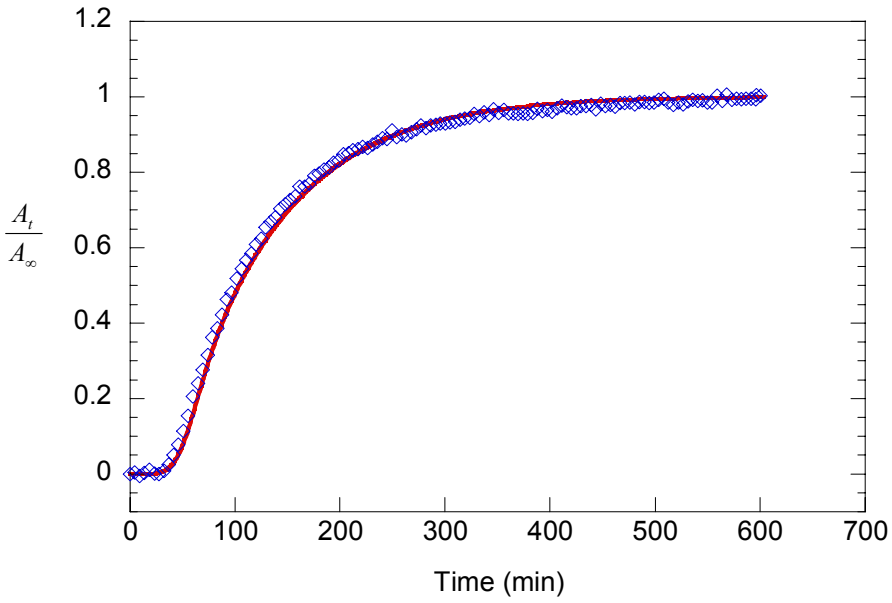

Figure 2.12 FTIR-ATR data for absorbance of acetonitrile in CA at activity 0.25 with the fit using the dual mode model with local equilibrium relaxation. T=25˚C and L=30.4 μm.

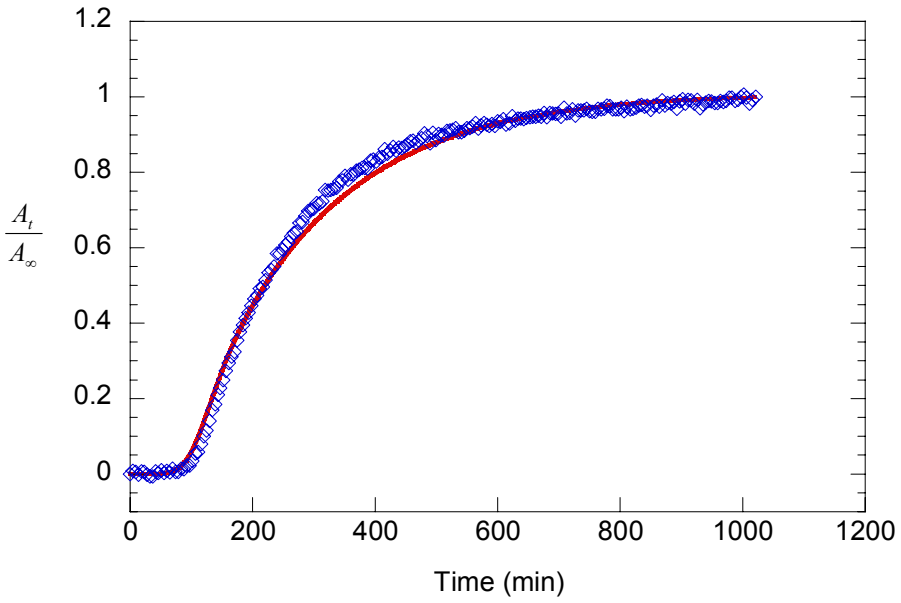

Figure 2.13 FTIR-ATR data for absorbance of acetonitrile in CA at activity 0.30 with the fit using the dual mode model with local equilibrium relaxation. T=25˚C and L=49.4 μm.

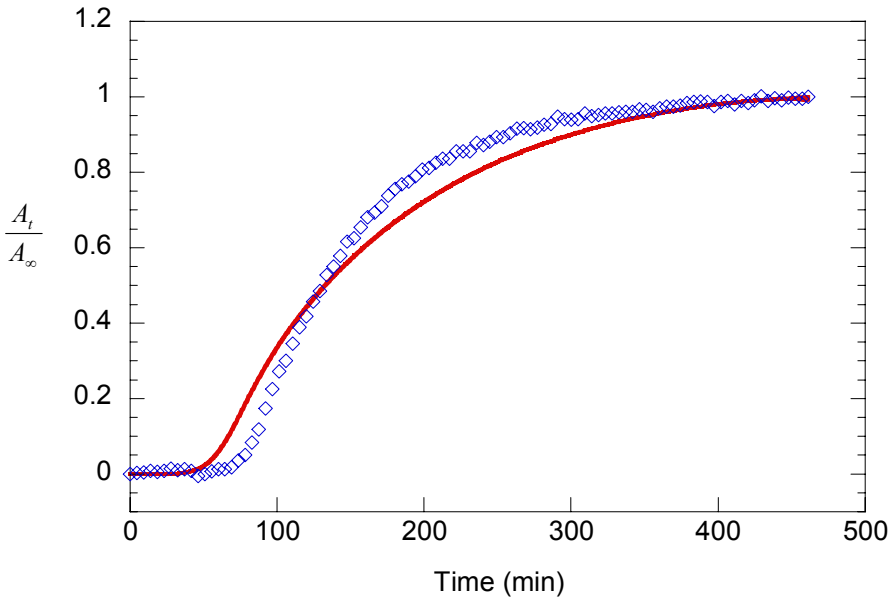

Figure 2.14 FTIR-ATR data for absorbance of acetonitrile in CA at activity 0.40 with the fit using the dual mode model with local equilibrium relaxation. T=25˚C and L=59.8 μm.

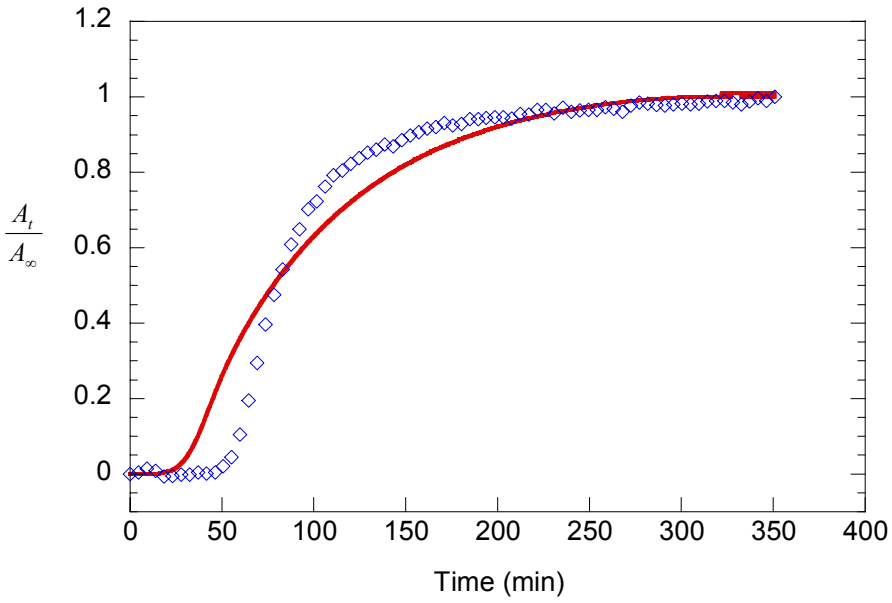

Figure 2.15 FTIR-ATR data for absorbance of acetonitrile in CA at activity 0.50 with the fit using the dual mode model with local equilibrium relaxation. T=25˚C and L=76.2 μm.

Table 2.2 D_D from the dualmode transport model with local equilibrium relaxation ($k_r = 4.85 \times 10^{-3}\ s^{-1}$).

Activity	$D_D \times 10^{10}\ cm^2/s$
0.06	1.91 ± 0.03
0.10	2.96 ± 0.02
0.15	4.66 ± 0.01
0.20	6.38 ± 0.04
0.25	7.04 ± 0.11
0.30	8.09 ± 0.06
0.40	18.1 ± 0.4
0.50	46.0 ± 3.5

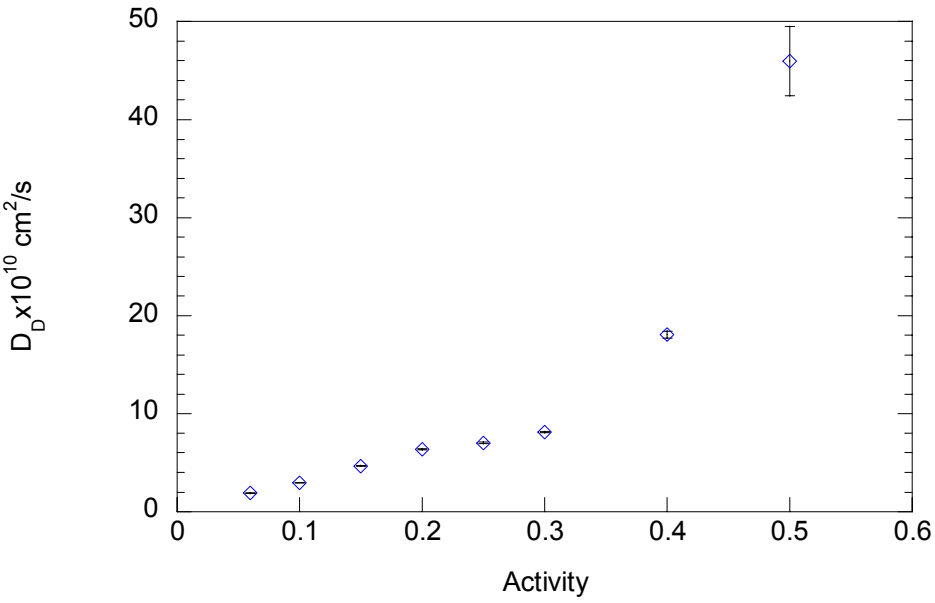

Figure 2.16 Diffusion coefficients obtained from the dual mode transport model with local equilibrium relaxation (k_r = 4.85 x 10^{-3} s^{-1}).

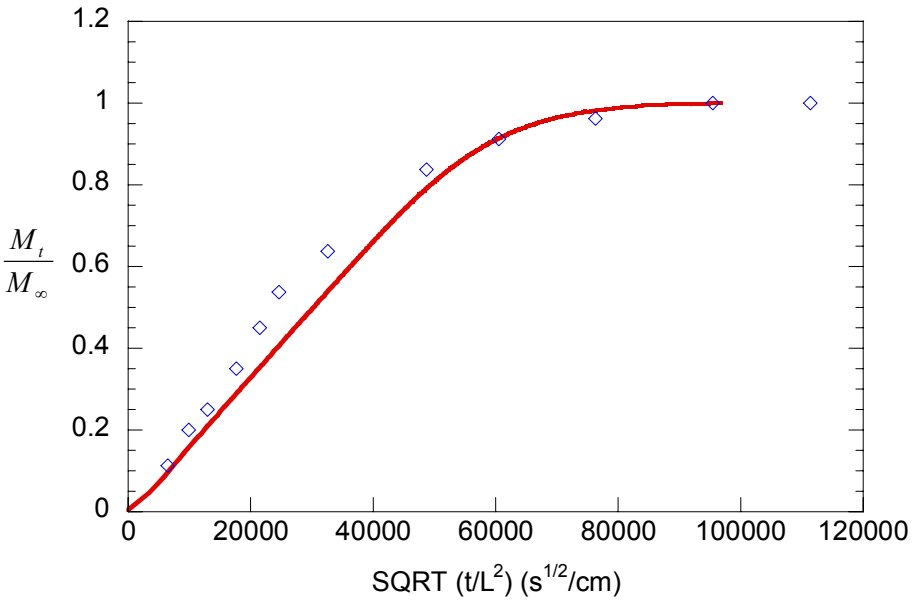

Figure 2.17 Prediction of mass uptake at activity 0.1 using the dual mode transport model with local equilibrium relaxation. Open diamonds represent actual mass uptake data. L=28.6 μm.

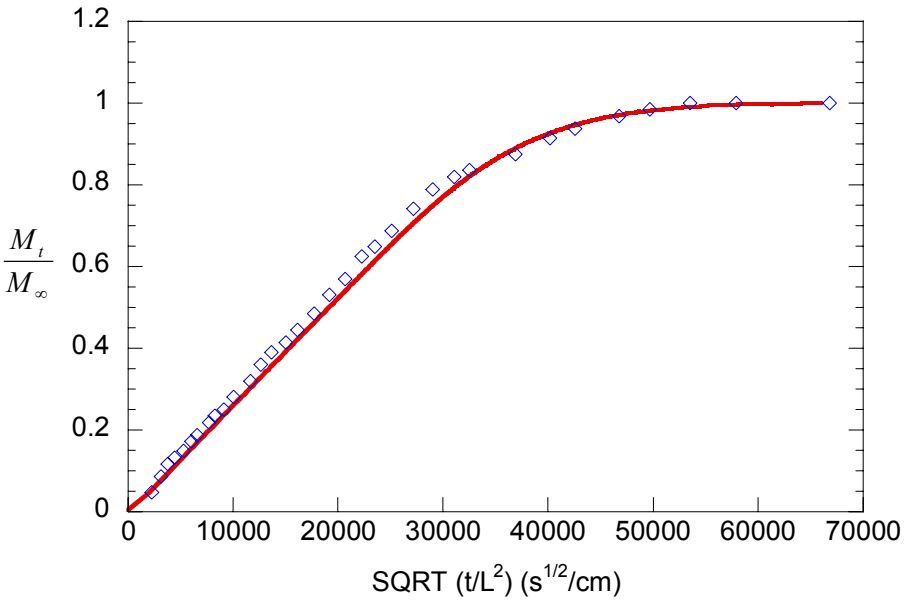

Figure 2.18 Prediction of mass uptake at activity 0.2 using the dual mode transport model with local equilibrium relaxation. Open diamonds represent actual mass uptake data. L=50.4 μm.

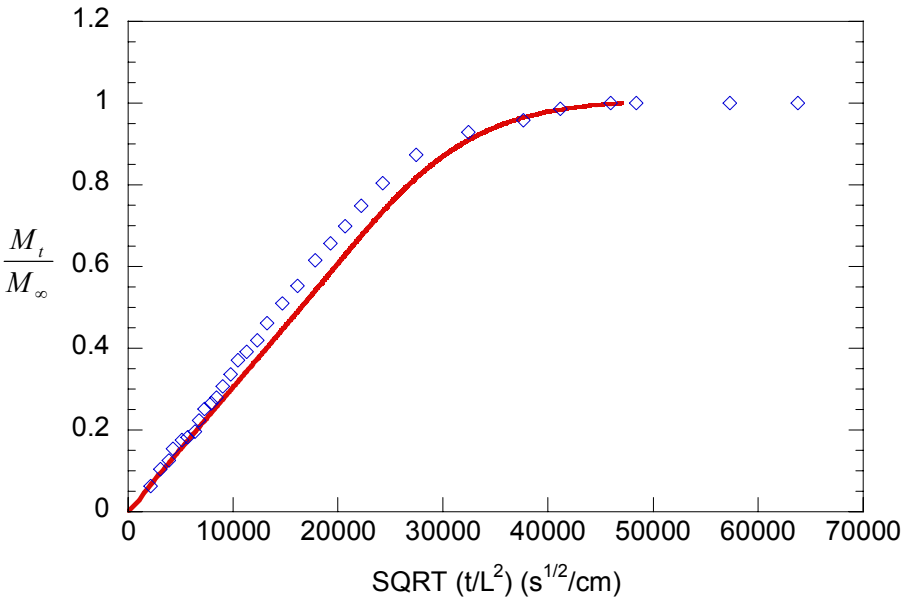

Figure 2.19 Prediction of mass uptake at activity 0.3 using the dual mode transport model with local equilibrium relaxation. Open diamonds represent actual mass uptake data. L=48.2 μm.

2.4 Conclusion

The results presented here indicate that the assumption of local equilibrium in the dual mode model must be relaxed when describing transient diffusion behavior in a glassy polymer. One of the strengths of FTIR-ATR spectroscopy applied to diffusion in a polymer film is that it effectively measures the concentration at a point, the polymer-crystal interface, provided the film thickness is much larger than the depth of penetration of the evanescent field into the film. Therefore, the technique can be a stringent test of transport models, such as the dual mode model, and can uncover phenomena that could be masked when measuring an integrated quantity, such as total mass in gravimetric measurements.

The dual mode transport model with local equilibrium relaxation is able to describe well the physics of acetonitrile diffusion in glassy cellulose acetate, particularly at low activities. The model appears rather robust in that a characteristic rate constant for the hole filling process (k_r) from one activity can be kept constant as activity is varied, leaving the diffusion coefficient for the dissolved population (D_D) as the only adjustable parameter. Physically, at low activities, the slight increase in D_D with activity suggests an increase in chain mobility. In contrast, a constant value of k_r suggests that chain mobility around pre-existing holes does not influence the rate of filling (or emptying) that hole. The model, as presented here, breaks down at higher activities, but the large increase in the magnitude of the diffusion coefficient at these activities suggests a glass transition or plasticization effect, which must be accounted for separately. Chapter 3 will address this transition with a moving boundary model.

The dual mode transport model with local equilibrium relaxation will also be challenged with desorption and dilation data in Chapters 4 and 6, respectively. A variation of this model to account for penetrant-induced plasticization (and hole disappearance) will be presented in Chapter 5.

Chapter 3

Moving Boundary Model for Diffusion in a Glassy Polymer Undergoing a Penetrant-Induced Glass Transition

3.1 Introduction

In the previous chapter, a dual model transport model with local equilibrium relaxation was proposed and successfully used to interpret the FTIR-ATR diffusion data of acetonitrile in cellulose acetate (CA) films below and at activity 0.3. However, the model broke down at higher activities, namely 0.4 and 0.5. Furthermore, the diffusion coefficients obtained gravimetrically suggest there may be a penetrant induced glass transition near activity 0.3. If this hypothesis is accurate, then there will be a position within the film at which the concentration reaches a glass transition concentration, C_g, and the location of this concentration will move away from the penetrant source until it reaches the polymer-crystal interface. Hence, during the diffusion process, there are two separated regions in the polymer film: (1) the region behind the moving boundary, in which the polymer is rubbery and diffusion is governed by simple Fickian diffusion, and (2) the region in front of the moving boundary, in which the polymer is glassy and, based on the results in the previous chapter, the diffusion is governed by dual mode transport with local equilibrium relaxation. The concept of a moving boundary (or front) during diffusion in glassy polymers has precedence, as it is the basis for many descriptions of Case II transport.[123-137]

3.2 Experimental Methods

The experimental measurement of the onset of desorption hysteresis was used to determined both the presence of a penetrant-induced glass transition and the concentration at which it occurs. The detailed sample preparation and experimental procedures have been discussed in Chapter 1. Unlike the sorption process, during which the final activity in the isotherm was approached in step-wise fashion, for the desorption experiments, the CA polymer samples were exposed directly to the acetonitrile vapor at the target activity from which desorption would be initiated. The equilibrium mass uptake obtained by exposing the CA to acetonitrile at the target activity was the same as that obtained from the gradual step-wise increase in activity up to the target value.

3.3 Moving Boundary Model

3.3.1 Model Formulation

To better describe the diffusion of acetonitrile in cellulose acetate undergoing a penetrant-induced glass transition, a moving boundary model is proposed in this chapter. First, in order to simplify the conditions of the problem, the swelling of the polymer is ignored. By making this assumption, the polymer is set in a fixed coordinate system as shown in Figure 3.1. The position of the moving boundary is a function of time, $X(t)$, and it starts moving from the polymer film surface exposed to the penetrant source (z=0) into the film.

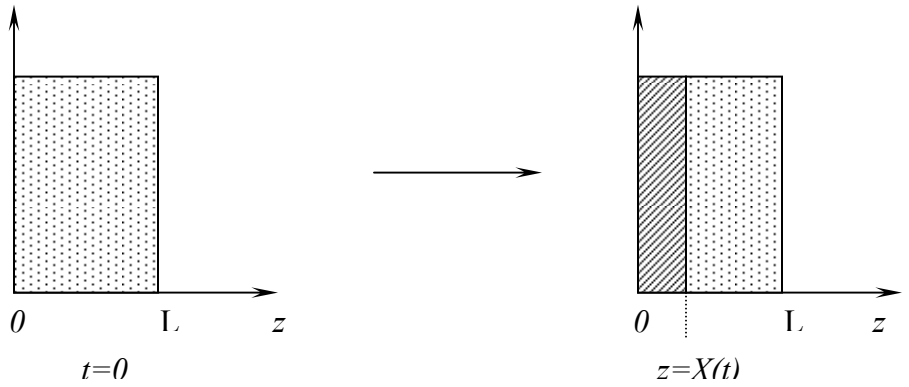

Figure 3.1 Schematic representation of a moving boundary, where the penetrant source is located at z=0. To facilitate the numerical solution of the moving boundary problem, the coordinate system used here is the opposite of that used in Chapter 2.

In the rubbery region $0 \le z \le X(t)$:

$$\frac{\partial C_r}{\partial t} = D_r \frac{\partial^2 C_r}{\partial z^2} \tag{3.1}$$

with

initial condition:

$t = 0$ (*all z*) $\quad C_r = 0$ (3.2)

stationary boundary condition:

$z = 0$ ($t>0$) $\quad C_r = C_L$ (3.3)

moving boundary condition:

$z = X(t)$ ($t>0$) $\quad C_r = C_g$ (3.4)

In the glassy region $X(t) \le z \le L$

$$\frac{\partial C_D}{\partial t} = D_D \frac{\partial^2 C_D}{\partial Z^2} - k_f C_D (C_H^{'} - C_H) + k_r C_H \tag{3.5}$$

$$\frac{\partial C_H}{\partial t} = k_f C_D (C_H^{'} - C_H) - k_r C_H \tag{3.6}$$

with

initial condition:

$t = 0$ (*all z*) $\quad C_D = 0, C_H = 0$ (3.7)

stationary boundary condition:

$z = L$ ($t>0$) $\quad \frac{dC_D}{dz} = 0, \frac{dC_H}{dz} = 0$ (3.8)

At the moving boundary, total concentration of the two species, Henry's law population and Langmuir population, is equal to the glass transition concentration,

$z = X(t)$ ($t>0$) , $C_D + C_H = C_g$ (3.9)

In addition to the continuity of concentration at the moving boundary, there must also be continuity of flux. In chapter 2, it was assumed that the Langmuir population residing in the pre-existing free volume (or holes) of the polymer does not contribute to the flux. Therefore, the flux in terms of concentration in the glassy region should only include the Henry's law population:

$z = X(t)$ ($t>0$) , $D_r \frac{dC_r}{dz} = D_D \frac{dC_D}{dz}$ (3.10)

In this model, $X(t)$ is the position of the moving boundary; C_r and D_r are the penetrant concentration and diffusion coefficient in the rubbery region, respectively; C_L is the concentration at the penetrant-polymer interface; C_g is the glass transition

concentration; C_D and C_H are the Henry's law and Langmuir concentrations in the glassy region, respectively; D_D is the diffusion coefficient in the glassy region; and k_r and k_f are the hole-emptying and hole-filling rate constants, respectively.

The solution to Equation (3.1), satisfying its stationary boundary condition at z=0, is [2]

$$C_r = C_L + B \cdot erf \frac{z}{2\sqrt{D_r t}} \tag{3.11}$$

where B is a constant. To make Equation (3.11) satisfy the continuity of concentration, moving boundary condition at $z=X(t)$, it can be written as

$$B \cdot erf \frac{X(t)}{2\sqrt{D_r t}} = C_g - C_L \tag{3.12}$$

Since B, C_g and C_r are fixed, Equation (3.12) indicates $X(t)$ must be proportional to $t^{1/2}$,

$$X(t) = kt^{1/2} \tag{3.13}$$

where k is a constant which can be obtained numerically. Hence, B can be given by

$$B = \frac{C_g - C_L}{erf \frac{k}{2\sqrt{D_r}}} \tag{3.14}$$

Substituting Equation (3.11) into the left side of the continuity of flux, moving boundary condition at $z=X(t)$, Equation (3.10) can be rewritten as

$$D_D \frac{dC_D}{dz} = \sqrt{\frac{D_r}{\pi t}} \cdot B \cdot \exp\left(-\frac{k^2}{4D_r}\right) \tag{3.15}$$

3.3.2 Numerical Solution Procedure

The model was numerically solved using the following procedure:

1. Initial estimates for the diffusion coefficient in the rubbery region, D_r and the moving boundary velocity constant k, designated as D_{r1} and k_1, respectively, are made.
2. At time t_1, from the initial estimate of k_1, the position of the moving boundary, $X(t_1)=k_1 t_1^{1/2}$ is obtained, and then the value of B is calculated from Equation (3.14). Then, in the rubbery region, $0 \le z \le X(t_1)$, Equation (3.11) is used to obtain the concentration as a function of position. In the glassy region, $X(t_1) \le z \le L$, Equations (3.5) and (3.6) with boundary condition (3.8) are used to obtain the concentrations, C_D and C_H, as functions of position. For both regions, the moving boundary conditions, Equations (3.4), (3.9) and (3.15) are employed.
3. Repeating step 2, at $t_L = (L/k_1)^2$, the moving boundary reaches the polymer-crystal interface. The concentration as a function of position at time t_L is obtained as described in step 2. The penetrant concentration at time t_L when the moving boundary reaches the interface is normalized to the value at the penetrant source, C_L, and compared to the experimental normalized absorbance data at t_L by obtaining the squared error. The value of k is then changed from k_1 to k_2, by adding a small increment, and step 3 is repeated until the squared error between calculated and experimental concentrations at t_L is minimized, giving the best value of k for D_{r1}.

4. Using D_{r1} and k, and the other known parameters, the entire penetrant concentration profile as a function of time is calculated and compared to the experimental data, and the sum of the squared errors is obtained. D_{r1} is incrementally changed to D_{r2}, and steps 2 and 3 are repeated until the sum of squared errors is minimized.

3.4 Results and Discussion

3.4.1 Penetrant-Induced Glass Transition and Desorption Hysteresis

In the previous chapter, a hypothesis was proposed that upon sorption of acetonitrile in cellulose acetate, a penetrant-induced glass transition might be occurring near activity 0.3. In order to validate this hypothesis, desorption experiments were conducted at two different "conditioning" activities, 0.4 and 0.3. The term "conditioning" refers to the sorption history prior to the measurement of the desorption isotherm. Here, the CA history was exposure to acetonitrile vapor at an activity of either 0.4 or 0.3, until the equilibrium mass uptake was reached. The desorption isotherms are plotted in Figure 3.2 alongside the sorption isotherm.

It can be seen that the desorption isotherm starting from activity 0.4 initially follows the sorption isotherm, departing near activity 0.25. It is well known that, for rubbery polymers, the sorption and desorption isotherms follow the same curve. Furthermore, it is also well established that desorption hysteresis is a characteristic of the glassy state and the onset of this hysteresis is often identified as the glass transition concentration. This behavior suggests that the acetonitrile/CA system is in a rubbery

state at activity 0.4 and a penetrant-induced glass transition occurs near activity 0.25. The desorption isotherm starting from activity 0.3 shows a more immediate departure from the sorption isotherm, but ultimately follows the desorption isotherm generated from activity 0.4. Since the glass transition is itself history dependent, these results suggest that the polymer at activity 0.3 may not have completely relaxed to a rubbery state, even though the sorption is considered to be at equilibrium, over the time allowed for the measurement. Based on the desorption isotherm starting at activity 0.4 and assuming that the polymer is fully relaxed at this activity, the glass transition is taken to be at activity 0.25. The glass transition concentration corresponding to activity 0.25 is $C_g = 0.0977 \frac{g_{nitrile}}{g_{polymer}}$.

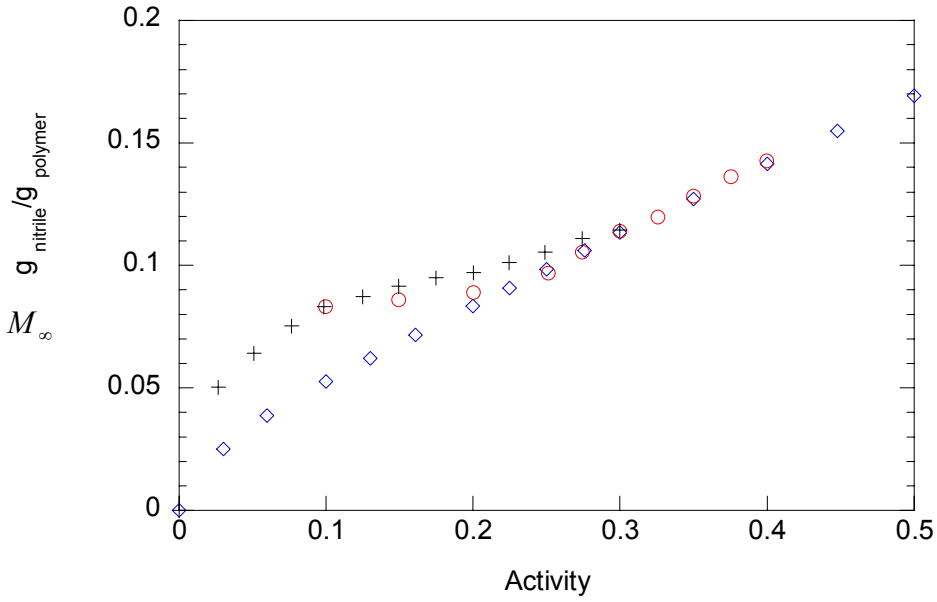

Figure 3.2 Desorption hysteresis of acetonitrile in cellulose acetate. Diamonds are the sorption isotherms; circles and crosses are the desorption isotherms starting from activities 0.4 and 0.3, respectively.

3.4.2 Application of Moving Boundary Model to Acetonitrile Diffusion in CA

Several of the parameters used to solve the moving boundary problem are fixed from the results obtained in Chapter 2:

$k_r = 4.85 \times 10^{-3} s^{-1}$,

$\frac{k_f}{k_r} = 135.3 \frac{g_{polymer}}{g_{nitrile}}$,

$C_H' = 0.030 \frac{g_{nitrile}}{g_{polymer}}$,

C_L for activity 0.3 is $0.1122 \frac{g_{nitrile}}{g_{polymer}}$,

C_L for activity 0.4 is $0.1406 \frac{g_{nitrile}}{g_{polymer}}$,

C_L for activity 0.5 is $0.1689 \frac{g_{nitrile}}{g_{polymer}}$.

Since the glass transition is assumed to be occuring at activity 0.25, the penetrant diffusion coefficient in the glassy region in the moving boundary model was fixed at the value at activity 0.25, the mean value of which was also obtained in the previous chapter, $D_D = 7.04 \times 10^{-10}\ cm^2/s$. The moving boundary velocity constant, k, was obtained numerically in terms of C_r, C_g, $C_{D,}$ and C_H. C_D and C_H were calculated from parameters D_D, k_r and k_f; and C_r was obtained by fitting the model to the data using the one remaining adjustable parameter, D_r. There is one unique value for k corresponding to the diffusion coefficient in the rubbery region at each activity.

3.4.3 Fitting the Moving Boundary Model to Diffusion Data

Following the procedure described above, the moving boundary model was numerically solved to fit the FTIR-ATR absorbance data at activities of 0.5, 0.4 and 0.3, and the results are plotted in Figures 3.3, 3.4 and 3.5, respectively. In these figures, "(a)" is the result from Chapter 2, using the dual model transport model with local equilibrium relaxation, and "(b)" is the result for fitting the same data with the moving boundary model. From the figures, it is clear that the moving boundary model captures the data very well, including the time delay characteristic of local equilibrium relaxation. The moving boundary model, combining simple Fickian diffusion and dual mode transport with local equilibrium relaxation, appears to describe the mechanism of penetrant diffusion in a polymer undergoing a penetrant-induced glass transition. To test the robustness of the model, FTIR-ATR data at different film thicknesses were fit using the model. The results are shown in Figures 3.6, 3.7 and 3.8 for activities 0.5, 0.4, and 0.3, respectively. The results indicate that the physics of the process is independent of the thickness of the films. The values of the diffusion coefficient for the rubbery region, D_r, obtained from the model fit are listed in Table 3.1.

The diffusion coefficients in Table 3.1 are plotted in Figure 3.9 with the diffusion coefficients obtained from gravimetric measurements and those in glassy CA obtained from the dual mode transport model with local equilibrium relaxation. As mentioned above, the penetrant diffusion coefficient for the glassy region in the moving boundary model was fixed at $7.04\times10^{-10}\ cm^2/s$ for activities at and above

0.3. From Figure 3.9, it can be seen that the diffusion coefficient in the rubbery region at activity 0.5 is more than one order of magnitude higher than that in the glassy region. This difference is typical of rubbery and glassy polymers. Furthermore, the diffusion coefficients from gravimetric measurements for activities 0.5 and 0.4 lie between the corresponding glassy and rubbery diffusion coefficients from the moving boundary model. This observation is expected since the diffusion coefficient from the mass uptake experiments is, in effect, an "averaged" value. Also, the diffusion coefficient obtained for the rubbery region at activity 0.3 is close to that used for the glassy region, suggesting that the glass transition concentration could be close to the equilibrium concentration at activity 0.3, $0.1122\frac{g_{nitrile}}{g_{polymer}}$, rather than that assumed here at activity 0.25, $0.0977\frac{g_{nitrile}}{g_{poly}}$.

It is interesting to note that the moving boundary model exhibits a discontinuity believed to be the result of the arrival of the moving boundary at the polymer crystal interface. For example, in Figure 3.3 (b), the value of *k*, the moving boundary velocity coefficient, was numerically calculated to be $1.06\times10^{-4}\ cm/s^{1/2}$. The time at which the moving boundary reaches the interface was calculated to be $t = L^2/k^2 = 86.1\text{min}$, which corresponds well to the time at which the discontinuity in the fitting curve in Figure 3.3 (b) occurs. The discontinuity is believed to be the result of the discontinuity in the concentration of the mobile species between the rubbery and glassy regions in the model.

Table 3.1 Diffusion coefficients for the rubbery region in the moving boundary model for acetonitrile in cellulose acetate.

Activity (N=3)	$D_r \times 10^9\ cm^2/s$
0.5	8.7 ± 0.2
0.4	3.1 ± 0.2
0.3	0.82 ± 0.02

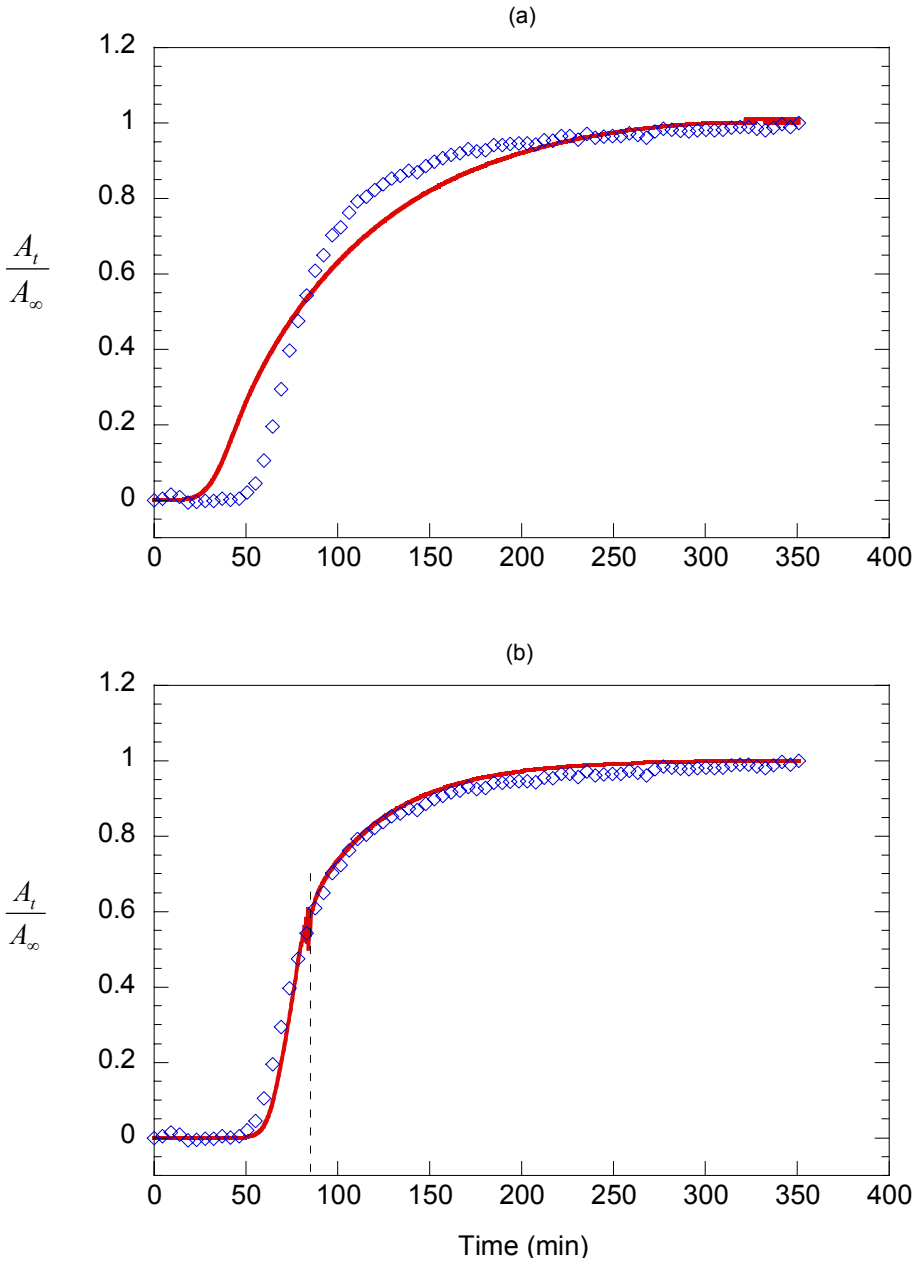

Figure 3.3 Acetonitrile diffusion in CA at activity 0.50. (a) Dual mode with local equilibrium relaxation. (b) Moving boundary model. L=76.2 μm and T=25˚C.

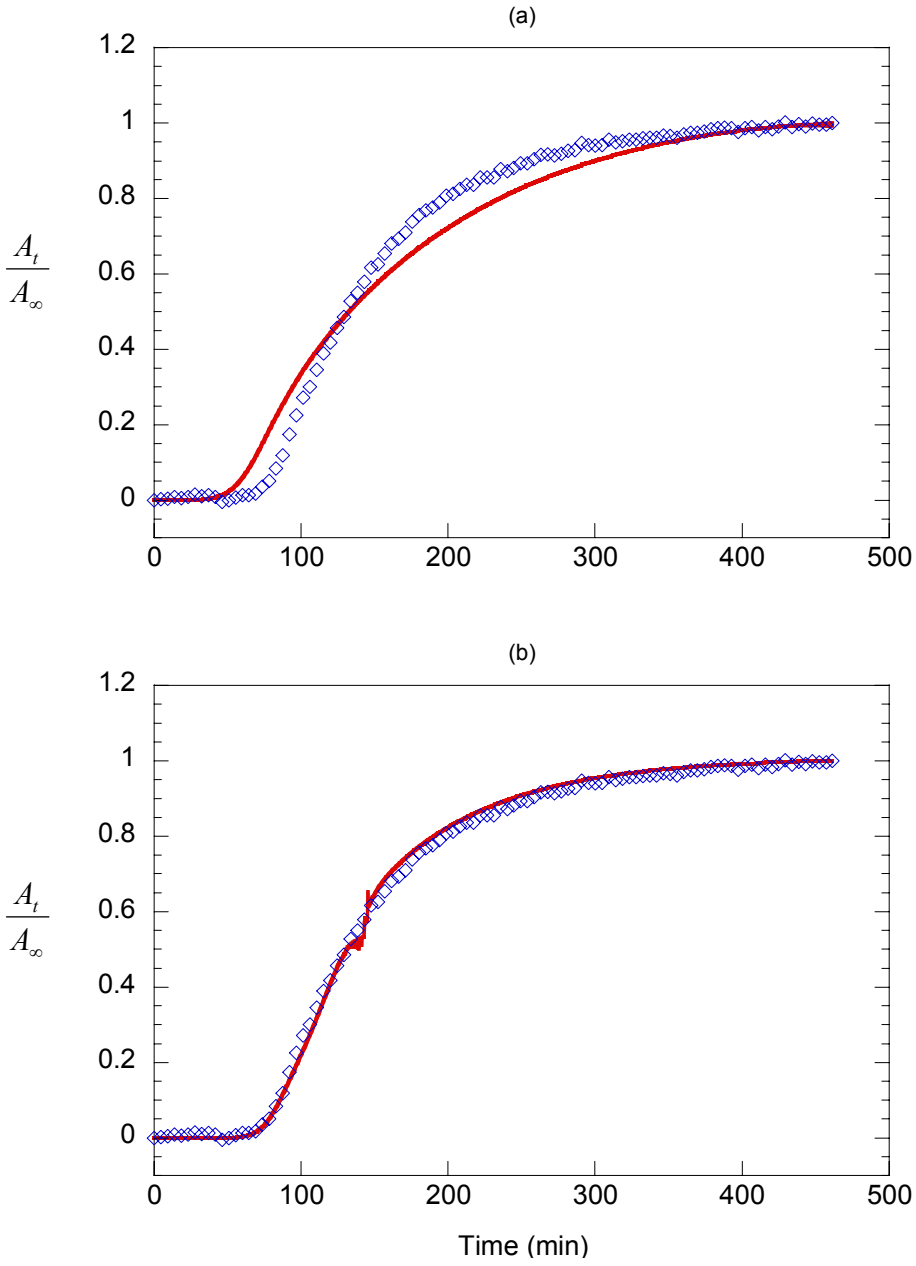

Figure 3.4 Acetonitrile diffusion in CA at activity 0.40. (a) Dual mode with local equilibrium relaxation. (b) Moving boundary model. L=59.8 μm and T=25˚C.

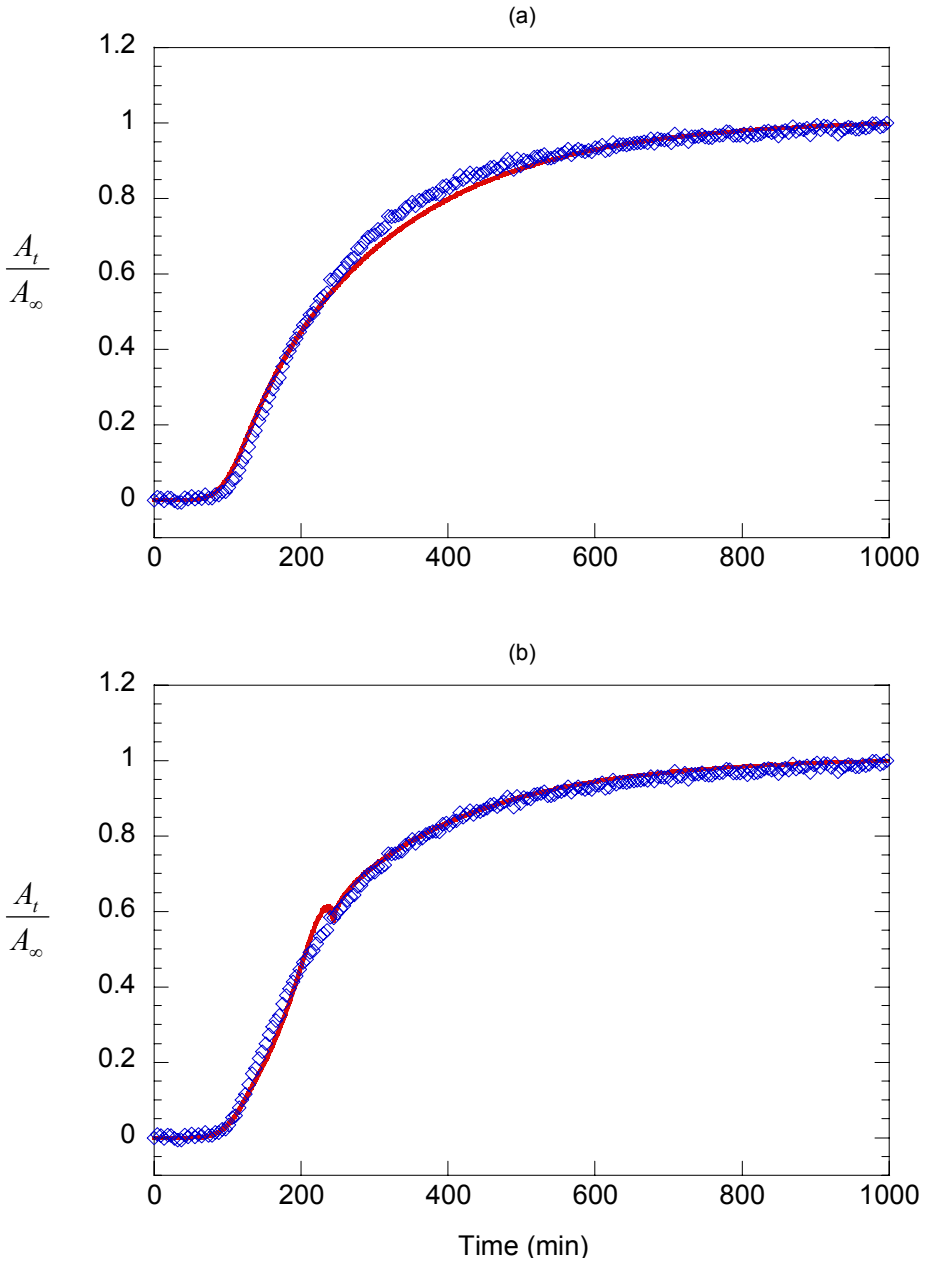

Figure 3.5 Acetonitrile diffusion in CA at activity 0.30. (a) Dual mode with local equilibrium relaxation. (b) Moving boundary model. L=49.4 μm and T=25˚C.

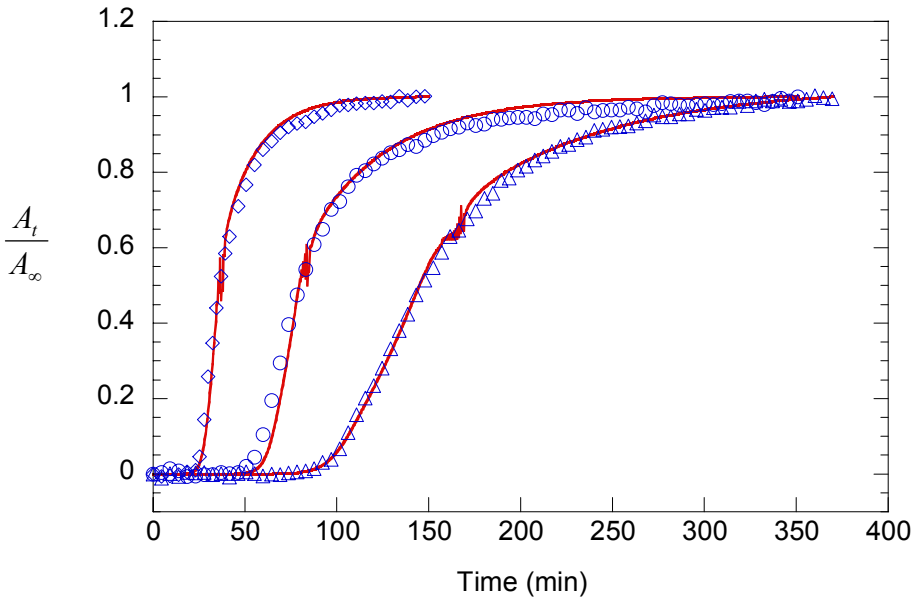

Figure 3.6 Acetonitrile diffusion in CA at activity 0.5 and different film thicknesses. Solid lines represent the best fit using the moving boundary model. Diamonds - L=47.3 μm; Circles - L=76.2 μm; Triangles - L=94.0 μm.

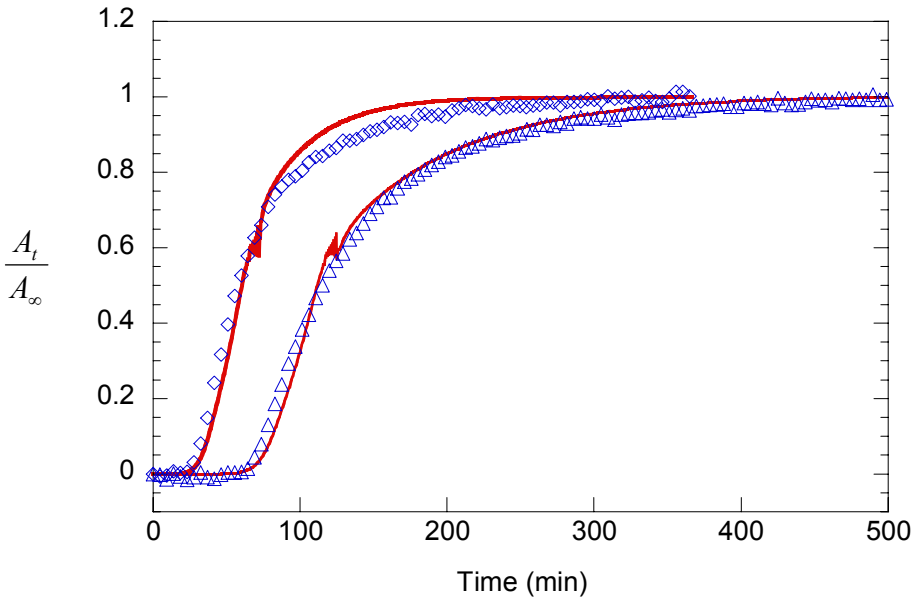

Figure 3.7 Acetonitrile diffusion in CA at activity 0.4 and different film thicknesses. Solid lines represent the best fit using the moving boundary model. Diamonds - L=42.7 μm; Triangles - L=60.7 μm.

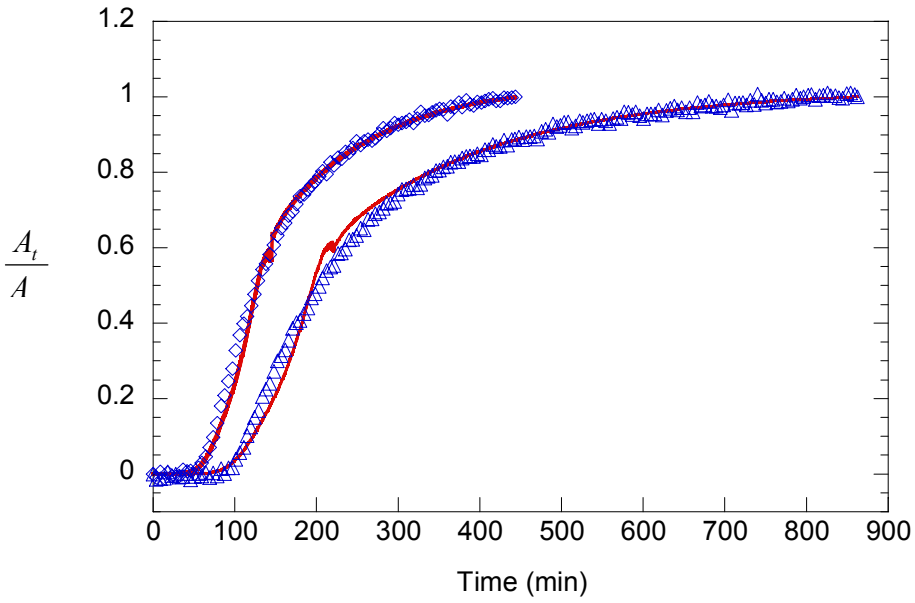

Figure 3.8 Acetonitrile diffusion in CA at activity 0.3 and different film thicknesses. Solid lines represent the best fit using the moving boundary model. Diamonds - L=39.4 μm; Triangles - L=48.3 μm.

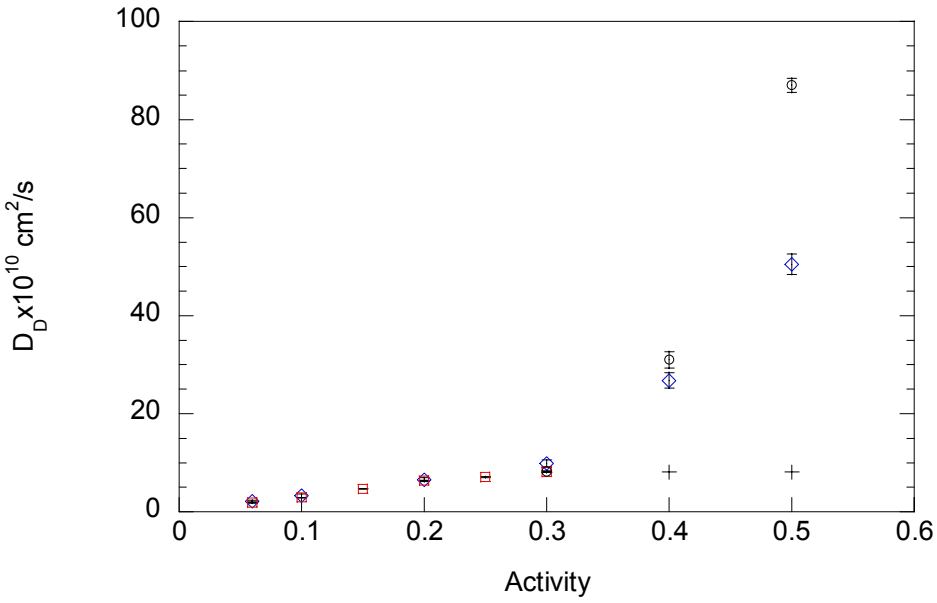

Figure 3.9 Diffusion coefficients from gravimetric measurements (diamonds); FTIR-ATR measurements with the dual mode model with local equilibrium relaxation (squares); and FTIR-ATR measurements with the moving boundary model (crosses for the glassy region and circles for the rubbery region). T=25˚C.

3.4.4 Prediction of Mass Uptake Using Moving Boundary Model

As a further validation of the moving boundary model, the mass uptake curves for activities 0.3, 0.4 and 0.5 were predicted using the moving boundary model with parameters from fitting the FTIR-ATR data. First, the total concentration profile was calculated numerically and then, the concentration profile was integrated over the film thickness to obtain the mass uptake. The calculated mass uptake is plotted as a function of $\sqrt{t/L^2}$ alongside the actual mass uptake data at activities 0.3, 0.4 and 0.5 in Figures 3.10, 3.11 and 3.12, respectively. In these figures, the open diamonds are the gravimetric data and the solid lines are the predictions. In general, the predictions are excellent.

3.5 Conclusion

A moving boundary model combining simple Fickian diffusion (for the rubbery region) and dual mode transport with local equilibrium relaxation (for the glassy region) successfully describes the physics of acetonitrile diffusion in cellulose acetate undergoing a penetrant-induced glass transition. The moving boundary model appears rather robust in that the hole-filling and hole-emptying rate constants and the diffusion coefficient in the glassy region can be kept constant, leaving the diffusion coefficient in the rubbery region as the only adjustable parameter. Furthermore, the moving boundary model predicted the mass uptake data from gravimetric measurements.

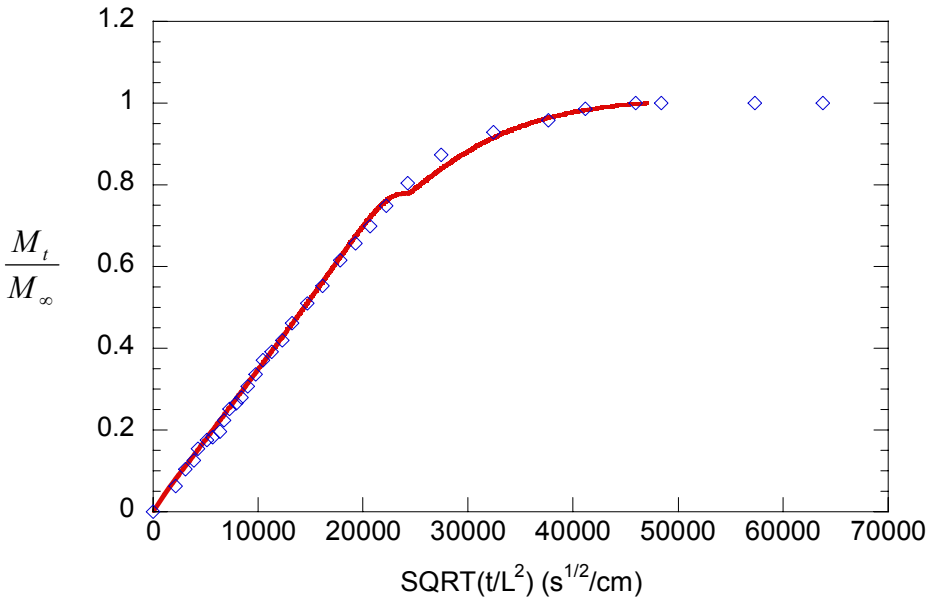

Figure 3.10 Mass uptake data versus $\sqrt{t/L^2}$ at activity 0.3 with the prediction from the moving boundary model. L=48.2 μm and T=25˚C.

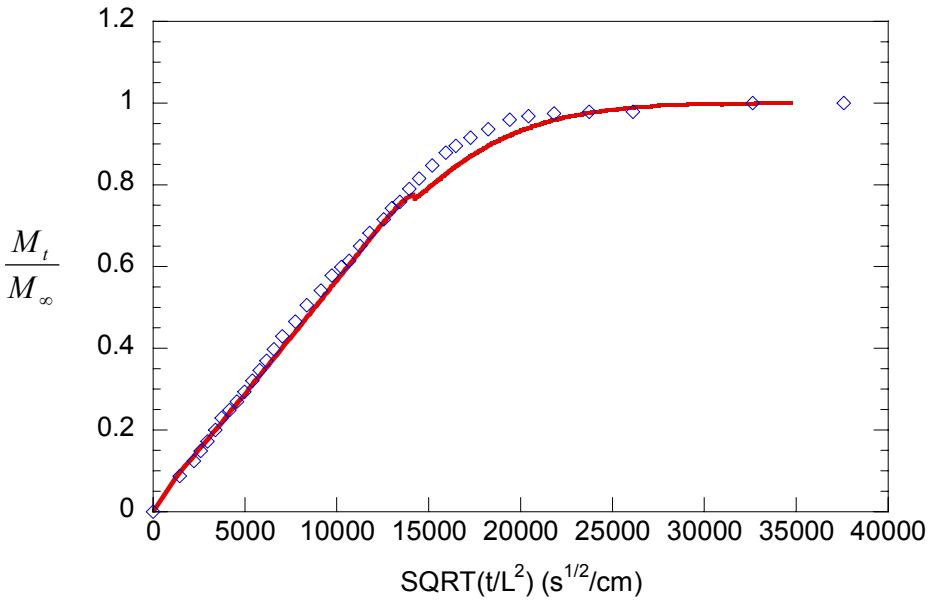

Figure 3.11 Mass uptake data versus $\sqrt{t/L^2}$ at activity 0.4 with the prediction from the moving boundary model. L=79.4 μm and T=25˚C.

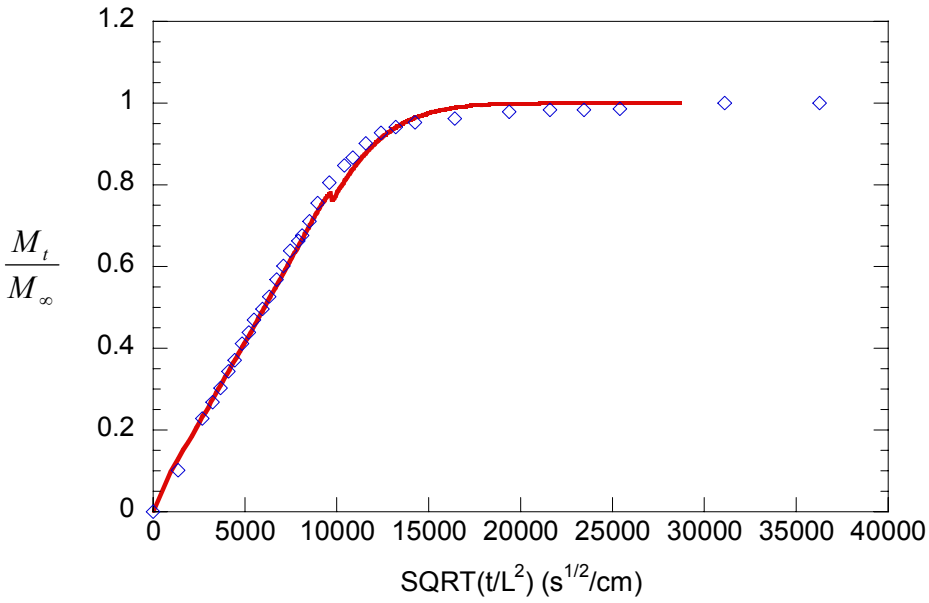

Figure 3.12 Mass uptake data versus $\sqrt{t/L^2}$ at activity 0.5 with the prediction from the moving boundary model. L=70.8 μm and T=25˚C.

Chapter 4

Application of The Dual Mode Transport Model with Local Equilibrium Relaxation to Desorption

4.1 Introduction

In Chapter 2, the sorption of acetonitrile from the vapor phase into cellulose acetate (CA) was studied by FTIR-ATR spectroscopy and a conventional gravimetric balance. A dual mode transport model with local equilibrium relaxation was proposed and used successfully to capture the diffusion behavior uncovered by FTIR-ATR spectroscopy for this system. In this chapter, the desorption of acetonitrile from CA films back into the vapor phase is studied by FTIR-ATR spectroscopy together with the gravimetric balance. The dual mode transport model with local equilibrium relaxation was used, with parameters from the sorption results, to predict the desorption behavior. The prediction was poor, which was not surprising given the fact that desorption hysteresis occurs in glassy polymers. Using the desorption isotherms and recognizing that hysteresis suggests a redistribution of the Henry's law and Langmuir populations, the dual mode model was used to fit the desorption kinetics.

4.2 Experimental Measurement of Desorption Kinetics

In addition to the sorption kinetic experiments described in Chapter 2 and the desorption isotherm measurements described in Chapter 3, FTIR-ATR desorption kinetics experiments were conducted following the procedure described below:

1. After the sorption process reached equilibrium, the valve connecting the vapor generation system and the ATR cell was turned off.
2. Vacuum is then pulled throughout the vapor generation system.
3. When the reading on the vacuum pressure gauge reached its lowest level (approximately 0.2 mmHg), the valve was reopened, marking the starting time for desorption ($t = 0$).

Because of the limitations of the vacuum pump, the vapor system cannot reach true vacuum condition (0 mmHg). However, since the pressure is low, relative to the lowest sorption pressure prior to desorption (13mmHg for activity 0.15), the pressure can be taken as 0 mmHg. Also, since the volume of the reservoir is much larger than that of the ATR cell, it is reasonable to assume that the surface of the CA film is exposed to vacuum (0 mmHg) immediately when the desorption experiment is started. The desorption spectra are captured by the FTIR-ATR spectrometer as a function of time as they were in the sorption experiments.

4.3 Transport Models for Desorption

4.3.1 Simple Fickian Diffusion

According to the Fickian model, the desorption process is governed by the same Fickian equation as is sorption:

$$\frac{\partial C}{\partial t} = D\frac{\partial^2 C}{\partial z^2} \tag{4.1}$$

where C is the penetrant concentration and D is the diffusion coefficient. With the initial condition:

t=0 (*all* z) $\quad C = C_L$

and the boundary conditions:

z=L (t>0) $\quad C = 0$

z=0 ($t \geq 0$) $\quad \frac{\partial C}{\partial z} = 0$

Equation (4.1) can be solved to obtain an analytical solution for C as follows:

$$\frac{C}{C_L} = \sum_{n=0}^{\infty} \frac{4(-1)^n}{\pi(2n+1)} \cos\left[\frac{\pi(2n+1)z}{2L}\right] \exp\left[-\frac{D\pi^2(2n+1)^2 t}{4L^2}\right] \tag{4.2}$$

In FTIR-ATR diffusion experiments, a penetrant-saturated polymer film of thickness L is attached to the surface of an ATR crystal and has one surface exposed to vacuum. With assumptions of weak infrared absorption and constant refractive index, an analogous expression to Equation (4.2) can be derived in term of absorbance:

$$\frac{A}{A_\infty} = \frac{8\gamma}{1-\exp(-2\gamma L)} \sum_{n=0}^{\infty} \exp(g) \left[\frac{\exp(-2\gamma L) f + 2\gamma(-1)^n}{\pi(2n+1)(4\gamma^2 + f^2)}\right] \tag{4.3}$$

where

$$g = \frac{-D(2n+1)^2 \pi^2 t}{4L^2},$$

$$f = \frac{(2n+1)\pi}{2L},$$

and

$$\gamma = \frac{2n_1 \pi \left(\sin^2 \alpha - (n_2/n_1)^2\right)^{1/2}}{\lambda}$$

where γ is the evanescent field decay coefficient, n_1 and n_2 are the refractive indices of the ATR crystal and polymer, respectively, α is the incidence angle, and λ is the wavelength of absorbed light. Under the experimental condition here, where $1/\gamma < 0.1L$, the ratio of absorbances on the left side of Equation (4.3) is well approximated by the ratio of C (z = 0) to C_L (see Chapter 2).

4.3.2 Dual Mode with Local Equilibrium Relaxation

According to the dual mode sorption model, there are two species of penetrant. One population, known as the Henry's law population, is dissolved in the dense, equilibrium portion of the polymer; the other one, known as the Langmuir population, resides in the pre-existing free volume or "holes". The dual mode sorption model gives the total concentration, C_T, of sorbed penetrant:

$$C_T = C_D + C_H = k_D a + C_H' \frac{ba}{1+ba} \tag{4.4}$$

where k_D is the Henry's law constant, a is the penetrant activity in the gas or vapor phase, $C_H^{'}$ is the Langmuir capacity constant, and b is the Langmuir affinity constant.

Equation (4.4) is used for both sorption and desorption. Desorption hysteresis distinguishes itself by a significantly higher value of $C_H^{'}$, which reflects a redistribution of the sorbed population from C_D to C_H.

Diffusion in glassy polymers at low concentrations is well represented by the partial immobilization model. According to this model, a fraction, F, of the Langmuir population, is mobile with the same diffusion coefficient as the Henry's law population, represented by D_D. Under these assumptions, the general dual mode transport model is:

$$\frac{\partial C_D}{\partial t} = D_D \frac{\partial^2 C_D}{\partial z^2} - k_f C_D (C_H^{'} - C_H) + k_r C_H \tag{4.5}$$

$$\frac{\partial C_H}{\partial t} = F D_D \frac{\partial^2 C_H}{\partial z^2} + k_f C_D (C_H^{'} - C_H) - k_r C_H \tag{4.6}$$

where k_f is the rate constant for hole filling and k_r is the rate constant for hole emptying in the Langmuir framework presented in Equation (4.4). The governing equations for desorption are the same as those for sorption. However, the initial condition and boundary conditions for desorption process are:

$t = 0$ ($all\ z$) $\quad C_D = C_{T_L} - C_H,\ C_H = C_H^{'} \dfrac{ba}{1+ba}$

$z = 0$ ($t > 0$) $\quad \dfrac{\partial C_D}{\partial z} = 0,\ \dfrac{\partial C_H}{\partial z} = 0$

$z = L$ ($t > 0$) $\quad C_D = 0,\ C_H = 0$

Equations (4.5) and (4.6) can be written in dimensionless form:

$$\frac{\partial \theta_D}{\partial \tau} = \frac{\partial^2 \theta_D}{\partial \xi^2} - \phi \theta_D \left(\theta_H^{'} - \theta_H \right) + \theta_H \tag{4.7}$$

$$\frac{\partial \theta_H}{\partial \tau} = F \frac{\partial^2 \theta_H}{\partial \xi^2} + \phi \theta_D \left(\theta_H^{'} - \theta_H \right) - \theta_H \tag{4.8}$$

where $\theta_D = \frac{C_D}{C_{T_L}}$;

$\theta_H = \frac{C_H}{C_{T_L}}$;

$\tau = tk_r$;

$\xi = \frac{z}{\sqrt{D_D / k_r}}$;

$\phi = \frac{k_f C_{T_L}}{k_r} = \frac{bC_{T_L}}{k_D}$;

$\theta_H^{'} = \frac{C_H^{'}}{C_{T_L}}$.

The initial condition and boundary conditions can be converted as well:

$\tau = 0 \ \left(0 \le \xi \le \frac{L}{\sqrt{D_D / k_r}} \right)$ $\qquad \theta_D = 1 - \theta_H^{'} \frac{ba}{1+ba}, \ \theta_H = \theta_H^{'} \frac{ba}{1+ba}$

$\xi = 0 \ (\tau > 0)$ $\qquad \frac{\partial \theta_D}{\partial \xi} = 0, \ \frac{\partial \theta_H}{\partial \xi} = 0$

$\xi = \frac{L}{\sqrt{D_D / k_r}} \ (\tau > 0)$ $\qquad \theta_D = 0, \ \theta_H = 0$

4.4 Results and Discussion

4.4.1 Simple Fickian Diffusion

The FTIR-ATR desorption kinetics experiments were conducted at starting activities of 0.25, 0.2, 0.15, 0.1 and 0.06. The integrated absorbances for acetonitrile in CA at activity 0.2 and a film thickness of 44.0 μm, normalized by the equilibrium absorbance, are plotted in Figure 4.1(a) for all time points. Equation (4.3) was used to obtain the best fit to the data, resulting in a diffusion coefficient of 5.0 x 10^{-10} cm^2/s. However, the fit is extremely poor. It is clear that the simple Fickian model cannot capture the desorption behavior for acetonitrile in cellulose acetate.

4.4.2 Dual Mode Transport Model with Local Equilibrium Relaxation for Desorption Kinetics Using Sorption Parameters

From the results in Chapter 2, the failure of the simple Fickian model could have been expected. Since the dual mode transport model with local equilibrium relaxation worked well in sorption kinetics, it is reasonable to assume that the same model may work for the desorption kinetics. To validate this expectation, Equations (4.7) and (4.8) were used to calculate the desorption data for acetonitrile in cellulose acetate at activity 0.2 and $F = 0$ (the Langmuir population is assumed immobile as discussed in Chapter 2). The parameters in the calculation, equilibrium sorption parameters k_D, C_H' and b, and sorption kinetics parameters, D_D and k_r, were obtained from fitting the sorption data at activity 0.2 in Chapter 2.

$$k_D = 0.282 \frac{g_{nitrile}}{g_{polymer}};$$

$$C'_H = 0.030 \frac{g_{nitrile}}{g_{polymer}};$$

$b = 38.1$.

$D_D = 6.38 \times 10^{-10}$ cm^2/s

$k_r = 4.85 \times 10^{-3}$ s^{-1}.

The prediction is compared to the experimental FTIR-ATR absorbance data in Figure 4.1(b). The result is slightly better than the case for simple Fickian diffusion, but the prediction cannot capture the FTIR-ATR desorption data.

4.4.3 Desorption Isotherms for Acetonitrile in Cellulose Acetate

It is well known that the physical properties of glassy polymer are history dependent. The so-called "conditioning" of the polymer upon sorption can change these properties significantly as reported in earlier studies. [141-145] Fleming and Koros (1990) [146] studied the hysteretic behavior in the sorption and desorption of high pressure CO_2 in polycarbonate (PC). In their studies, the polycarbonate films were exposed to CO_2 at pressures of 900 psia , 600 psia and 300 psia prior to desorption. Their desorption data are re-plotted in Figure 4.2 along with the sorption isotherm. Equation (4.4) was used to fit the sorption data shown in Figure 4.2 to obtain the dual mode parameters. From the sorption isotherm, the following dual mode sorption parameters were obtained:

$$k_D = 0.0560 \frac{cm^3(STP)}{cm^3(polymer) \cdot psia}$$

$$C_H^{'} = 1.327 \frac{cm^3(STP)}{cm^3(polymer)}$$

b=$0.1332\,(psia)^{-1}$

It is worth noting here that $cm^3(STP)$, where *STP* refers to standard temperature and pressure, is commonly used in gas sorption studies where 1 $mole = 22{,}420\,cm^3(STP)$.

In desorption processes, it is reasonable to assume that conditioning does not affect the interaction between the penetrant molecules from the vapor phase and the pre-existing Langmuir sites or holes. To test this assumption, the well-characterized CO_2-PC desorption isotherms were fit using Equation (4.4) keeping the value of *b* fixed at $0.1332\,(psia)^{-1}$. With k_D and $C_H^{'}$ as the adjustable parameters, the desorption dual mode parameters were obtained for each desorption isotherm, and are listed in Table 4.1. Comparing the sorption parameters, k_D for desorption is less than that for sorption and is essentially constant for all three conditioning pressures. $C_H^{'}$ for desorption changes significantly, increasing with increasing conditioning pressure. These results imply that the sorption process changes the physical properties of the glassy polymer. It appears that the Henry's law and Langmuir populations redistribute during sorption. Physically, sorption according to Henry's law implies that the polymer chains must expand to accommodate the penetrant, in contrast to Langmuir sorption, which occurs in pre-existing holes. Owing to the rigid nature of the glassy state, it is reasonable that some of the Henry's law molecules, upon desorption, leave a hole behind. These molecules, which would have been included in C_D during sorption, would now be treated as part of C_H in desorption.

Table 4.1 Dual mode desorption parameters for the PC/CO_2 system with sorption conditioning at various pressures holding *b* constant at $0.1332\,(psia)^{-1}$. Data from Fleming and Koros [141] in Figure 4.2.

Pressure (psia)	k_D $\frac{cm^3(STP)}{cm^3(polymer)\cdot psia}$	C'_H $\frac{cm^3(STP)}{cm^3(polymer)}$
900	0.02198	4.751
600	0.02434	3.626
300	0.02413	2.705

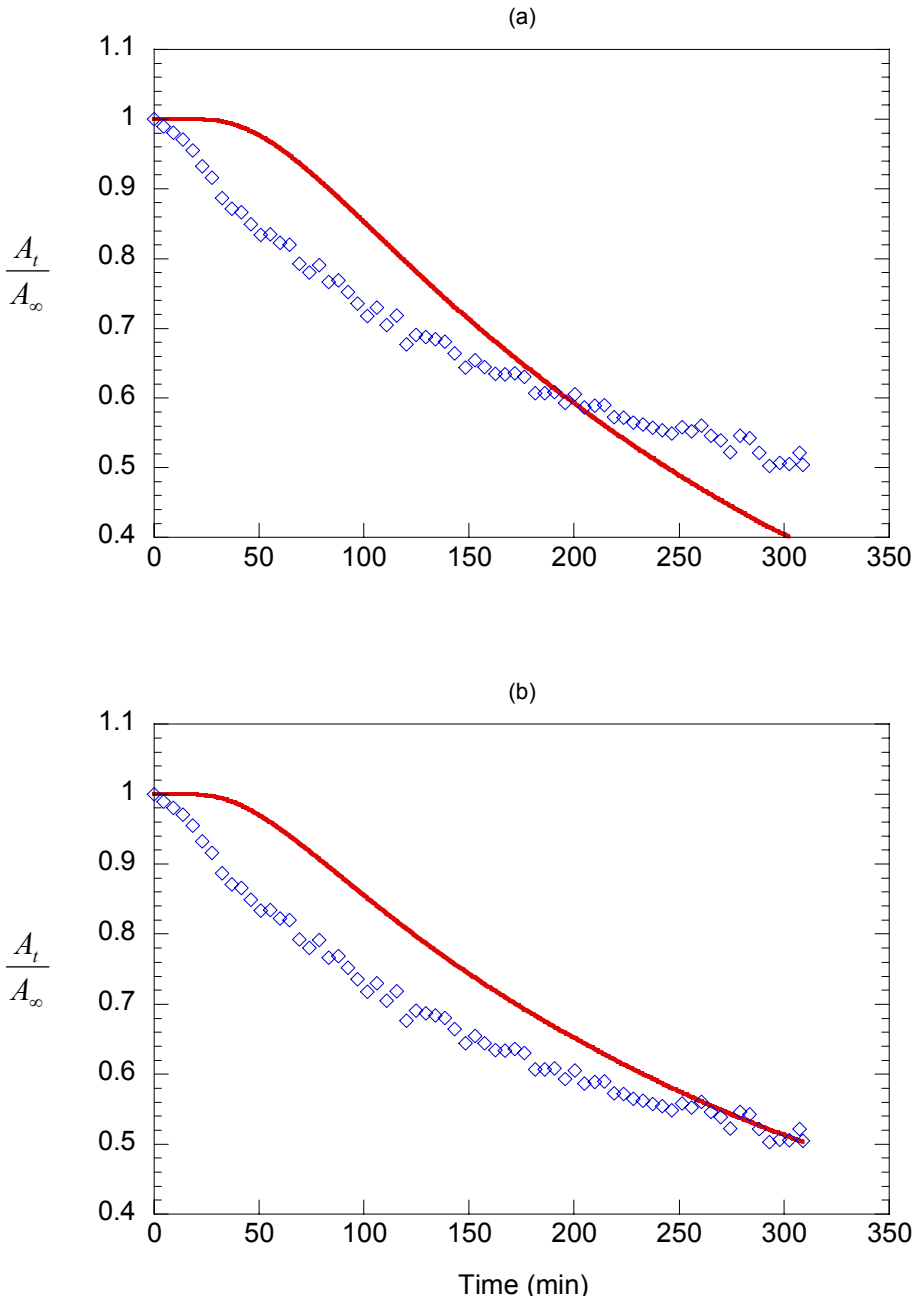

Figure 4.1 Desorption FTIR-ATR absorbance data at activity 0.2 (diamonds) with (a) simple Fickian model fit and (b) prediction using dual mode parameters from sorption. L = 44.0 μm and T = 25ºC.

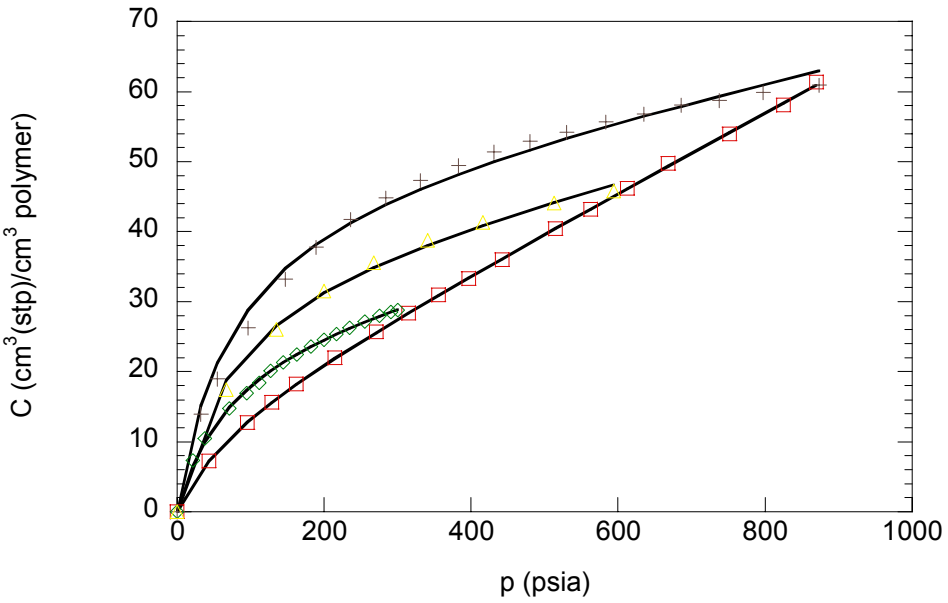

Figure 4.2 CO_2 sorption in PC at 35ºC and desorption after conditioning pressures of 300, 600 and 900 psia, Fleming and Koros. [141] The squares are the sorption isotherms, and the diamonds, triangles and crosses are the desorption isotherms starting from 300, 600 and 900 psia, respectively. Solid lines are the curves from the dual mode model

This re-examination of Fleming and Koros' data shows that one can consider the holes during desorption to be physically the same as those in sorption, which is reflected in b, the affinity constant from the vapor phase. The redistribution between C_D and C_H is reflected in k_D and C_H'. A similar conditioning effect should also occur in the acetonitrile/CA system. In order to validate this hypothesis and obtain the dual mode desorption parameters, desorption isotherms were measured at three different "conditioning" activities, 0.15, 0.20 and 0.25. The results are plotted in Figure 4.3. To determine the dual mode desorption parameters, the value of *b* was fixed at the value from the sorption isotherm, 38.1. The desorption parameters, k_D and C_H', from fitting the desorption isotherms using Equation (4.4), are listed in Table 4.2. The value of k_D from desorption is much smaller than the value from sorption and is essentially constant at $k_D = 0.0593 \pm 0.0008 \frac{g_{nitrile}}{g_{polymer}}$. Also, the desorption hole saturation constants for these three activities can be linearly related to the concentration of Henry's law population, $C_D = k_D a$.

$$C_H' = C_{H0}' + \varphi \cdot k_D a \tag{4.9a}$$

where C_{H0}' is the hole saturation constant for the pure unconditioned polymer, which is fixed at $0.030 \frac{g_{nitrile}}{g_{polymer}}$ from sorption, φ is the proportionality constant, k_D is the Henry's law constant and *a* is activity. By fitting the C_H' parameters at activities 0.15, 0.20 and 0.25, one can obtain the expression for C_H' in terms of activity *a* (r^2 = 0.9988):

$$C_H' = C_{H0}' + 0.256a \tag{4.9b}$$

C_H' at activities 0.1 and 0.06 were calculated from Equation (4.9b) and are listed in Table 4.2.

Table 4.2 Dual mode desorption parameters for acetonitrile/CA at various sorption conditioning activities.

Activity	k_D $\frac{g_{nitrile}}{g_{polymer}}$	C_H' $\frac{g_{nitrile}}{g_{polymer}}$
0.25	0.05852	0.0940
0.20	0.06017	0.0804
0.15	0.05915	0.0680
0.10	0.05928*	0.0556**
0.06	0.05928*	0.0454**

* fixed at average value from activities 0.15, 0.2 and 0.25

** calculated from Equation (4.9b)

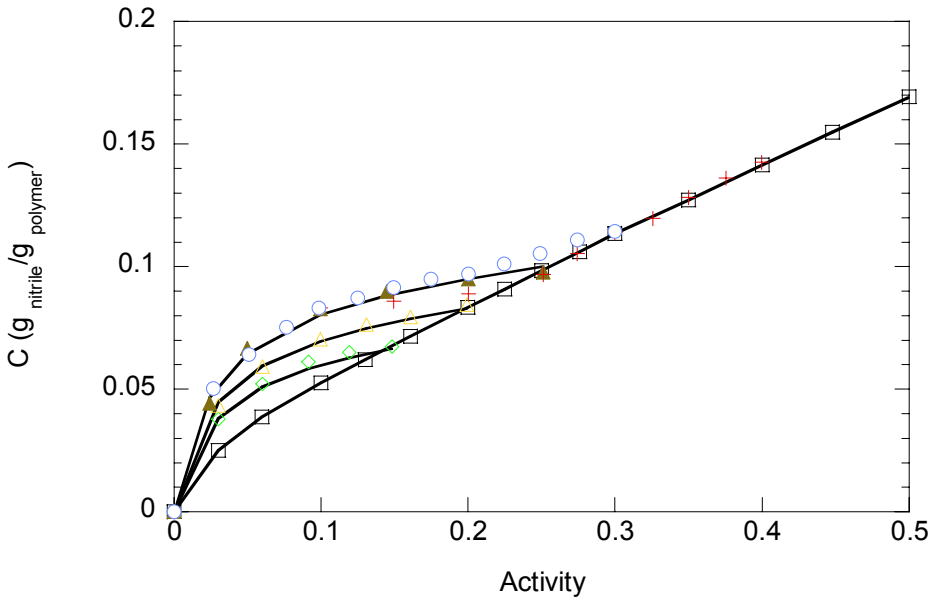

Figure 4.3 Initial acetonitrile sorption and desorption after conditioning activities of 0.15, 0.20, 0.25, 0.30 and 0.40. The squares are the sorption data, and the diamonds, triangles, stars, circles and crosses are the desorption data from activities 0.15, 0.20 0.25, 0.3 and 0.4, respectively. The solid lines are the dual mode model fits.

The desorption experiments conducted at conditioning activities of 0.30 and 0.40, which were discussed in Chapter 3, are also plotted in Figure 4.3 for comparison. The fact that the desorption data starting from activity 0.25 follows the same isotherm as those starting from 0.3 and 0.4, strongly supporta a penetrant-induced glass transition at activity 0.25 or $C_g = 0.0977 \frac{g_{nitrile}}{g_{polymer}}$.

4.4.4 Dual Mode Transport Model with Local Equilibrium Relaxation for Desorption Kinetics Using the Desorption Isotherms

The dual mode desorption parameters, k_D, C_H', and b, for activity 0.2, were combined with the diffusion coefficient, D_D = 6.38 x 10^{-10} cm^2/s, and hole-emptying rate constant, k_r = 4.85 x 10^{-3} s^{-1}, from sorption to predict the desorption FTIR-ATR data, as shown in Figure 4.4(a). The predictions show obvious disagreements with the experimental data. Since there is a redistribution of C_D and C_H populations between sorption and desorption, it is reasonable to assume that the local chain mobility is different between sorption and desorption, resulting in different values for k_r and D_D. To examine the results of this assumption, k_r and D_D were treated as adjustable parameters to fit the desorption FTIR-ATR absorbance data coupled with the dual mode desorption parameters. The result is plotted in Figure 4.4(b) at activity 0.25. The model captures the data very well. From triplicate experiments at activity 0.2, the mean value of D_D and k_r were determined to be 6.53(±1.01) x 10^{-9} cm^2/s and 5.46(±0.18) x 10^{-4} s^{-1}, respectively.

To test the robustness of the model and its physical interpretation, the rate constants for hole-filling and emptying were assumed to be independent of activity. Fixing the value of k_r at 5.46 x 10^{-4} s^{-1}, FTIR-ATR data for desorption diffusion at activities 0.06, 0.1, 0.15 and 0.25 were fit with D_D as the only adjustable parameter. Representative fits for each of these activities are shown in Figures 4.5 to 4.8 and the mean values of D_D are listed in Table 4.3.

Table 4.3 Diffusion coefficients obtained from fitting desorption FTIR-ATR absorbance data using dual mode transport model with local equilibrium relaxation and the desorption isotherms.

Activity	$D_D \times 10^9\ cm^2/s$
0.06	0.78 ± 0.039
0.10	1.56 ± 0.25
0.15	3.24 ± 0.06
0.20	6.53 ± 1.01
0.25	13.1 ± 2.05

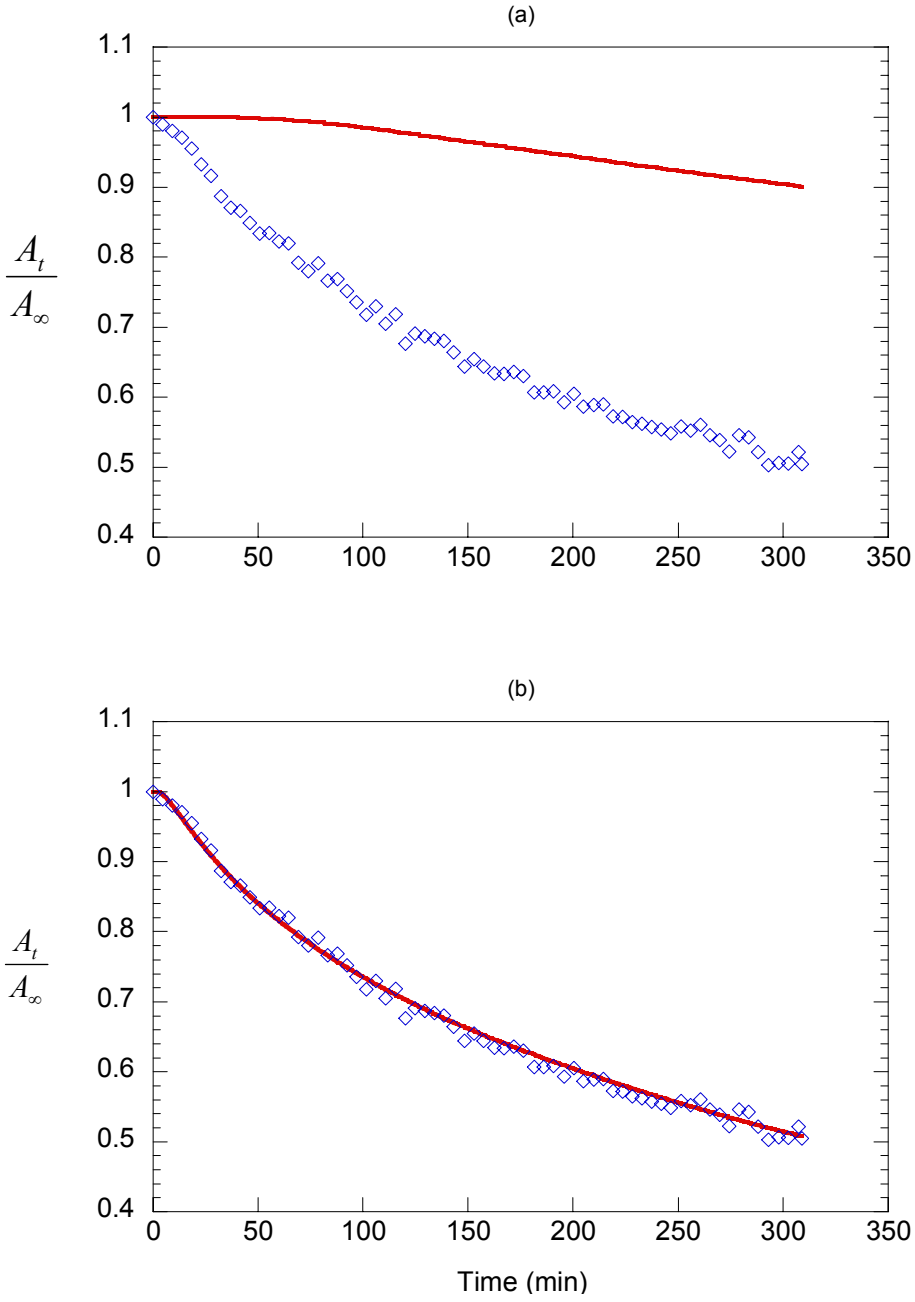

Figure 4.4 Desorption FTIR-ATR absorbance data at activity of 0.20 with (a) prediction with desorption dual mode parameter and sorption diffusion coefficient and hole-emptying constant (b) fit with diffusion coefficient and hole-emptying constant adjustable. L=44.0 μm and T = 25ºC.

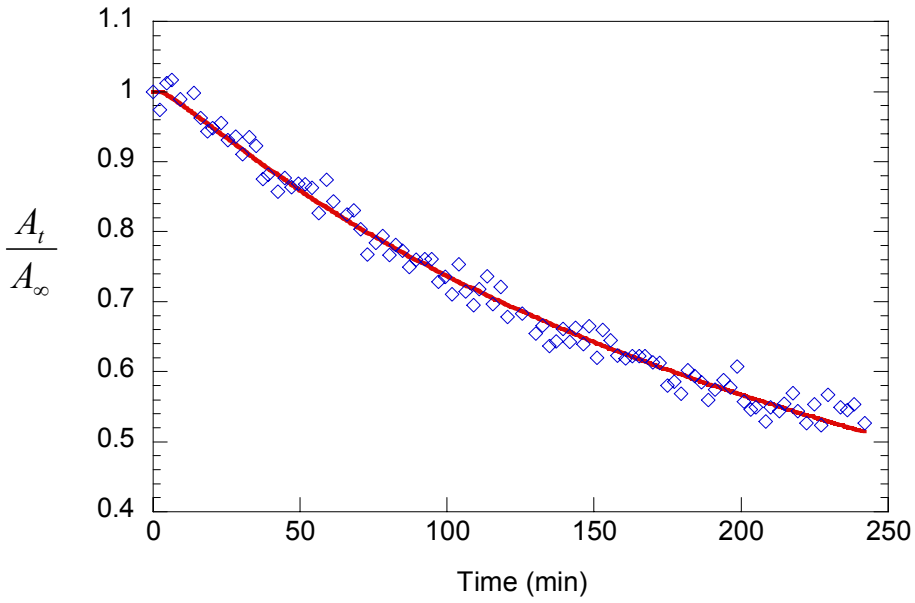

Figure 4.5 Desorption FTIR-ATR absorbance data with fit curve at activity 0.06, L=15.2 μm and T = 25ºC.

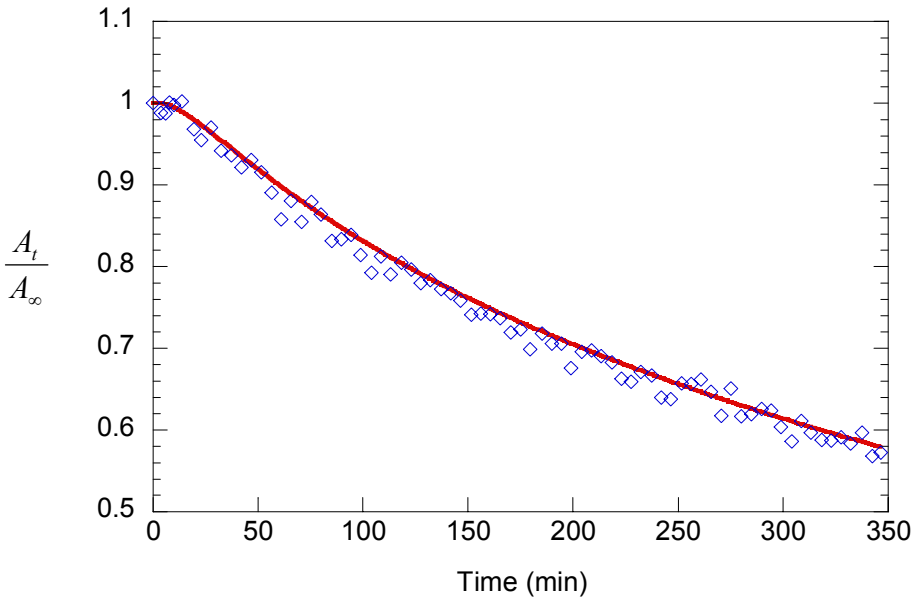

Figure 4.6 Desorption FTIR-ATR absorbance data with fit curve at activity 0.10, L=29.8 μm and T = 25ºC.

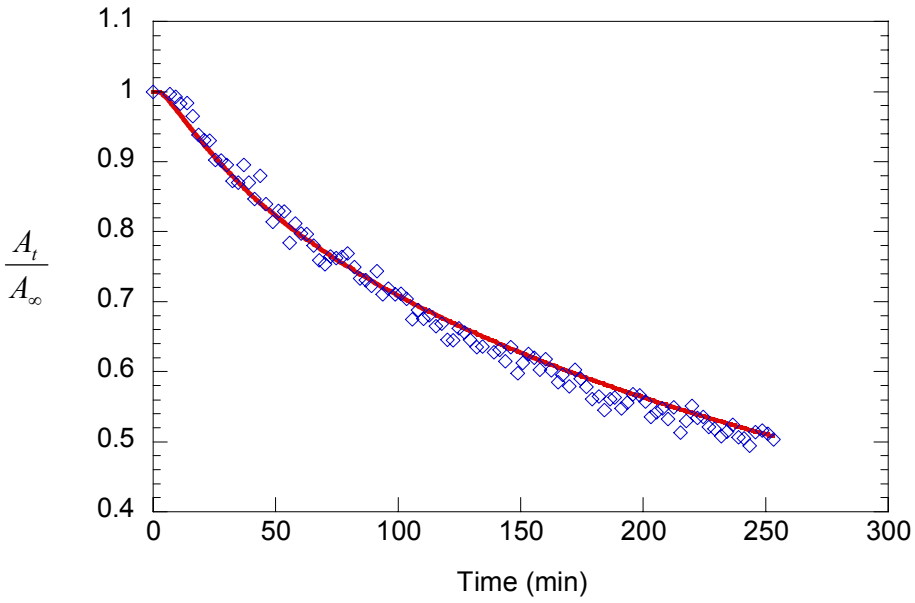

Figure 4.7 Desorption FTIR-ATR absorbance data with fit curve at activity 0.15, L=29.2 μm and T = 25ºC.

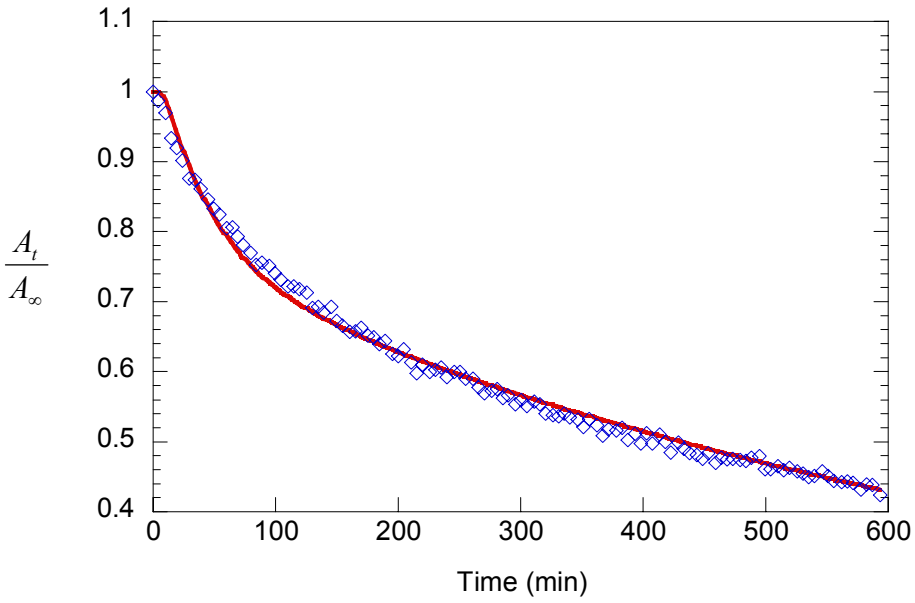

Figure 4.8 Desorption FTIR-ATR absorbance data with fit curve at activity 0.25, L=60.8 μm and T = 25ºC.

4.5 Conclusion

The desorption isotherms further support the finding in Chapter 3 that cellulose acetate undergoes a penetrant-induced glass transition at higher activities. The glass transition concentration is $C_g = 0.0977 \frac{g_{nitrile}}{g_{polymer}}$.

The dual mode model was not able to interpret the desorption FTIR-ATR data utilizing the parameters obtained from the sorption isotherm. Parameters for dual mode desorption were obtained from the hysteretic desorption isotherms, and these parameters were used with the dual mode transport model with local equilibrium relaxation to successfully model the FTIR-ATR desorption data. The desorption Henry's law constant, k_D, is much smaller than that for sorption, while the hole saturation constant, C_H', is much larger than that for sorption. These results indicate that the sorption of acetonitrile has a conditioning effect on cellulose acetate, which causes a large portion of the Henry's law population to behave as part of the Langmuir population during desorption. In this process, additional holes are created by that portion of the Henry's law population. The new holes created by penetrant molecules pushing apart the polymer chains upon sorption, generate low energy sites, compared to the pre-existing ones, resulting in a higher energy barrier for the molecule to leave. This leads to a hole-emptying rate constant for desorption, 5.46 x 10^{-4} s^{-1} that is one order of magnitude lower than that for sorption, 4.85 x 10^{-3} s^{-1}.

Conversely, the desorption diffusion coefficients are considerably higher than those from sorption at the same activity, even higher than those obtained from the moving boundary model in the rubbery region, a physically unrealistic outcome. If the Langmuir population is considered to be totally immobilized and the Henry's law population is the only species allowed to diffuse, then the redistribution of species in favor of the Langmuir population results in a small driving force for diffusion, as shown in Figure 4.9 at activity 0.25. As a result, mathematically, a high value for the diffusion coefficient is needed to capture the desorption data.

The dual mode transport model as presented in this work is limited in its ability to describe desorption with physically realistic parameters. This may be caused by the nature of the dual mode sorption framework in which the number of unoccupied holes is fixed throughout both the sorption and the desorption processes. In this framework, there is a discontinuity in the concentration of the mobile species at the glass transition. In the next chapter, a modified dual mode model is proposed to remove this constraint, allowing the number of unoccupied holes to disappear as concentration increases so that there are none at the glass transition.

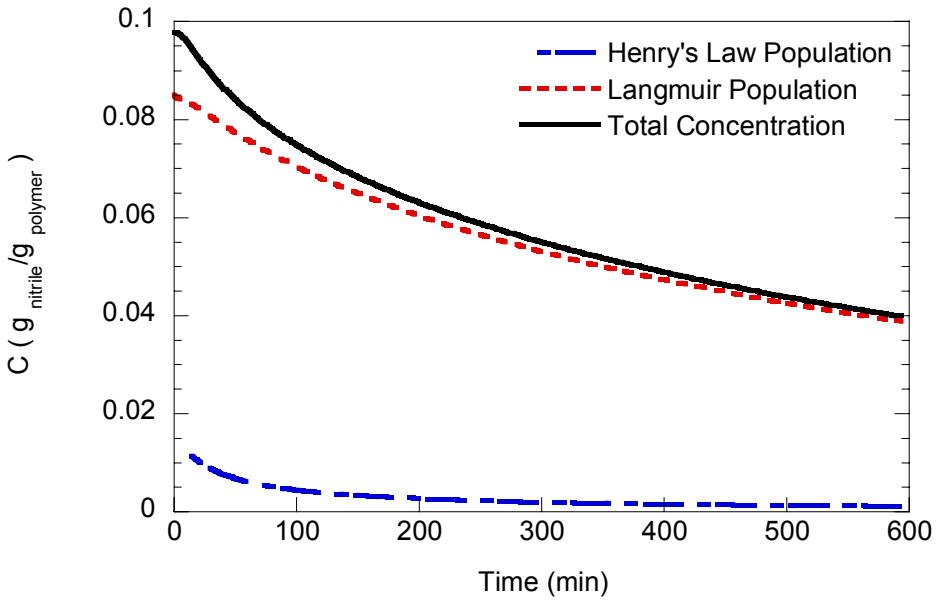

Figure 4.9 Penetrant concentrations as a function of time in desorption at activity 0.25, L = 60.8 μm and T = 25ºC.

Chapter 5

Modification of The Dual Mode Transport Model to Account for Plasticization

5.1 Introduction

In this thesis thus far, the interpretation of the observed diffusion behavior was based on a transport model that incorporated the well-accepted dual mode sorption model with the assumption of local equilibrium relaxation and total immobilization of the hole population. Although this model can fit the FTIR-ATR sorption and desorption data very well, leading to a reasonable description of the diffusion mechanism, its limitation was suggested in the last chapter with respect to the magnitude of desorption diffusion coefficients. In the framework of the classical dual mode sorption model, the number of holes is fixed. Alternatively, it is reasonable to consider that the glassy polymer may be plasticized upon the sorption of penetrant molecules. Plasticization increases local chain mobility causing holes to "relax" and thus be removed as a potential sorption site. In this chapter, the dual mode sorption model is modified to take into account plasticization induced by penetrant molecules, as originally proposed by Kamiya and coworkers. Consequently, the dual mode transport model with local equilibrium relaxation was reconstructed with Kamiya's model. The FTIR-ATR absorbance data for acetonitrile diffusion in cellulose acetate for both sorption and desorption were studied using the modified dual mode transport model.

5.2 Experimental Measurement of Film Elongation

In addition to the experiments already described, elongation measurements of the cellulose acetate film upon sorption of acetonitrile were conducted. The only difference in sample preparation for these measurements is that the films were prepared on a glass slide (7.5 cm x 2 cm), and after removal from the slide, were cut into a strip (3 cm x 0.5cm). The polymer strip was hung directly on the quartz spring in the sorption chamber with a weight of 0.10 g fixed at the lower end to prevent the film from curling. The sorption of acetonitrile took place in the glass chamber connected to the vapor generation system, and the elongation was determined from the film strip extension using a cathetometer, as a function of time, until equilibrium extension was reached. The elongation results are used to determine a parameter in Kamiya's sorption model.

5.3 Transport Model

5.3.1 Modification of the Dual Mode Sorption Model

Although the dual mode sorption model, which was used in the previous chapters, is the most accepted model to describe the sorption of gases or vapors in glassy polymers, there are some sorption behaviors that cannot be explained by this model. Berens [141] studied vinyl chloride monomer in glassy ploy(vinyl chloride) over a wide range of relative pressure; Stannett, *et al.* (1980) [147] published a study on the sorption of water vapor in glassy polyacrylonitrile. The sorption isotherms in both studies over a wide range of pressures were found to have a sigmoidal form, which could not be

described by the classical dual mode model. Mauze and Stern [32,33, 148] re-examined these two systems and proposed a modification of the classical dual mode model by taking into account the plasticization effect induced by penetrant molecules in the dissolved mode. They assumed for these systems that C_D is a much stronger function of penetrant concentration, that is:

$$C_D = S(C)a = \left[k_D \exp(\sigma C)\right]a \tag{5.1}$$

where $S(C) = \left[k_D \exp(\sigma C)\right]$ is a solubility coefficient, σ is a parameter characterizing the concentration dependence of *S(C),* and k_D is the Henry's law parameter. By substituting Equation (5.1) into the classical dual mode sorption equation, they obtained the following expression to interpret the sigmoidal sorption isotherms:

$$C = \left[k_D \exp(\sigma C)\right]a + C_H^{'} \frac{ba}{1+ba} \tag{5.2}$$

However, in this expression, the effect of plasticization on $C_H^{'}$ is not considered. Since plasticization should decrease the pre-existing free volume in a glassy polymer, as does an increase temperature, the change in $C_H^{'}$ due to plasticization should be considered. Pace and Datyner [149] pointed out the possibility that a decrease of $C_H^{'}$ is caused by the plasticizing effect of sorbed gases or vapors. They assumed that the presence of a significant quantity of the Henry's law population might plasticize the polymer to allow relaxation of some of the initial pre-existing free volume over the experimental time scale. This possibility was also suggested by Petropoulos. [150] Kamiya and coworkers found similar results in a broad variety of studies, [34,151-158] such as high pressure CO_2 in poly(vinyl benzoate), polysulfone, polycarbonate, LDPE, poly(vinyl butyral), poly(ethylene terephthalate) and poly(ethyl methacrylate);

high pressure Ar in poly(vinyl benzoate) and polycarbonate; N_2 in poly(vinyl benzoate), LDPE and polysulfone; CH_4 in polysulfone; C_2H_6 in polysulfone and poly(ethyl methacrylate); and C_2H_4 and C_3H_8 in poly(ethyl methacrylate). They concluded that, even below the glass transition temperature, T_g, the transition from a glassy to rubbery state could occur by an increase in penetrant concentration. The concentration at the transition point where the pre-existing free volume would disappear was designated as the glass transition concentration, C_g, at a given temperature.

According to Kamiya and coworkers, the amount of pre-existing (hole) free volume in a unit volume of a penetrant-polymer system can be written as

$$V_H = \Delta\alpha_T \left[\beta C_g - (T_{g0} - T_g)\right] \tag{5.3}$$

where $\Delta\alpha_T$ is the difference between the cubic coefficients of thermal expansion for the rubbery and glassy states, β is a proportionality constant between the temperature and the concentration at the glass transition of the penetrant-polymer system and T_{g0} is the glass transition temperature of the pure polymer. The glass transition temperature as a function of penetrant concentration decreases linearly with increasing concentration. Hence the following expression is obtained:

$$T_g = T_{g0} - \beta C^* \tag{5.4}$$

where C^* is the effective concentration of sorbed penetrant, given by:

$$C^* = C_D + fC_H \qquad 0 \le f \le 1 \tag{5.5}$$

where f is the ratio of the plasticizing ability of the Langmuir population to that of the Henry's law population.

The relationship between the hole saturation constant C_H' and the amount of pre-existing free volume was given by Koros and Paul: [159]

$$C_H' = \gamma V_H \tag{5.6}$$

where γ is a constant related to the molar volume of sorbed penetrant.

Substituting Equations (5.3) and (5.5) into Equation (5.6), the hole saturation constant can be expressed as:

$$C_H' = C_{H0}'(1 - C^*/C_g) \tag{5.7}$$

where C_{H0}' is the hole saturation constant at C^*=0.

Substituting Equation (5.7) into Equation (5.2) yields the following equation for the sorption isotherm with a term accounting of the plasticization of polymer induced by the penetrant:

$$C = \left[k_D \exp(\sigma C^*)\right]a + C_{H0}' \frac{ba(1 - C^*/C_g)}{1 + ba} \tag{5.8}$$

where C^* replaces C in the first term, because in the glassy state the plasticization of polymer by penetrant should be described by the effective concentration defined in Equation (5.5).

In the above extension of the dual mode sorption model, the hole affinity constant b is assumed to be a constant at a given temperature. This is based on the idea that plasticization induced by penetrant molecules can cause the number of Langmuir sorption sites to decrease without affecting the interaction between the penetrant and the sorption sites. The possibility of b being constant with temperature was also suggested experimentally by Chan and Paul. [160]

5.3.2 Modification of The Dual Mode Transport Model

The dual mode transport model can be modified to include Kamiya's sorption model by using Equation (5.7) for $C_H^{'}$:

$$\frac{\partial C_D}{\partial t} = D_D \frac{\partial^2 C_D}{\partial z^2} - k_f C_D \left[C_{H0}^{'}(1 - \frac{C_D + fC_H}{C_g}) - C_H \right] + k_r C_H \tag{5.9}$$

$$\frac{\partial C_H}{\partial t} = FD_D \frac{\partial^2 C_H}{\partial z^2} + k_f C_D \left[C_{H0}^{'}(1 - \frac{C_D + fC_H}{C_g}) - C_H \right] - k_r C_H \tag{5.10}$$

The initial and boundary conditions for sorption are:

t = 0 (*all* z) $\quad C_D = 0\,,\ C_H = 0$

z = 0 (t > 0) $\quad \frac{\partial C_D}{\partial z} = 0\,,\ \frac{\partial C_H}{\partial z} = 0$

$z = L$ (t > 0) $\quad C_H = C_{T_L} - C_D\,,\ C_D = k_D a$

The initial and boundary conditions for desorption are:

t = 0 (*all* z) $\quad C_H = C_{T_L} - C_D\,,\ C_D = k_D a$

z = 0 (t > 0) $\quad \frac{\partial C_D}{\partial z} = 0\,,\ \frac{\partial C_H}{\partial z} = 0$

$z = L$ (t > 0) $\quad C_D = 0\,,\ C_H = 0$

where C_{T_L} is the total concentration at z=L.

At equilibrium:

$$k_f C_D (C_H^{'} - C_H) = k_r C_H \tag{5.11}$$

Using Kamiya's model for $C_H^{'}$, Equation (5.11) becomes:

$$k_f C_D \left[C'_{H0}(1 - \frac{C^*}{C_g}) - C_H \right] = k_r C_H \tag{5.12}$$

From Equation (5.12):

$$C_H = \frac{k_f C_D C'_{H0}(1 - C^*/C_g)}{k_r + k_f k_D a} \tag{5.13}$$

Also, from Equation (5.8):

$$C_H = C'_{H0} \frac{ba(1 - C^*/C_g)}{1 + ba} \tag{5.14}$$

From Equations (5.13) and (5.14), one can obtain the following relationship, which is identical to that obtained in the classical dual mode sorption model:

$$\frac{b}{k_D} = \frac{k_f}{k_r} \tag{5.15}$$

5.4 Results and Discussion

5.4.1 Evaluation of Kamiya's Model Parameters for Sorption

From Chapter 2, it can be seen that the sorption isotherm is linear at high activity, hence σ, the exponential constant in Equation (5.8) is zero. Substituting $\sigma = 0$ and Equation (5.5) into Equation (5.8), gives:

$$C = \frac{k_D a + \frac{C'_{H0} ba}{1 + ba}\left[1 - \frac{k_D a(1 - f)}{C_g}\right]}{1 + \frac{C'_{H0} ba}{1 + ba}\frac{f}{C_g}} \tag{5.16}$$

There are four parameters in Equation (5.16) to evaluate, k_D, f, b and C'_{H0}. In this equation, k_D has been shown to be not sensitive to the value of f. [151] This means that

the value of k_D can be obtained by fitting Equation (5.16) taking k_D, b and C'_{H0} as three adjustable parameters with an arbitrary value of f from 0 to 1. To test the insensitivity of k_D in the model to f, five different values of f were used to fit Equation (5.16) with a least-squares analysis. As expected, k_D was not sensitive to the value of f (see Table 5.1).

Table 5.1 Values of k_D using different values of f in Equation (5.16)

f	0	0.2	0.4	0.6	0.8	1.0
k_D ($g_{nitrile}/g_{polymer}$)	0.3769	0.3759	0.3764	0.3764	0.3762	0.3754

From Table 5.1, the mean value of k_D was obtained for later fitting purposes:

$k_D = 0.3762 \pm 0.0004\, g_{nitrile}/g_{polymer}$.

The value of f was then evaluated from the relation between dilation (elongation) and concentration. The elongation of the polymer film during sorption can be written as:[151]

$$l_s = \left[\tau_G \beta \alpha_{T_G} / 3(1 - \tau_G \beta \alpha_{T_G} C_g)\right] C^* \qquad (5.17)$$

where τ_G is the coefficient correlating sorptive dilation with the concentration at the glass transition, β is the proportionality constant ($\beta = -dT_g/dC_g$), and α_{T_G} is the thermal expansion coefficient of the pure polymer in the glassy state.

When $\sigma C^* << 1$, one may simplify the effective concentration as:

$$C^* = \left[(1-f)k_D a + fC\right] / \left[1-(1-f)\sigma k_D a\right] \tag{5.18}$$

Substituting Equation (5.18) into Equation (5.17) with $\sigma=0$, one can obtain the following relationship between dilation and concentration:

$$l_s = \left[\tau_G \beta \alpha_G / 3(1-\tau_G \beta \alpha_G C_g)\right] \cdot \left[(1-f)k_D a + fC\right] \tag{5.19}$$

Equation (5.19) must hold at the glass transition regardless of the value of f, and hence the constant factor, $\left[\tau_G \beta \alpha_G / 3(1-\tau_G \beta \alpha_G C_g)\right]$, in the equation is the slope of the line connecting the coordinate origin and the glass transition concentration on the l_s versus C curve. The sorptive dilation experiment was conducted for acetonitrile in cellulose acetate as described above, and the film elongation was plotted as a function of total acetonitrile concentration (Figure 5.1). In this figure, the diamonds are the elongation data. As discussed in the previous chapters, the glass transition concentration is $C_g = 0.0977 \frac{g_{nitrile}}{g_{polymer}}$. The slope of the line between the origin and this point, which is shown in Figure 5.1 as the dotted line, is

$$\left[\tau_G \beta \alpha_G / 3(1-\tau_G \beta \alpha_G C_g)\right] = 0.2972 \frac{cm \cdot g_{polymer}}{g_{nitrile}}.$$

Hence, f is the only unknown parameter remaining in Equation (5.19), and it can be obtained by a least-squares analysis. The best fit value of f was demonstrated to be 0. The dilation curve for f=0 is plotted in Figure 5.1 as the solid line. As a comparison, the simulated dilation curves for f = 0.5 and f = 1 are plotted in Figure 5.1.

Using the values of k_D and f, Langmuir parameters b and C'_{H0} were determined by a least-squares regression analysis of the sorption isotherm using Equation (5.16):

$$C'_{H0} = 0.0259 \frac{g_{nitrile}}{g_{polymer}} \text{ and } b = 40.1$$

The fitting curve is plotted alongside the experimental sorption isotherm in Figure 5.2.

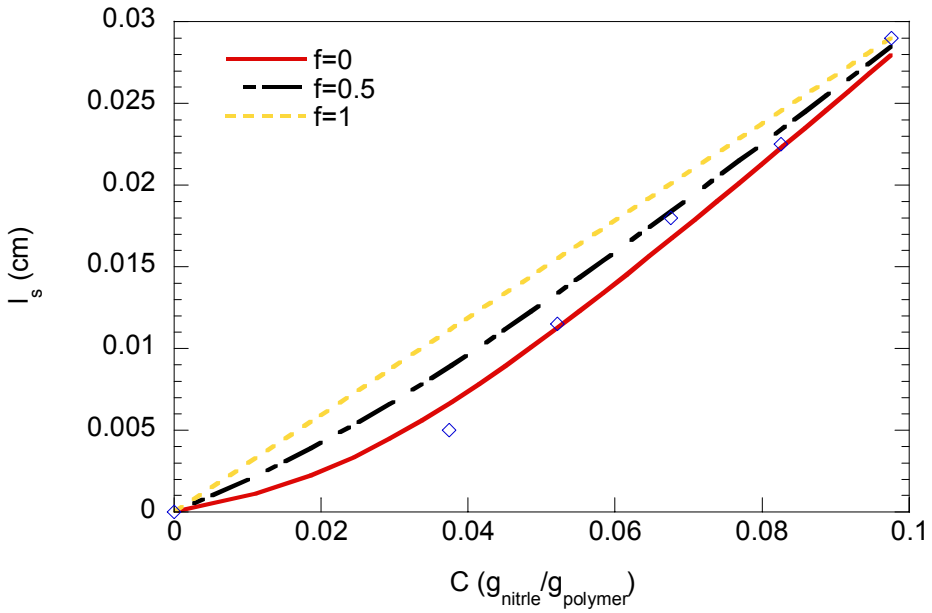

Figure 5.1 Dilation (elongation) of a cellulose acetate film during the sorption of acetonitrile as a function of concentration.

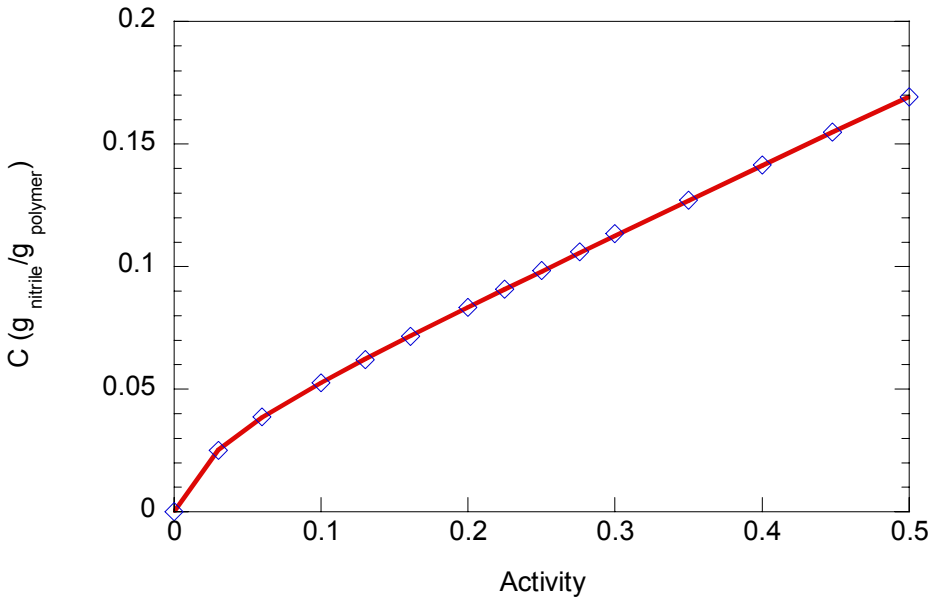

Figure 5.2 Sorption isotherm for acetonitrile in cellulose acetate using Kamiya's model.

5.4.2 Application of Modified Dual Mode Transport Model to Sorption Kinetics

FTIR-ATR absorbance data were analyzed using the modified dual mode transport model, Equations (5.9) and (5.10). The Henry's law population was assumed to be immobile (F=0), because preliminary results using F as an adjustable parameter resulted in values near zero for the best fit, as mentioned in Chapter 2. Also, from Equation (5.15), the ratio of the hole-filling rate constant, k_f, to the hole-emptying rate constant, k_r, is equal to that of b to k_D, which was obtained from the sorption isotherm. Hence, there are only two adjustable parameters in the modified dual mode transport model, the diffusion coefficient, D_D, and hole-emptying rate constant, k_r. The result of fitting FTIR-ATR absorbance data with this model at activity 0.2 is shown in Figure 5.3. The model captures the data very well. From triplicate experiments at activity 0.2, the mean values of D_D and k_r were determined to be $(4.76 \pm 0.14) \times 10^{-10}\ cm^2/s$ and $(4.74 \pm 0.11) \times 10^{-3}\ s^{-1}$, respectively.

As was done in Chapter 2 to test the robustness of the model and the physical interpretation of its parameters, the rate constant for hole-emptying was assumed to be independent of activity. Fixing the value of k_r at $4.74 \times 10^{-3}\ s^{-1}$, FTIR-ATR data for diffusion at activities of 0.06, 0.1, 0.15, 0.25, 0.3, 0.4 and 0.5 were fitted with D_D as the only adjustable parameter. Representative fits for each of these activities is shown in Figures 5.4 to 5.10, and the mean values of D_D are listed in Table 5.2. From Figures 5.9 and 5.10, it can be seen that the modified dual mode transport model breaks down at activities of 0.4 and 0.5, just as in Chapter 2. This means that this model is no better than the transport model based on classical dual mode

sorption, with respect to the interpretation of diffusion in a glassy polymer undergoing a glass transition induced by penetrant molecules. As was the case with the classical model, a moving boundary model will be necessary to capture the behavior at activities 0.4 and 0.5.

The Henry's law constant, k_D, hole saturation constant, C_H', (C_{H0}' for Kamiya's model), Langmuir affinity constant, b, and hole-emptying rate constant, k_r from both dual mode models are listed in Table 5.3. Also, the diffusion coefficients from both models for the glassy state ($a \leq 0.3$) are plotted in Figure 5.11. From Table 5.3 and Figure 5.11, it can be seen that the transport parameters are very similar, as is the Langmuir capacity of the pure polymer. The primary difference is in k_D, which affects the distribution of the penetrant molecules between the two populations. In Kamiya's model, the Langmuir concentration goes through a maximum and eventually becomes zero at the glass transition concentration. Conversely, this concentration in the classical dual mode model asymptotically approaches the saturation value reflected by C_H'. The total penetrant concentration, C_D and C_H in sorption from both models are plotted in Figure 5.12 as a function of activity.

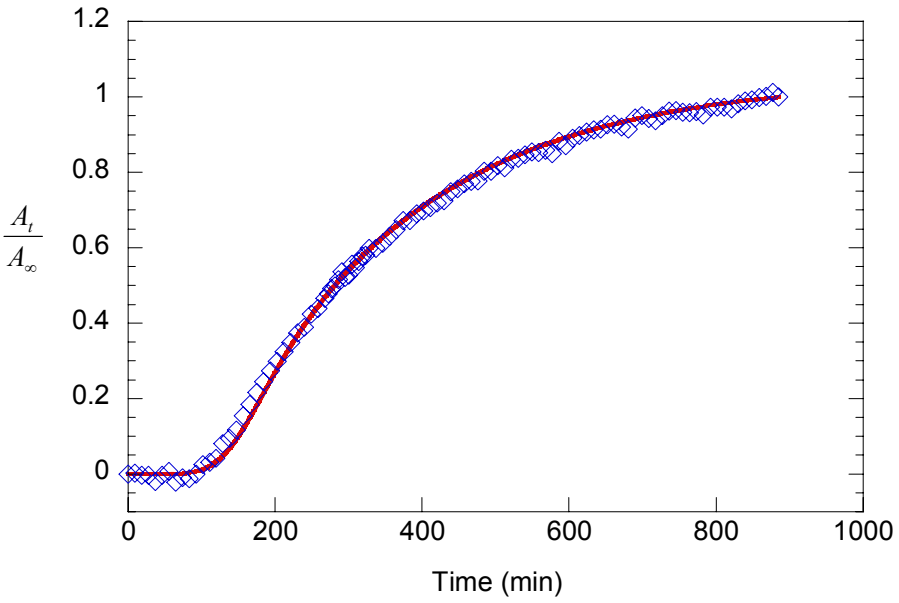

Figure 5.3 FTIR-ATR absorbance data of acetonitrile in CA at activity 0.2 with the fit using the dual mode transport model with local equilibrium relaxation and Kamiya's model. L = 49.2 μm and T = 25^{o} C.

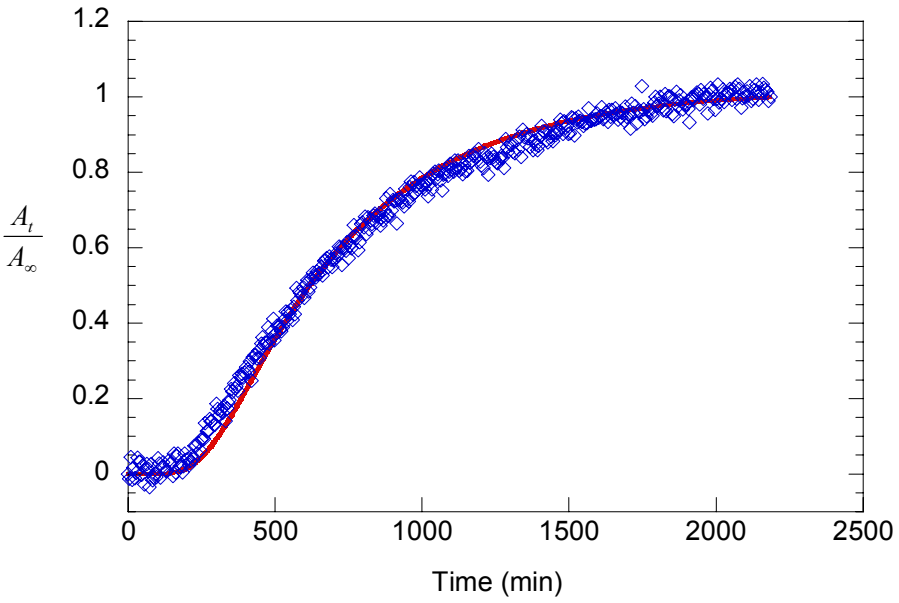

Figure 5.4 FTIR-ATR absorbance data of acetonitrile in CA at activity 0.06 with the fit using the dual mode transport model with local equilibrium relaxation and Kamiya's model. L = 30.8 μm and T = 25^{o} C.

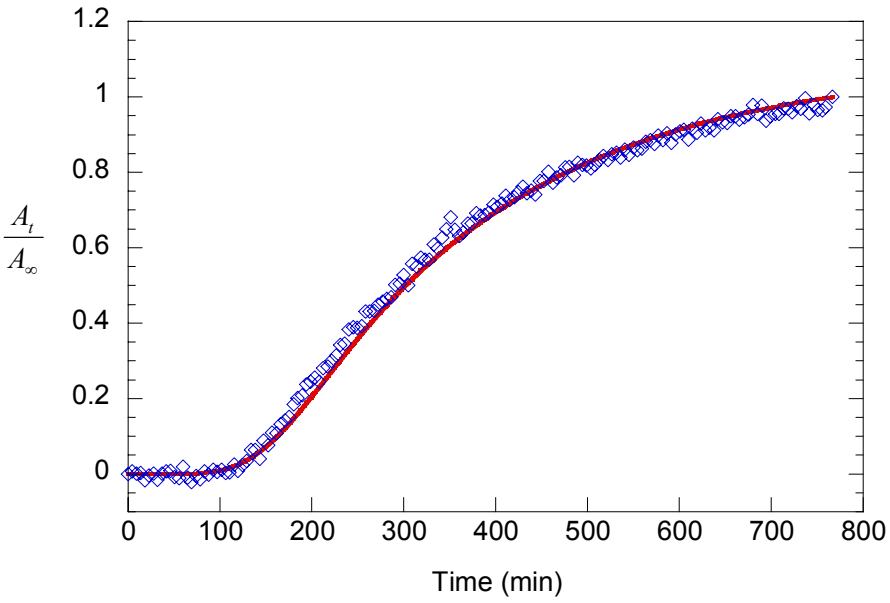

Figure 5.5 FTIR-ATR absorbance data of acetonitrile in CA at activity 0.1 with the fit using the dual mode transport model with local equilibrium relaxation and Kamiya's model. L = 29.8 μm and T = 25^{o} C.

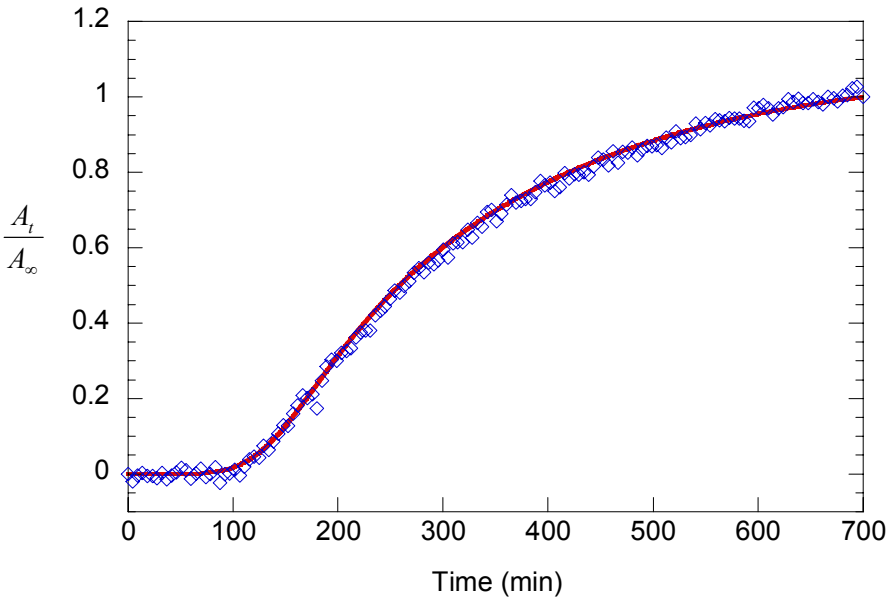

Figure 5.6 FTIR-ATR absorbance data of acetonitrile in CA at activity 0.15 with the fit using the dual mode transport model with local equilibrium relaxation and Kamiya's model. L = 38.4 μm and T = 25^{o} C.

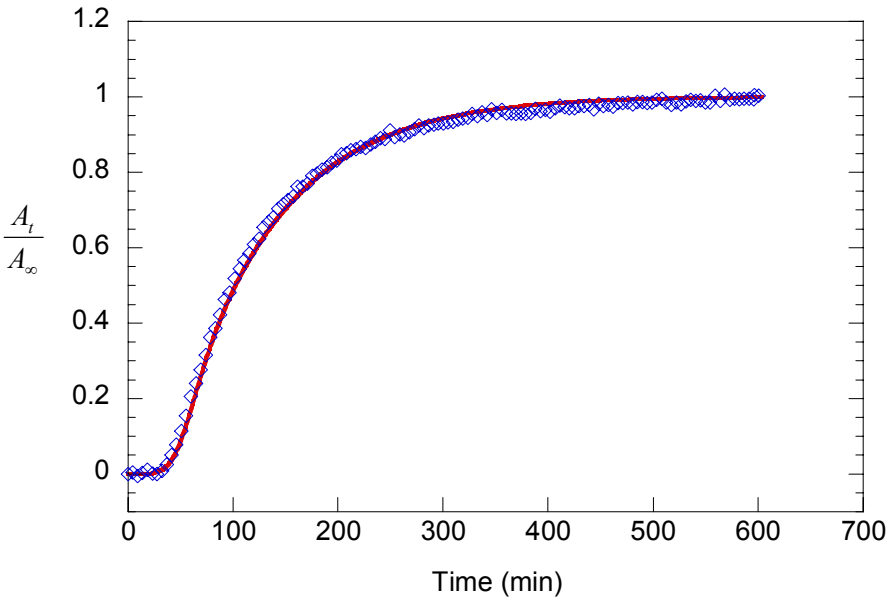

Figure 5.7 FTIR-ATR absorbance data of acetonitrile in CA at activity 0.25 with the fit using the dual mode transport model with local equilibrium relaxation and Kamiya's model. L = 30.4 μm and T = 25^{o}C.

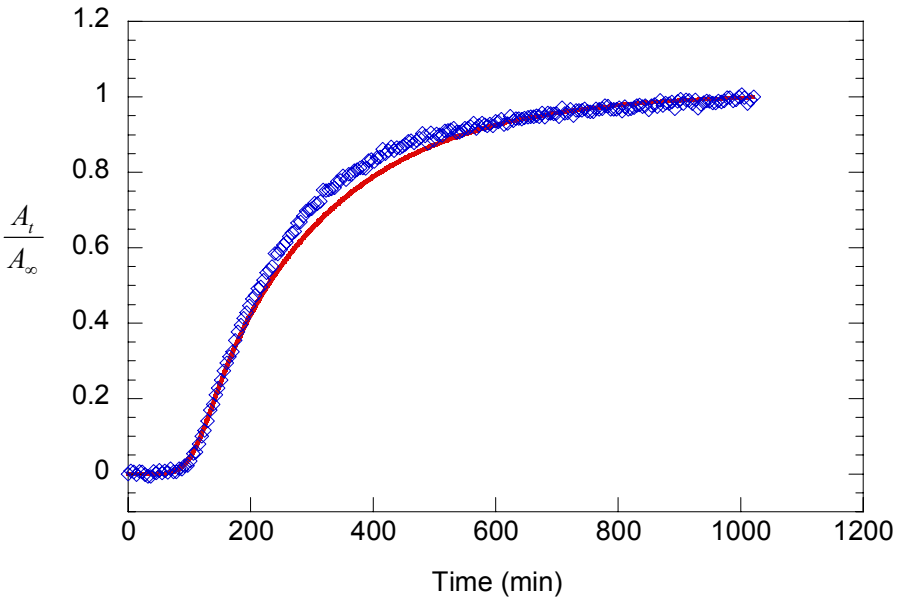

Figure 5.8 FTIR-ATR absorbance data of acetonitrile in CA at activity 0.3 with the fit using the dual mode transport model with local equilibrium relaxation and Kamiya's model. L = 49.4 μm and T = 25^{o}C.

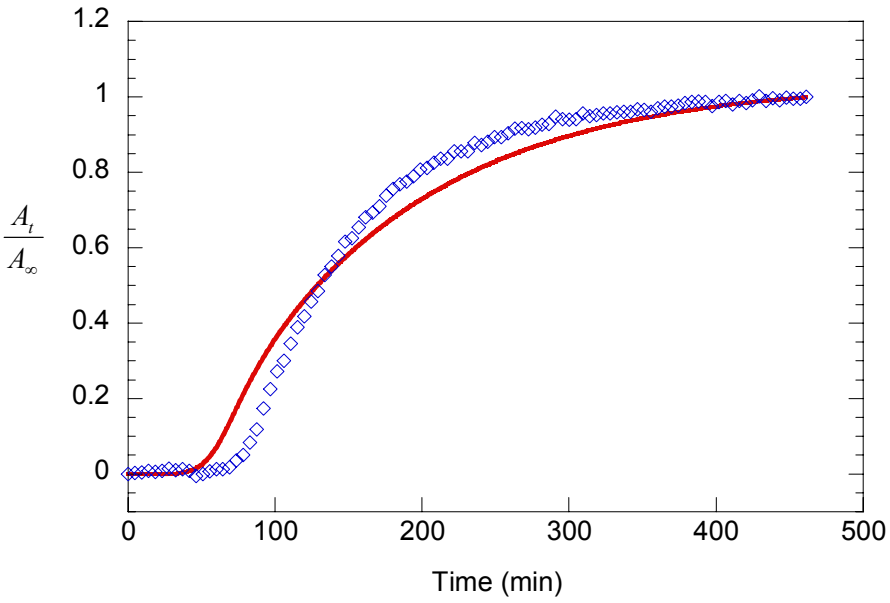

Figure 5.9 FTIR-ATR absorbance data of acetonitrile in CA at activity 0.4 with the fit using the dual mode transport model with local equilibrium relaxation and Kamiya's model. L = 59.8 μm and T = 25^{o} C.

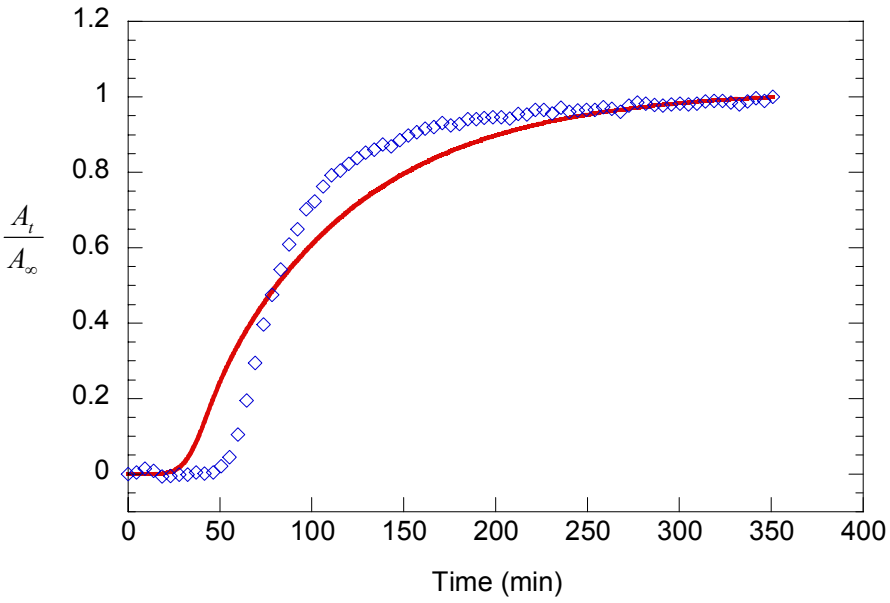

Figure 5.10 FTIR-ATR absorbance data of acetonitrile in CA at activity 0.5 with the fit using the dual mode transport model with local equilibrium relaxation and Kamiya's model. L = 76.2 μm and T = 25^{o} C.

Table 5.2 Diffusion coefficients for sorption of acetonitrile in cellulose acetate obtained by fitting the dual mode transport model with local equilibrium relaxation and Kamiya's sorption model.

Activity (N=3)	$D_D \times 10^{10}\ cm^2/s$
0.06	1.43 ± 0.07
0.10	2.20 ± 0.06
0.15	3.47 ± 0.20
0.20	4.76 ± 0.14
0.25	5.64 ± 0.47
0.30	6.30 ± 0.18
0.40	15.2 ± 1.10
0.50	36.9 ± 1.80

Table 5.3 Sorption parameters from Kamiya's model and classical dual mode model.

Parameters	k_D $(g_{nitrile}/g_{polymer})$	C_H' , C_{H0}' $(g_{nitrile}/g_{polymer})$	b	k_r (x 10^3 s^{-1})
Kamiya Model	0.376	0.026	40.1	4.74
Classical Dual Mode Model	0.282	0.030	38.1	4.85

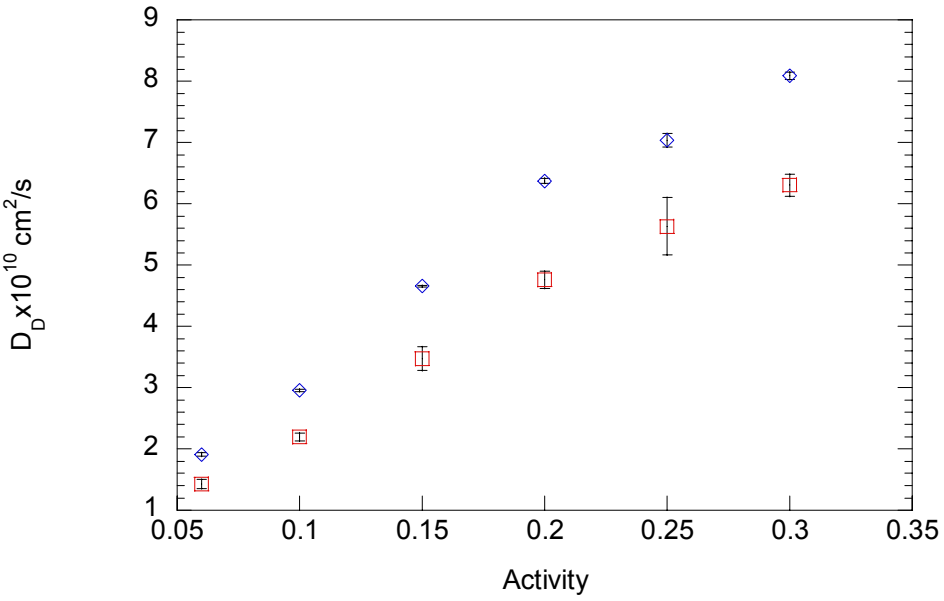

Figure 5.11 Diffusion coefficients for sorption form the classical dual mode transport model (diamonds) and the modified version (squares) as a function of activity.

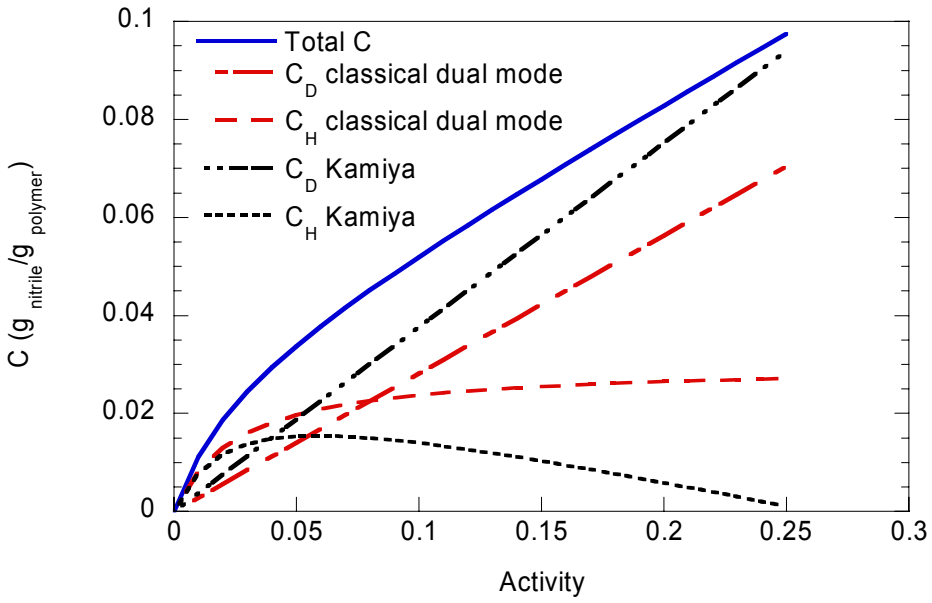

Figure 5.12 C_D and C_H distributions of the classical dual mode model and the Kamiya's model.

5.4.3 Mass Uptake Prediction Using the Modified Dual Mode Transport Model

As a further validation of the modified dual mode transport model, accounting for plasticization, the mass uptake was predicted from the parameters obtained from the FTIR-ATR data. First, the total concentration profile was calculated numerically and then, the concentration profile was integrated over the film thickness to obtain the mass uptake. The calculated mass uptakes using the mean values listed in Table 5.2 for D_D are plotted as a function of $\sqrt{t/L^2}$ alongside the actual mass uptake data at activities 0.1, 0.2 and 0.3, in Figures 5.13, 5.14 and 5.15, respectively. In these figures, the open diamonds are the experimental data and the solid lines are the prediction from the modified dual mode transport model. In general, the prediction is very good.

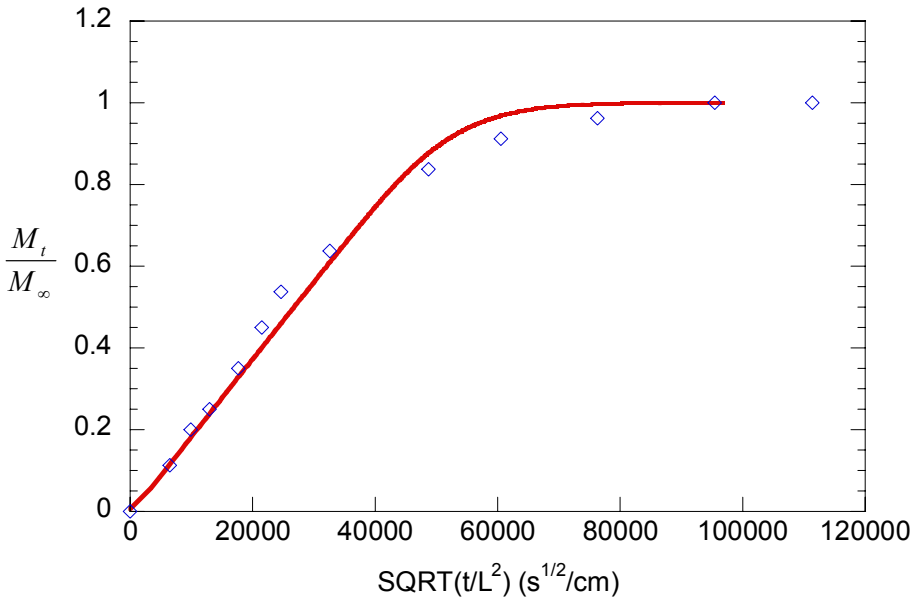

Figure 5.13 Mass uptake data at activity of 0.10 with prediction using modified dual mode transport model. L = 28.6 μm, T = 25° C.

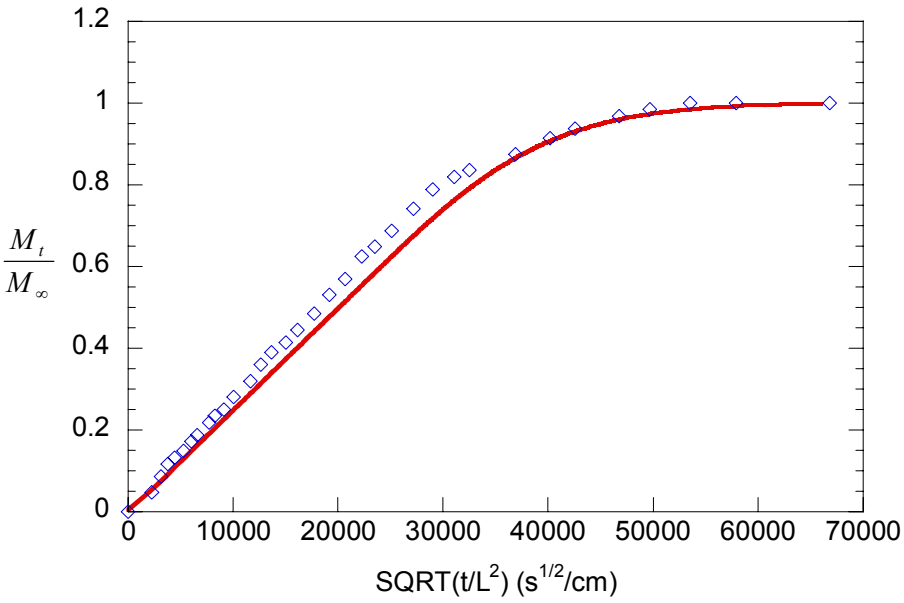

Figure 5.14 Mass uptake data at activity of 0.20 with prediction using modified dual mode transport model. L = 50.4 μm, T = 25° C.

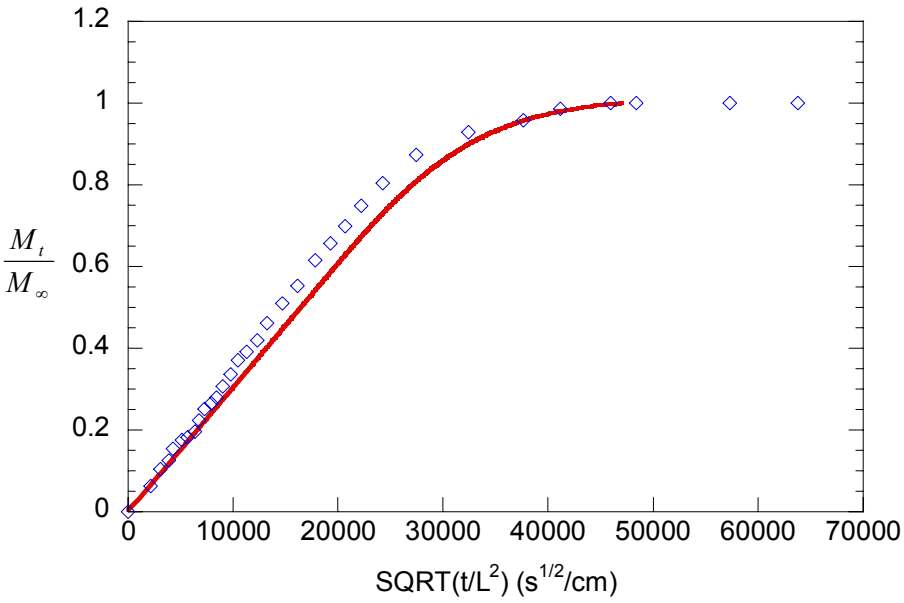

Figure 5.15 Mass uptake data at activity of 0.30 with prediction using modified dual mode transport model. L = 48.2 μm, T = 25^{o} C.

5.4.4 Application of Modified Dual Mode Transport Model to Desorption Kinetics

In order to apply the modified dual mode transport model to the FTIR-ATR desorption data, it was assumed that $f = 0$ on the basis that sorption and desorption were mechanistically similar. Equation (5.16) was then used to fit the desorption isotherms at activities 0.15, 0.2 and 0.25 to obtain values of k_D, C'_{H0} and b. For the sake of comparison, another three arbitrary f values, 0.25, 0.5 and 0.75, were picked to obtain desorption parameters. In fitting the desorption isotherms with arbitrary f values, b was expected to vary with f, since the Langmuir population can plasticize the polymer with a non-zero value of f. The fitting results are shown in Table 5.4, and the fitting curves are shown in Figure 5.16. At each activity, the value of k_D is independent of the f values, which is consistent with the sorption results.

The parameters in Table 5.4 were used with Equations (5.9) and (5.10) to fit the desorption FTIR-ATR absorbance data at activity 0.15. From triplicate experiments at activity 0.15, the mean values of D_D and k_r were determined to be (1.60±0) x 10^{-9} cm^2/s and (5.90±0.15) x 10^{-4} s^{-1}, respectively. Also, the values of D_D and k_r at each activity were found to be independent of f. As was done before, the rate constant for hole-emptying was assumed to be independent of activity. Hence, the value of k_r was fixed at 5.90 x 10^{-4} s^{-1}, and FTIR-ATR absorbance data for desorption at activities 0.2 and 0.25 were fitted with D_D as the only adjustable parameter. Representative fits for each of these activities are shown in Figures 5.17 to 5.19 and the mean values of D_D are listed in Table 5.5.

The diffusion coefficients for desorption from both transport models are plotted in Figure 5.20. From Figure 5.20, it can be seen that the desorption diffusion coefficients from the modified model are much lower than the corresponding diffusion coefficients from the original dual mode model and are physically more realistic. This observation suggests that the Kamiya model may be better for describing the desorption mechanism because it takes into account the plasticization effect induced by the penetrant.

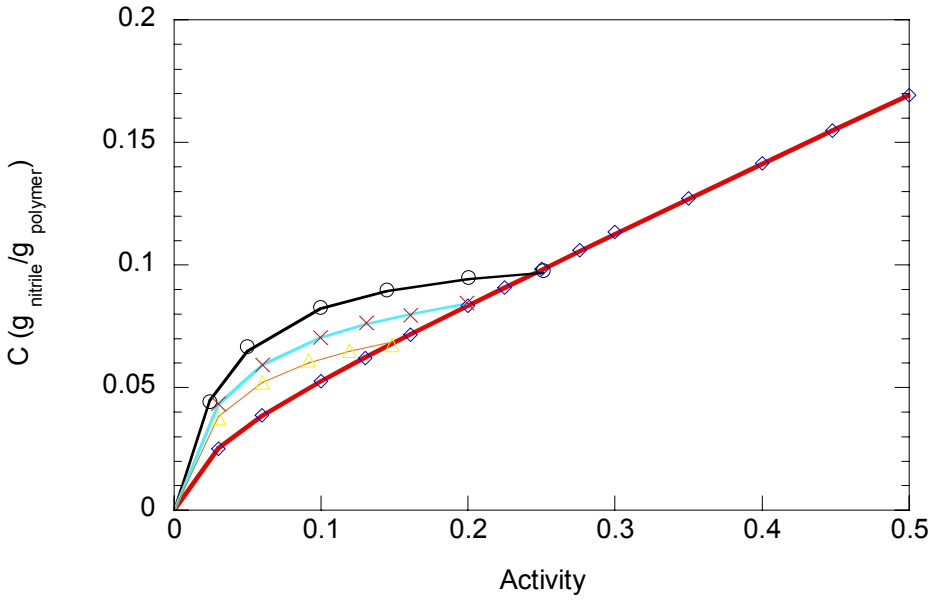

Figure 5.16 Desorption isotherms for acetonitrile from cellulose acetate using Kamiya's model. Circles for activity 0.25, crosses for activity 0.2 and triangles for activity 0.15.

Table 5.4 Parameters for Kamiya's model for desorption of acetonitrile from cellulose acetate at various activities.

Activity	k_D $(g_{nitrile}/g_{poly})$	C'_{H0} $(g_{nitrile}/g_{poly})$	b	f	D_D $\times 10^9\ cm^2/s$	k_r $\times 10^4\ s^{-1}$
		0.1016	26.2	0		
0.25	0.3531	0.1373	19.4	0.25	1.83±0.06	5.46
		0.2117	12.6	0.5		
		0.4618	5.8	0.75		
		0.0806	30.3	0		
0.2	0.2583	0.1016	24.1	0.25	1.47±0.15	5.46
		0.1373	17.8	0.5		
		0.2116	11.6	0.75		
		0.0727	31.2	0		
0.15	0.1512	0.0893	25.4	0.25	1.4±0	5.46
		0.1158	19.6	0.5		
		0.1646	13.8	0.75		

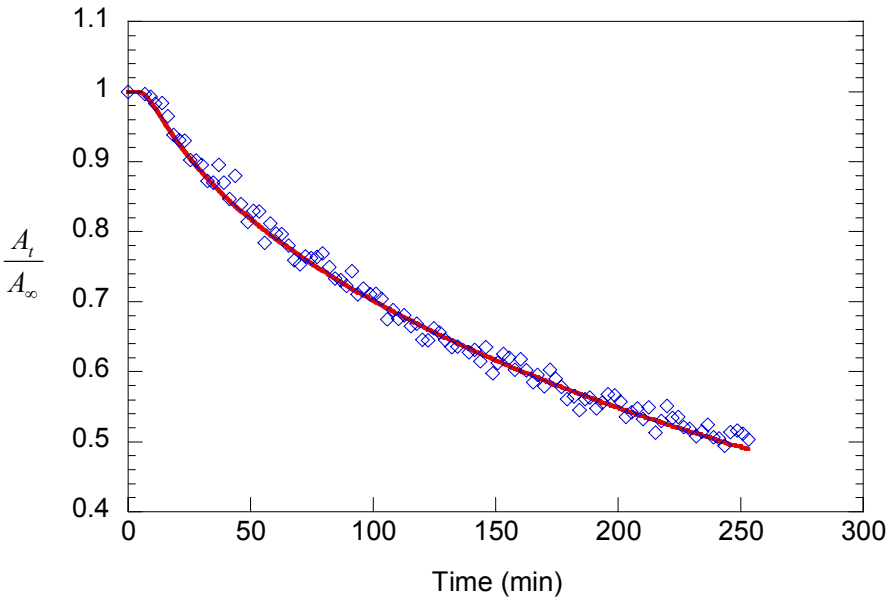

Figure 5.17 Desorption FTIR-ATR absorbance data with fit from modified dual mode transport model at activity 0.15, L = 29.2 μm, T = 25° C.

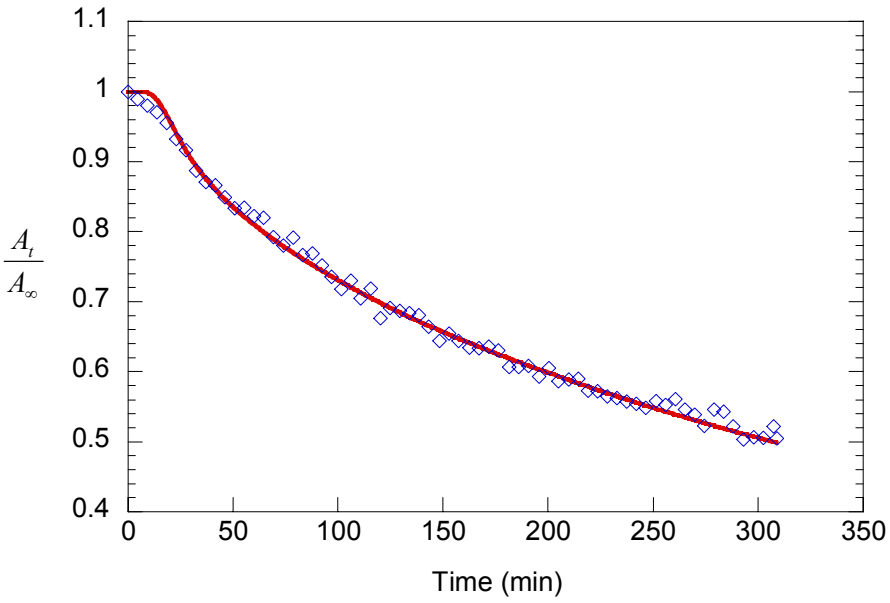

Figure 5.18 Desorption FTIR-ATR absorbance data with fit from modified dual mode transport model at activity 0.2, L=44.0 μm, T = 25° C.

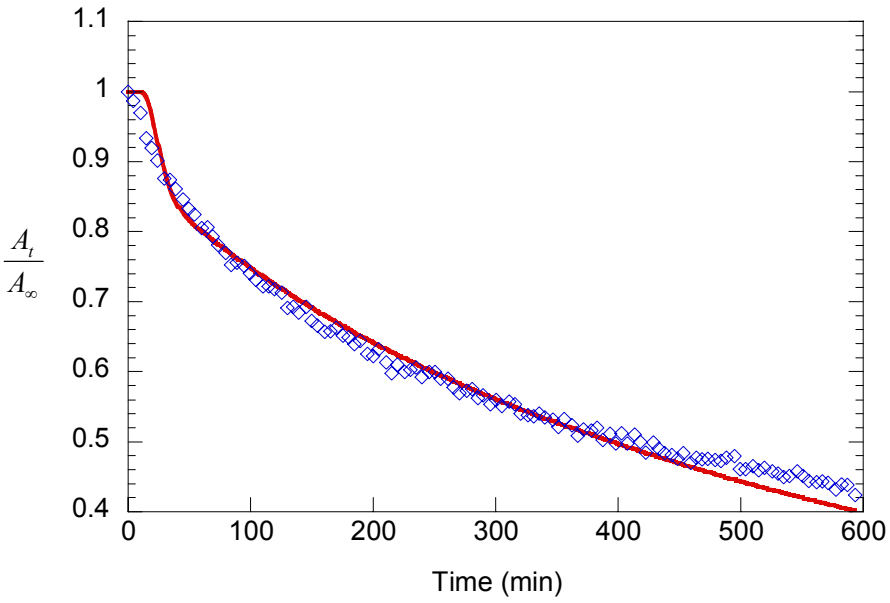

Figure 5.19 Desorption FTIR-ATR absorbance data with fit from modified dual mode transport model at activity 0.25, L=60.8 μm, T = 25° C.

Table 5.5 Diffusion coefficients for desorption obtained from the modified dual mode transport model taking plasticization into account.

Activity (N=3)	$D_D \times 10^9\ cm^2/s$
0.15	1.40±0
0.2	1.47±0.15
0.25	1.83±0.06

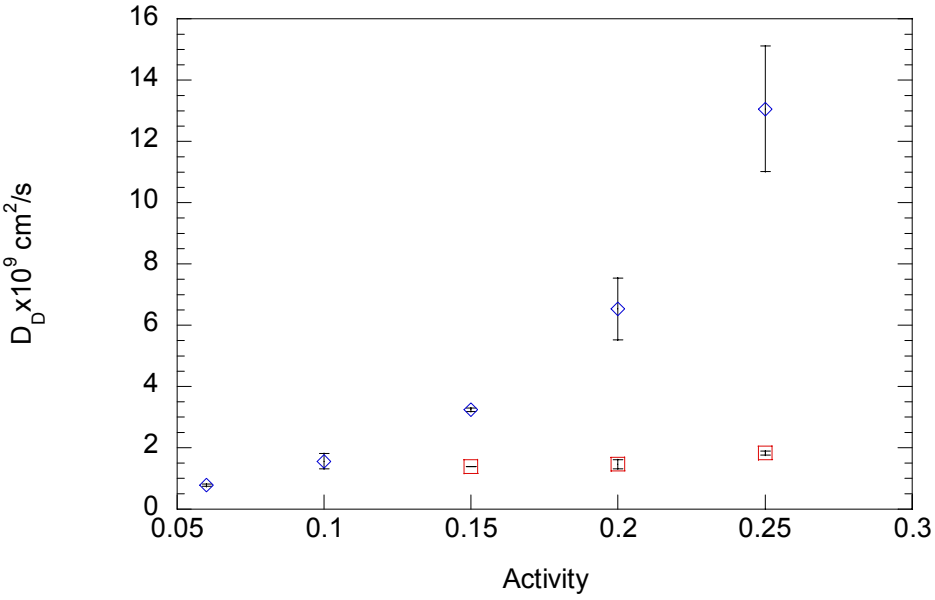

Figure 5.20 Diffusion coefficients for desorption form the dual mode transport model from Chapter 4 (diamonds) and the modified one (squares) as a function of activity.

5.5 Conclusion

The dual mode transport model with local equilibrium relaxation based on a modification of dual mode sorption proposed by Kamiya *et al*. was demonstrated to be a reasonable model to interpret the sorption and desorption behavior of acetonitrile in cellulose acetate. It provides a somewhat different physical interpretation for the distribution of sorbed populations, of which only the Henry's law mode is mobile. According to the Kamiya model, penetrant molecules making up the Henry's law population, alone or with part of the Langmuir species, plasticize the polymer upon sorption, or anti-plasticize the polymer during desorption. Hence, unlike in the classical dual mode model, in which the number of unoccupied holes is constant, in the Kamiya model, the unoccupied hole concentration changes gradually as a function of local concentration of penetrant molecules with plasticizing capability. In the next chapter, both the classical dual mode and Kamiya models will be utilized to study the swelling and deswelling kinetics of cellulose acetate induced by the sorption and desorption, respectively, of acetonitrile to further investigate the physics of the transport mechanism.

Chapter 6

FTIR-ATR Study of the Kinetics of Swelling and Deswelling

6.1 Introduction

There are only a few prior studies that utilize the *in situ* capability of the FITR-ATR technique to study polymer swelling. Balik and Xu [70] studied the swelling of latex paint induced by the sorption of water. Their FTIR-ATR data indicated swelling of the paint film because of the decrease in the local absorbance of the C-H stretch. Swelling was confirmed by a direct volume measurement. Yarwood and coworkers [89] utilized FTIR-ATR spectroscopy to study the swelling of a PET film upon sorption of methanol. Sarti and coworkers [108] studied the swelling of three different polymers, polycarbonate (glassy state), poly(vinyl acetate) and poly(ether urethane) (rubbery state), induced by the sorption of vapor phase acetonitrile. In their study, they compared direct volume change measurements to FTIR dilation data, and obtained good agreement. The swelling (dilation) was thermodynamically interpreted using lattice fluid models.

In this chapter, the swelling of cellulose acetate films induced by the sorption of vapor-phase acetonitrile is studied using the FTIR-ATR spectroscopy technique combined with a direct elongation measurement to obtain the corresponding change in volume. The results from these two methods are compared and found to be in good agreement, which demonstrates that FTIR-ATR spectroscopy can be an excellent

alternative for studying polymer swelling in sorption. Moreover, although not done here, the FTIR-ATR technique has the added potential of being able to provide information about the swelling process at the molecular level. Deswelling measurements were also done using the FTIR-ATR technique.

The previous chapters in this dissertation focused on the interpretation of the diffusion mechanism for acetonitrile in cellulose acetate from the vapor phase using a dual mode transport model with local equilibrium relaxation. This model was developed into two versions with different physical interpretations of the two populations. One is based on the classical dual mode sorption model, and the other is based on a modification that takes into account the plasticization effect caused by penetrant molecules. These two models are used in this chapter to predict the swelling and deswelling behavior, and the results of the predictions are compared to the actual FTIR-ATR data.

6.2 Dual Mode Transport Models

The transport models developed in the previous chapters are summarized here. The classical dual mode sorption model is

$$C = C_D + C_H = k_D a + C_H' \frac{ba}{1+ba} \tag{6.1}$$

and the modified version accounting for plasticizing effects (Kamiya's model) is

$$C = k_D a + C_{H0}' \frac{ba[1-(C_D + fC_H)/C_g]}{1+ba} \tag{6.2}$$

where k_D is the Henry's law constant, a is the penetrant activity in the gas or vapor phase, $C_H^{'}$ and $C_{H0}^{'}$ are the Langmuir capacity constants for the pure polymer in these two models, b is the Langmuir affinity constant, f is the ratio of the plasticizing ability of a Langmuir species to that of a Henry's law species, and C_g is the glass transition concentration.

From Chapters 2 and 4, the Langmuir population of the penetrant was taken as totally immobilized in order to capture the FTIR-ATR data completely. Based on this assumption, the classical dual mode transport model becomes:

$$\frac{\partial C_D}{\partial t} = D_D \frac{\partial^2 C_D}{\partial Z^2} - k_f C_D (C_H^{'} - C_H) + k_r C_H \tag{6.3}$$

$$\frac{\partial C_H}{\partial t} = k_f C_D (C_H^{'} - C_H) - k_r C_H \tag{6.4}$$

and the modified (Kamiya) model becomes:

$$\frac{\partial C_D}{\partial t} = D_D \frac{\partial^2 C_D}{\partial z^2} - k_f C_D \left[C_{H0}^{'} (1 - \frac{C_D + f C_H}{C_g}) - C_H \right] + k_r C_H \tag{6.5}$$

$$\frac{\partial C_H}{\partial t} = k_f C_D \left[C_{H0}^{'} (1 - \frac{C_D + f C_H}{C_g}) - C_H \right] - k_r C_H \tag{6.6}$$

where D_D is the diffusion coefficient of the Henry's law population, k_f is the rate constant for hole-filling, and k_r is the rate constant for hole-emptying.

For sorption in glassy cellulose acetate, the initial and boundary conditions are:

$t = 0$ ($all\ z$) $\quad C_D = 0$, $C_H = 0$

$z = 0$ ($t > 0$) $\quad \frac{\partial C_D}{\partial z} = 0$, $\frac{\partial C_H}{\partial z} = 0$

$z = L$ ($t > 0$) $\quad C_H = C_{T_L} - C_D$, $C_D = k_D a$

and for desorption in cellulose acetate, the initial and boundary conditions are:

$t = 0$ (*all z*) $\quad C_H = C_{T_L} - C_D$, $C_D = k_D a$

$z = 0$ ($t > 0$) $\quad \frac{\partial C_D}{\partial z} = 0$, $\frac{\partial C_H}{\partial z} = 0$

$z = L$ ($t > 0$) $\quad C_D = 0$, $C_H = 0$

where C_{T_L} is the total concentration at $z=L$.

6.3 Results and Discussion

6.3.1 Swelling Measurements and Analysis

The swelling of cellulose acetate during the sorption of vapor-phase acetonitrile was measured separately by either direct observation of sample elongation with a cathetometer (equilibrium) or monitoring carbonyl (C=O) stretches peak in the polymer during the diffusion experiments with the FTIR-ATR technique (equilibrium and kinetics). As described in Chapter 5, the equilibrium elongation of the CA strip was measured as a function of activity. The volume change, ΔV, of the CA films can be expressed in terms of the elongation, L: [161]

$$\frac{\Delta V}{V_0} = \left(\frac{L}{L_0}\right)^3 - 1 = \left(1 + \frac{\Delta L}{L_0}\right)^3 - 1 \qquad (6.7)$$

where V_0 and L_0 are the volume and length of the pure polymer strip, respectively. The swelling was calculated from Equation (6.7) and is plotted as a function of activity in Figure 6.1.

Combining measurements of acetonitrile mass uptake and swelling allows one to use a straightforward thermodynamic approach to determine the partial molar volume of the acetonitrile in CA. The definition of the partial molar volume is given by [123, 162]

$$\overline{V_i} = \left(\frac{dV_t}{dn_i} \right)_{T,P,n_j} \tag{6.8}$$

where V_t is total volume of the system, n_i is the moles of species i, and $\overline{V_i}$ is the partial molar volume of i. Equation (6.8) is not convenient for the calculation of numerical values from experimental data, because data are normally expressed on a molar (or unit-mass) basis. An equation relating the partial molar volume to the molar volume of the system (V) and to mole fractions is expressed as: [123]

$$\overline{V_i} = V - \sum_{j \neq i} \left[x_j \left(\frac{dV}{dx_j} \right)_{T,P,x_k \neq j,i} \right] \tag{6.9}$$

The index i denotes the component of interest, whereas j identifies any other component. The subscript x_k indicates that the partial derivative is taken with all mole fractions held constant except i and j. A more practical expression for penetrant-polymer systems is the definition for the partial specific volume given by

$$v_i = \left(\frac{dV_t}{dm_i} \right)_{T,P,m_j} \tag{6.10}$$

where m_i is the mass of species i and v_i is the partial specific volume of species i. For a binary system like acetonitrile/CA, the partial specific volumes of CA and acetonitrile can be derived from Equations (6.9) and (6.10), [123,162]

$$v_1 = v_t - \omega_2\left(\frac{dv_t}{d\omega_2}\right) \tag{6.11a}$$

$$v_2 = v_t + (1-\omega_2)\left(\frac{dv_t}{d\omega_2}\right) \tag{6.11b}$$

where v_1 and v_2 are the partial specific volumes of the CA and acetonitrile, respectively. ω_2 is the acetonitrile weight fraction. Hence, the partial specific volume of the acetonitrile can be determined from the tangent slope of the specific volume of the acetonitrile/CA system, plotted against the weight fraction of acetonitrile. The total specific volume of the system and the mass fraction of acetonitrile, respectively, can be derived as,

$$v_t = \frac{V_0 + \Delta V}{C(V_0\rho_{polymer}) + V_0\rho_{polymer}} = \frac{1 + \Delta V/V_0}{\rho_{polymer}(1+C)} \tag{6.12}$$

$$\omega_{nitrile} = \frac{C\rho_{polymer}V_0}{C\rho_{polymer}V_0 + \rho_{polymer}V_0} = \frac{C}{1+C} \tag{6.13}$$

where C is the acetonitrile concentration in CA at equilibrium ($\frac{g_{nitrile}}{g_{polymer}}$), which was obtained as a function of activity in Chapter 2.

The density of the as-received CA powder is 1.3 g/cm^3, as provided by the supplier. However, CA film density may be different due to the film formation process. Based on the study of Puleo and Paul, [163] who measured the density of a CA film that was

made from a similar powder as used in the present study (39.8 wt% acetyl content and 2.45 Degree of Substitution) and the same solution-casting method (acetone as solvent), the density is 1.327 g/cm^3. Using this value, the specific volume of the acetonitrile/CA system was plotted as a function of mass fraction of acetonitrile, as shown in Figure 6.2. One can convert from partial specific volume to partial molar volume for the acetonitrile by simply multiplying the acetonitrile specific volume by its molecular weight, 41g/mole. The partial molar volume of acetonitrile in the acetonitrile/CA system is plotted as a function of activity in Figure 6.3. From the results in Figure 6.3, it can be seen that the partial molar volume of acetonitrile is concave to the activity axis, and asymptotically approaches a value of 44 cm^3/mole. As discussed in previous chapters, the acetonitrile/CA system is in a rubbery state when equilibrium is reached at activity 0.4 and 0.5. Therefore, the partial molar volume of acetonitrile at these activities should correspond to a value expected in liquid or rubbery polymers. From the study of Sarti, *et al*. [108], the partial molar volume of acetonitrile in poly(vinyl acetate) and poly(ether urethane), both rubbery polymers, was 43 and 42 cm^3/mole, respectively. The value calculated in the present study compares well to those values.

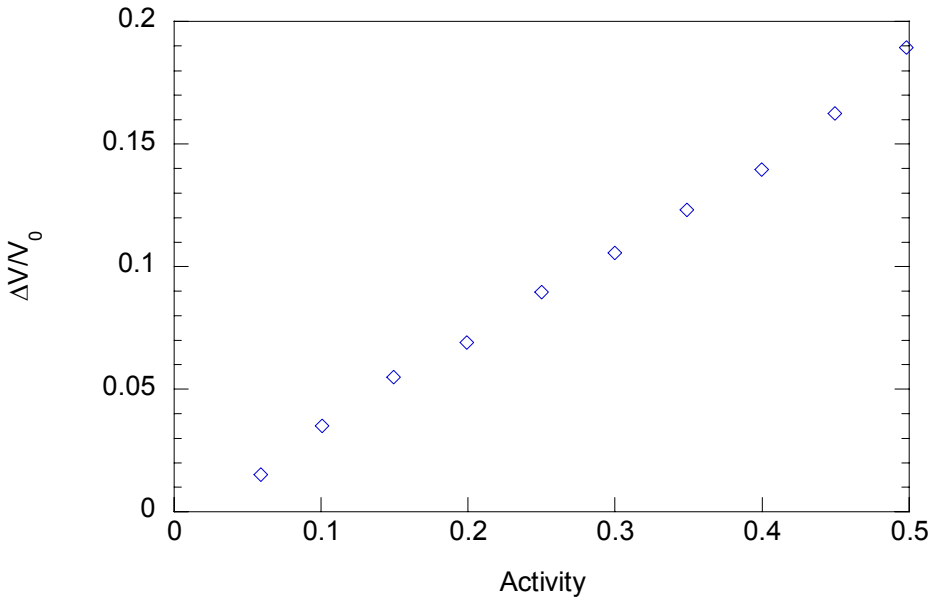

Figure 6.1 Swelling of CA by acetonitrile as a function of activity at T = 25° C.

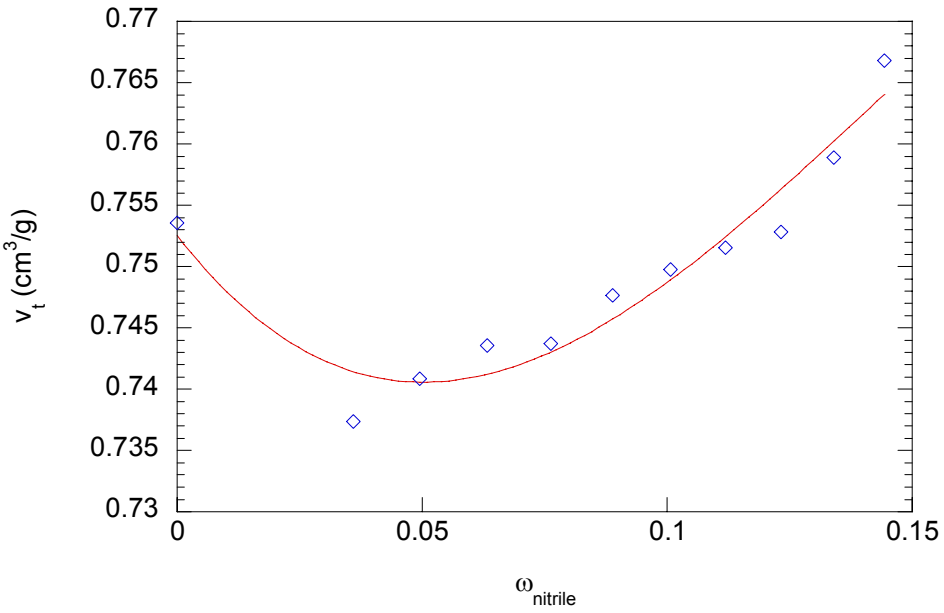

Figure 6.2 Total specific volume of the acetonitrile/CA system as a function of acetonitrile mass fraction. T = 25° C.

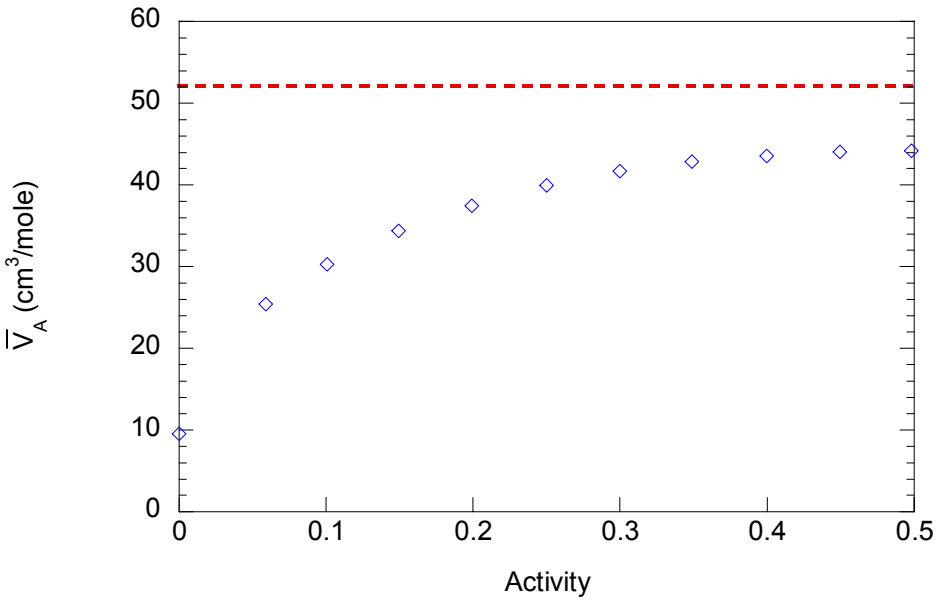

Figure 6.3 Partial molar volume of acetonitrile in the acetonitrile/CA system as a function of activity at T = 25^{o}C. The dashed line represents the molar volume of pure acetonitrile.

6.3.2 FTIR-ATR Swelling Data

When the polymer swells during penetrant sorption, the local concentration of polymer chains decreases such that the number of local polymer functional groups that can absorb IR radiation is also lowered. In this study, the characteristic functional group for monitoring the swelling of cellulose acetate is the carbonyl group, C=O, from wavenumber 1600 cm^{-1} to wavenumber 1850 cm^{-1}. A series of time-evolved absorbance spectra for the carbonyl group during the swelling of the CA film is shown in Figure 6.4. The spectrum of the pure polymer has been subtracted from each time point to highlight the decrease in C=O groups upon sorption. The presence of two C=O peaks reflects free and hydrogen-bound states within the polymer. Hydrogen bounding occurs with available OH group in CA.

If changes in the polymer functional group being monitored for dilation are relatively minor, then one may assume a linear relationship between the IR absorbance of a polymer peak and the polymer dilation, which leads to [108]

$$\frac{\Delta V}{V_0} = -\frac{\Delta A}{A_0} \tag{6.14}$$

where ΔA and ΔV represent the changes in IR absorbance and sample volume, respectively, relative to their pure polymer values, A_0 and V_0.

To fully characterize polymer swelling, the elasticity of the system should be considered. Under linear elasticity conditions, the total strain can be expressed by the principle of superposition: [108]

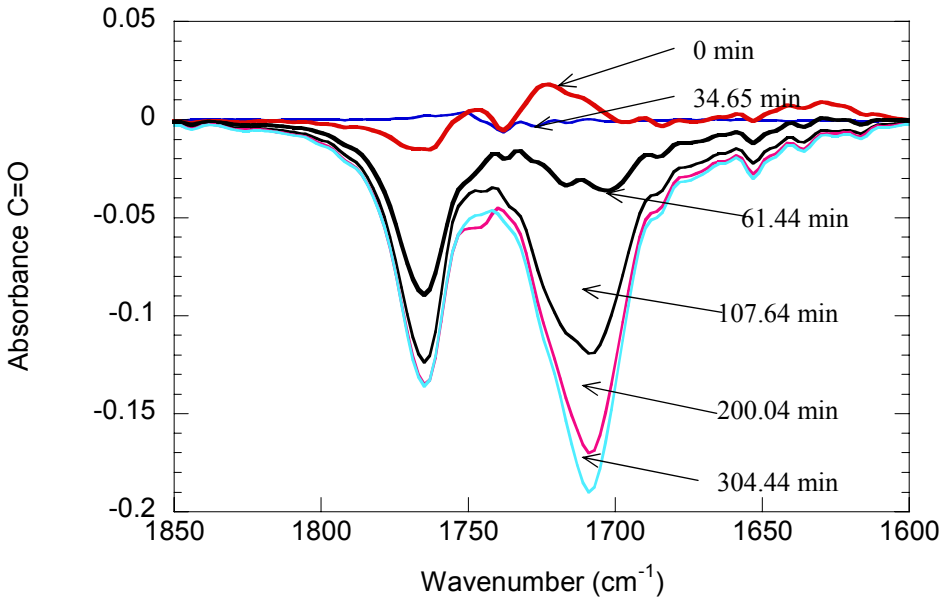

Figure 6.4 Time-resolved carbonyl absorbance spectra in cellulose acetate at activity 0.2 and T = 25° C shown as differences relative to the pure polymer.

$$\varepsilon = \varepsilon^{M} + \varepsilon^{D} \tag{6.15}$$

where ε^{M} is the contribution from mechanical forces and ε^{D} is from stress-free, diffusion-induced strains. By considering the symmetry of both the stress and strain tensors and the isotropy of the CA polymer samples, no shear effects are present, so the mechanical stress tensor σ can be expressed by the relation:

$$\sigma = \mathrm{E}(\varepsilon - \beta) \tag{6.16}$$

where σ and ε are vectors, E (Young's Modulus) is a second order elastic tensor, and β is a swelling function dependent on the actual penetrant concentration in the polymer.

In the present study, two experimental methods involving two different mechanical conditions were employed, a free sample for the direct measurement by cathetometer and a constrained sample with an attached surface in the FTIR-ATR experiments, where only out-of-plane deformation is allowed. In the first case, the swelling is only due to the diffusion process, no external mechanical forces are active, and σ = 0. Therefore, Equation (6.16) leads to $\varepsilon = \beta$. The overall volumetric change can then be expressed by: [108,164]

$$\frac{\Delta V}{V_0} = \varepsilon_{xx} + \varepsilon_{yy} + \varepsilon_{zz} = 3\beta \tag{6.17}$$

In the case of FTIR-ATR experiments, the CA film sample is clamped in the ATR cell and only the out-of-plane mechanical stress can be assumed to be zero. This description can be written as:

$$\varepsilon_{zz} = \left(\frac{2\nu}{1-\nu} + 1\right)\beta\,,\ \varepsilon_{xx} = 0\,,\ \varepsilon_{yy} = 0 \tag{6.18}$$

where ν is the Poisson ratio for cellulose acetate. Hence, in the FTIR-ATR experiments, the overall volumetric change is

$$\frac{\Delta V}{V_0} = \varepsilon_{xx} + \varepsilon_{yy} + \varepsilon_{zz} = \left(\frac{2\nu}{1-\nu} + 1\right)\beta \tag{6.19}$$

Comparing Equation (6.19) to (6.17), one can obtain

$$\left(\frac{\Delta V}{V_0}\right)_{free-sample} = \frac{3(1-\nu)}{\nu+1}\left(\frac{\Delta V}{V_0}\right)_{FTIR-ATR} \tag{6.20}$$

Taking this relationship into account in Equation (6.14), the swelling data obtained by the FTIR-ATR technique must be increased by a factor of $\frac{3(1-\nu)}{\nu+1}$ to be properly compared with the corresponding data from the direct measurement.

$$\frac{3(\nu-1)}{\nu+1}\frac{\Delta A}{A_0} = \frac{\Delta V}{V_0} \tag{6.21}$$

The Poisson ratio for cellulose acetate can be calculated from the relationship between bulk modulus, *B* and Young's modulus, *E*:

$$E = 3B(1-2\nu) \tag{6.22}$$

Young's modulus for cellulose acetate is $2GPa$, [165] and the bulk modulus can be estimated by [165]

$$B = (\mathbf{U}/\mathbf{V})^6 \rho_{poly} \tag{6.23}$$

where **U** is the Rao function or molar sound velocity function and **V** is the molar volume per structural unit of cellulose acetate. Using a group contribution method for the Rao function, it was calculated to be **U** = 24860. **V** = M/ ρ_{poly}, where M = 678.6, the molecular weight of the structural unit of cellulose acetate. From the density of

CA film, 1.327 g/cm^3, **V** = 511.4 $cm^3/mole$. Therefore, the bulk modulus can be calculated from Equation (6.23), and is B = 1.75 GPa. The Poisson ratio for cellulose acetate was then estimated to be 0.31. Hence the swelling data obtained with FTIR-ATR method should be multiplied by a factor of -1.58 to be properly compared with the direct swelling measurement for the free sample. From the literature, [166] the average Poisson ratio of cellulose acetate was found to be 0.30, which is in good agreement with the value calculated above.

The FTIR-ATR absorbance of the carbonyl group in the pure polymer, A_0, was obtained by integrating the carbonyl region of a pure CA film. The mean value of A_0, from 10 experiments, was 80.0 ± 1.9. The change in the absorbance of the carbonyl group as a function of activity, at equilibrium, was obtained by integration of the carbonyl region at each activity. The swelling data obtained from the FTIR-ATR experiments are plotted in Figure 6.5 alongside those from direct measurement. The two methods are in good agreement. Hence, the FTIR-ATR technique is an excellent alternative for the measurement of polymer swelling and was used to study swelling and deswelling kinetics.

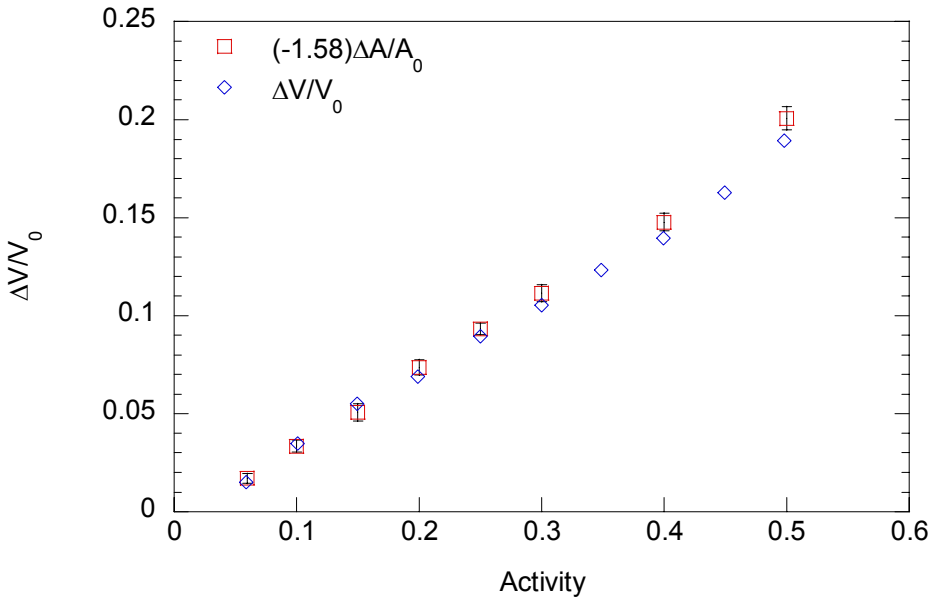

Figure 6.5 Swelling from both direct measurement and FTIR-ATR absorbance as function of activity.

6.3.3 Study of Swelling Kinetics by FTIR-ATR

According to the dual mode sorption model, there are two penetrant populations: those "dissolved" in the equilibrium portion of the matrix, represented by C_D, and those residing in the "holes" created by pre-existing free volume in the matrix, represented by C_H. A common hypothesis is that only penetrant molecules from the Henry's law population participate in swelling the polymer, while the Langmuir population resides in the pre-existing free volume without contributing to the system dilation. Based on the classical dual mode sorption model, the swelling induced by sorption of penetrant molecules is predictable in terms of the partial molar volume, $\overline{V}_{A_D}$, and concentration, C_D, of the Henry's law species:

$$\frac{\Delta V}{V_0} = \frac{[V_0 + C_D(t)\frac{\overline{V}_{A_D}}{M_{W_A}}\rho_{poly}V_0] - V_0}{V_0} = C_D(t)\frac{\overline{V}_{A_D}}{M_{W_A}}\rho_{poly} \tag{6.24}$$

where V_0 is the original volume, M_{W_A} is the molecular weight of acetonitrile and ρ_{poly} is the density of cellulose acetate. The value of $\overline{V}_{A_D}$ is assumed to be equal to the value of the partial molar volume in the rubbery state, which was determined to be 44 $cm^3/mole$ from Figure 6.3. The values of $\overline{V}_{A_D}$ in the glassy state ($a < 0.3$) in Figure 6.3 correspond to weighted averages of $\overline{V}_{A_D}$ and $\overline{V}_{A_D} = 0$ at each activity.

In Kamiya's model, the Henry's law population still swells the polymer, but it can also plasticize the polymer to reduce the number of holes. Reducing the number of holes results in volume collapse. From Equation (6.5), the number of holes at any given concentration is given by

$$C_H^{'} = C_{H0}^{'}\left(1 - \frac{C_D + fC_H}{C_g}\right) \tag{6.25}$$

If $f = 0$, as was determined previously in this study, then the amount of volume lost as a result of plasticization can be expressed as

$$\left(\frac{\Delta V}{V_0}\right)_{lost} = C_{H0}^{'}\frac{C_D}{C_g}\frac{\overline{V}_{A_D}}{M_{W_A}}\rho_{poly} \tag{6.26}$$

Therefore, based on the Kamiya model, the swelling of the polymer during sorption can be written as

$$\frac{\Delta V}{V_0} = \left(C_D(t) - C_{H0}^{'}\frac{C_D(t)}{C_g}\right)\frac{\overline{V}_{A_D}}{M_{W_A}}\rho_{poly} \tag{6.27}$$

In Equation (6.27), the first term represents the swelling by C_D in the absence of plasticization and the second term represents the volume lost through hole collapse as a result of plasticization.

FTIR-ATR spectroscopy allows one to simultaneously obtain acetonitrile diffusion data, which represents the total concentration of penetrant, and carbonyl group data, which represents the swelling of the CA. The relationships between polymer swelling and penetrant concentration given in Equations (6.24) and (6.27), can then be used to predict the kinetics of swelling. For both models, the Henry's law concentration as a function of time, $C_D(t)$, for acetonitrile can be calculated either with Equations (6.3) and (6.4) for classical dual mode model, or with Equations (6.5) and (6.6) for Kamiya's model, under the same initial and boundary conditions. All the parameters needed for the calculation were obtained in Chapters 2 and 5, and are listed in Tables 6.1 and 6.2. Specifically, C_D for acetonitrile in glassy cellulose acetate at activities

0.1, 0.15, 0.2 and 0.25 were calculated. Then, either Equation (6.24) or (6.27) was used to calculate the swelling as a function of time. Lastly, Equation (6.21) was applied to convert the calculated swelling of the polymer to FTIR-ATR absorbance data. The prediction of the ATR absorbance is plotted along with the actual experimental FTIR-ATR absorbance data in Figures 6.6 to 6.9 for both models.

Table 6.1 Parameters from the dual mode transport model with local equilibrium relaxation obtained from Chapter 2.

Activity	$D_D \times 10^{10} cm^2/s$	$k_r \times 10^3 s^{-1}$	k_D $(g_{nitrile}/g_{poly})$	$C_H^{'}$ $(g_{nitrile}/g_{poly})$	b
0.1	2.96				
0.15	4.66				
0.2	6.38	4.85	0.282	0.030	38.1
0.25	7.04				

Table 6.2 Parameters from the dual mode transport model with local equilibrium relaxation based on Kamiya sorption obtained from Chapter 5.

Activity	$D_D \times 10^{10} cm^2/s$	$k_r \times 10^3 s^{-1}$	k_D $(g_{nitrile}/g_{poly})$	C'_{H0} $(g_{nitrile}/g_{poly})$	f	b
0.1	2.20					
0.15	3.47					
0.2	4.76	4.74	0.376	0.0259	0	40.1
0.25	5.64					

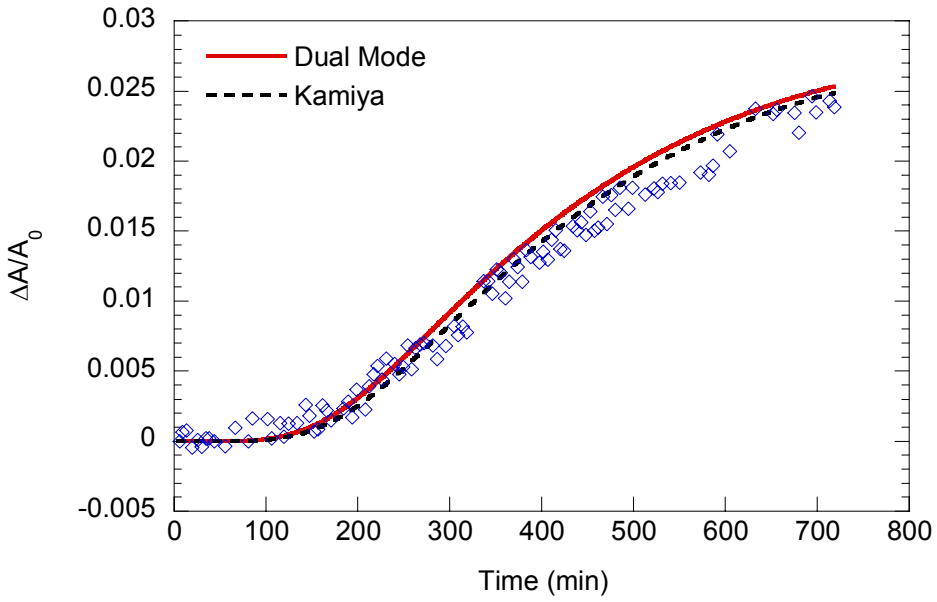

Figure 6.6 FTIR-ATR swelling kinetics data and the prediction from both classical dual mode and Kamiya models at activity 0.1. L = 29.8 μm and T = 25° C.

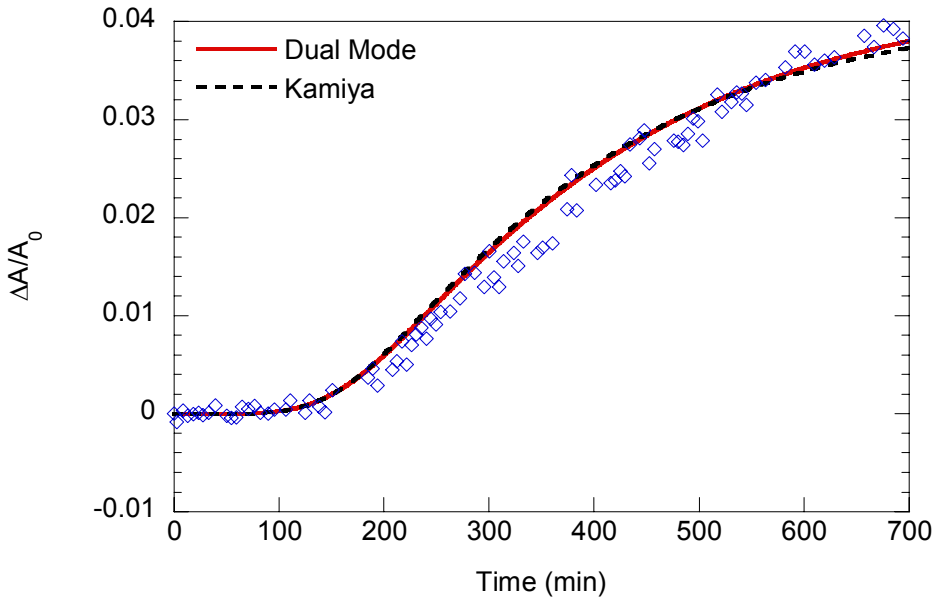

Figure 6.7 FTIR-ATR swelling kinetics data and the prediction from both classical dual mode and Kamiya models at activity 0.15, L = 38.4 μm and T = 25° C.

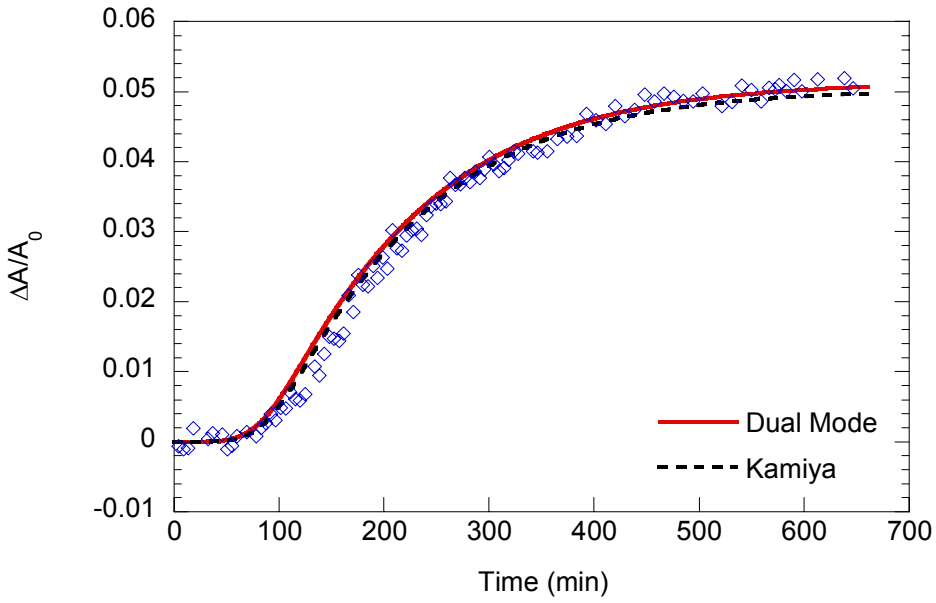

Figure 6.8 FTIR-ATR swelling kinetics data and the prediction from both classical dual mode and Kamiya models at activity 0.2, L = 34.2 μm and T = 25° C.

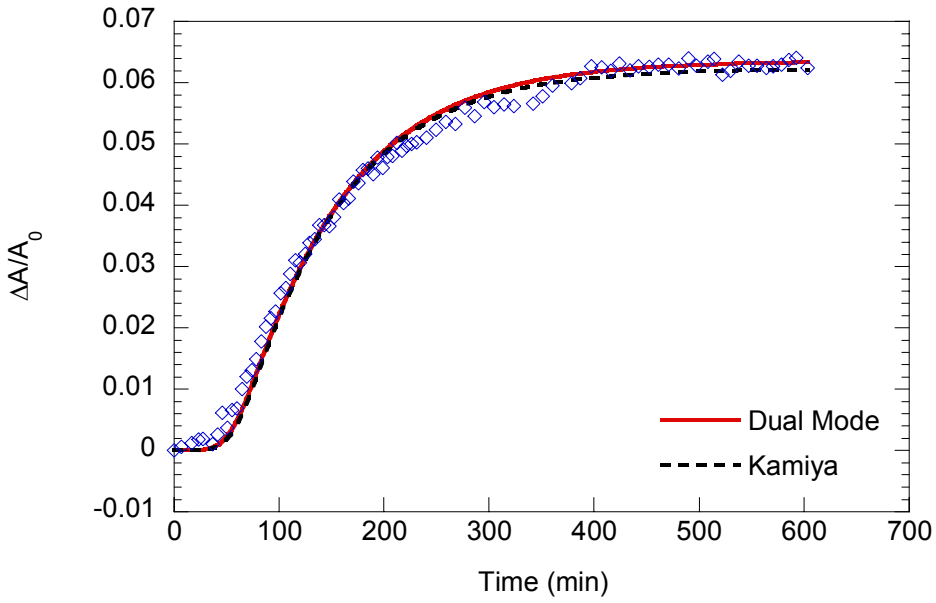

Figure 6.9 FTIR-ATR swelling kinetics data and the prediction from both classical dual mode and Kamiya models at activity 0.25, L = 30.4 μm and T = 25° C.

From these figures, it is clear that both models do an excellent job predicting the FTIR-ATR swelling kinetics. These results support the hypothesis that only the Henry's law population causes polymer swelling, and in the Kamiya model, also causes volume loss through hole collapse due to plasticization.

6.3.4 Study of Deswelling Kinetics by FTIR-ATR

In the application of the classical dual mode sorption model to predicting swelling, the final equilibrium value of the Henry's Law population from sorption, C_D^{SF}, determines the initial condition for deswelling:

$$\frac{\Delta V}{V_0} = C_D^{SF} \frac{\overline{V}_{A_D}}{M_{W_A}} \rho_{poly} \tag{6.28}$$

For the Kamiya model, plasticization by the Henry's law population must be taken into account. Hence, the initial condition for deswelling of polymer is

$$\frac{\Delta V}{V_0} = \left(C_D^{SF} - C_{H0}'^{S} \frac{C_D^{SF}}{C_g} \right) \frac{\overline{V}_{A_D}}{M_{W_A}} \rho_{poly} \tag{6.29}$$

where C_g is the glass transition concentration and $C_{H0}^{'S}$ represents the number of unoccupied holes in the pure polymer prior to sorption and obtained from the sorption isotherm.

As shown in Chapters 4 and 5, sorption-desorption hysteresis results in a redistribution between the C_D and C_H populations for desorption relative to those for sorption. If the initial Henry's law population for desorption is denoted by C_D^{DI}, then $C_D^{SF} + C_H^{SF} = C_D^{DI} + C_H^{DI} = C_\infty$, where C_∞ is the total concentration at equilibrium

sorption (or the total concentration initially for desorption). As desorption starts, if the Henry's law population is still assumed to be the only species responsible for deswelling, the loss in volume is associated with the amount of the Henry's law population that has left, or $C_D^{DI} - C_D(t)$. In the classical dual mode framework, the deswelling of the polymer can then be written as:

$$\frac{\Delta V}{V_0} = \left[C_D^{SF} - \left(C_D^{DI} - C_D(t)\right)\right]\frac{\overline{V}_{A_D}}{M_{W_A}}\rho_{poly} \tag{6.30}$$

Analogously, the volumetric decrease in the Kamiya framework can be written as:

$$\frac{\Delta V}{V_0} = \left[C_D^{SF} - C_{H0}'^{S}\frac{C_D^{SF}}{C_g} - \left(C_D^{DI} - C_D(t)\right) + C_{H0}'^{D}\left(\frac{C_D^{DI} - C_D(t)}{C_g}\right)\right]\frac{\overline{V}_{A_D}}{M_{W_A}}\rho_{poly} \tag{6.31}$$

where $C_{H0}'^{D}$ represents the number of unoccupied holes in the pure polymer at the end of desorption when all of the penetrant has left. Physically, the ratio $\frac{C_D^{SF}}{C_g}$ represents the fraction of the initial number of unoccupied holes in the pure polymer that has collapsed at the end of sorption due to plasticization. The ratio $\frac{C_D^{DI} - C_D(t)}{C_g}$ represents the fraction of the final number of unoccupied holes in the pure polymer that have been formed at the end of desorption due to "anti-plasticization".

The predictions of deswelling kinetics along with the actual ATR absorbance data at activities 0.15, 0.2 and 0.25 are plotted in Figures 6.10, 6.11 and 6.12, respectively. The Henry's law concentration as a function of time, $C_D(t)$, was calculated from either Equations (6.3) and (6.4) for the classical dual mode model or Equations (6.5) and (6.6) for the Kamiya model, under the desorption initial and boundary conditions.

The parameters needed in the calculation were obtained from Chapters 2 and 5, and are listed in Tables 6.3 and 6.4. In the Kamiya model framework, f is assumed to be zero as discussed in Chapter 5.

Table 6.3 Parameters from the classical dual mode transport model for desorption obtained from Chapter 2.

Activity	$D_D \times 10^9 cm^2/s$	$k_r \times 10^4 s^{-1}$	k_D $(g_{nitrile}/g_{poly})$	C_H' $(g_{nitrile}/g_{poly})$	b
0.15	3.24			0.068	
0.2	6.53	5.46	0.0593	0.0804	38.8
0.25	13.1			0.094	

Table 6.4 Parameters from the Kamiya transport model for desorption obtained from Chapter 5.

Activity	$D_D \times 10^9 cm^2/s$	$k_r \times 10^4 s^{-1}$	k_D $(g_{nitrile}/g_{poly})$	C_{H0}' $(g_{nitrile}/g_{poly})$	f	b
0.15	1.40		0.151	0.073		26.2
0.2	1.47	5.90	0.258	0.081	0	30.3
0.25	1.83		0.353	0.102		31.2

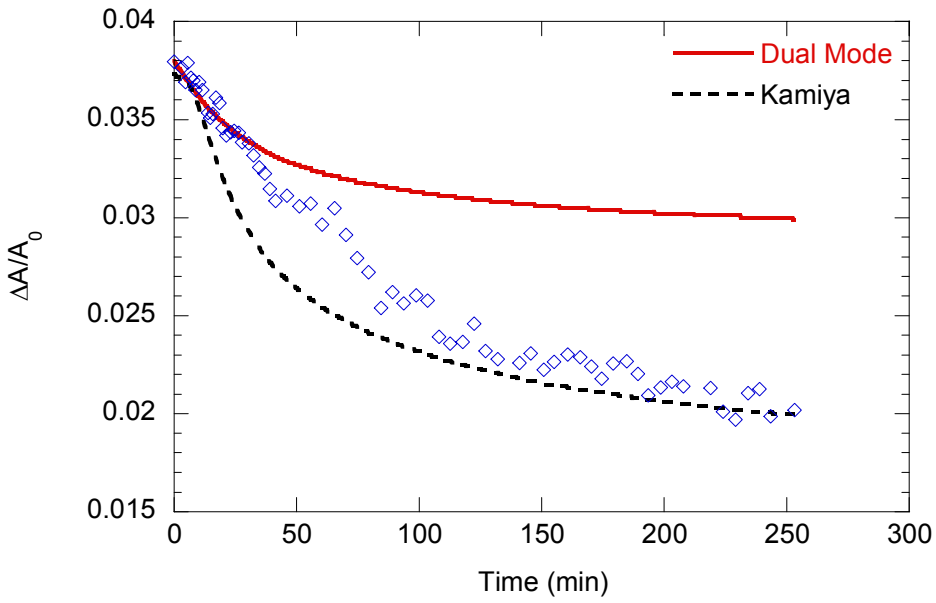

Figure 6.10 Prediction of deswelling FTIR-ATR data at activity 0.15, based on the assumption that only the Henry's law population contributes to volume loss. L = 38.4 μm and T = 25° C.

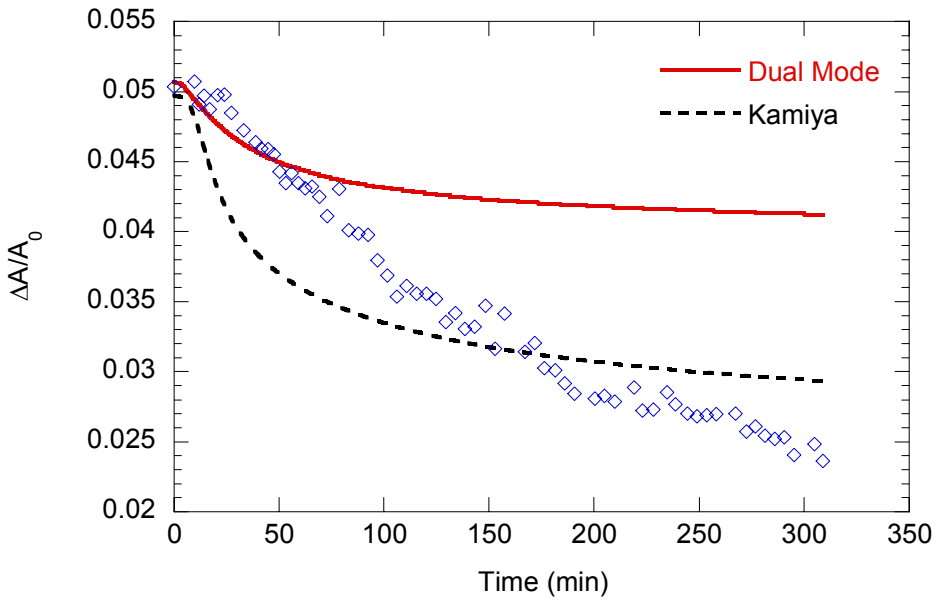

Figure 6.11 Prediction of deswelling FTIR-ATR data at activity 0.2, based on the assumption that only the Henry's law population contributes to volume loss. L = 34.2 μm and T = 25° C.

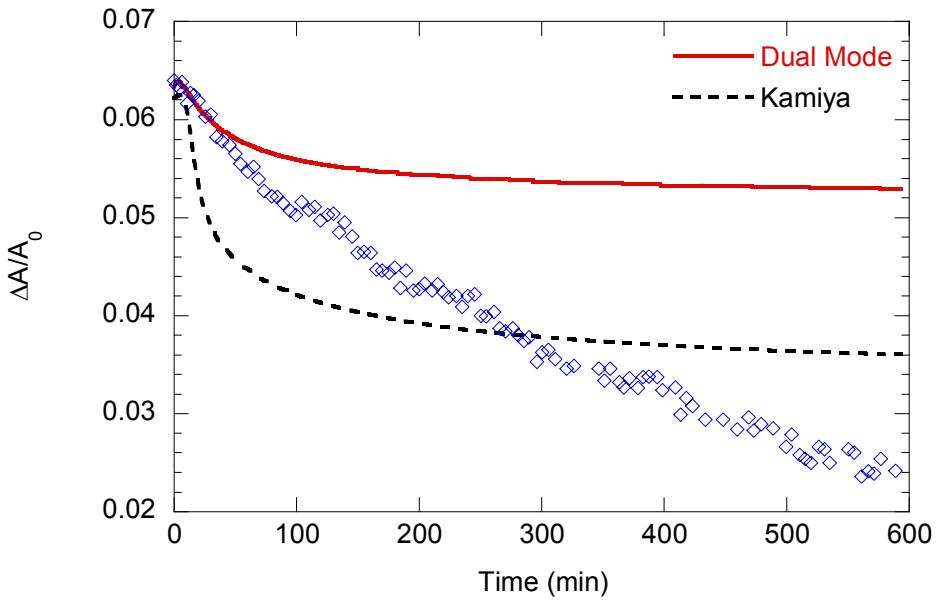

Figure 6.12 Prediction of deswelling FTIR-ATR data at activity 0.25, based on the assumption that only the Henry's law population contributes to volume loss. L = 30.4 μm and T = 25° C.

From Figures 6.10 to 6.12, it can be seen that neither Equation (6.30) nor Equation (6.31) can predict the deswelling absorbance data very well. However, the Kamiya prediction at least bisects the data, unlike the classical dual mode prediction, which lies above the actual data over the nearly the entire time course of the experiment. The results for deswelling suggest that a more complicated mechanism is involved; one that likely involves the Langmuir population and its effect on swelling.

6.4 Conclusion

In this chapter, time-resolved FTIR-ATR spectroscopy was used to study the swelling and deswelling behavior of cellulose acetate induced by the sorption and desorption, respectively, of acetonitrile. The ATR absorbance data for swelling were compared to direct measurements made independently with a quartz spring apparatus, and they were in very good agreement. It was demonstrated that the FTIR-ATR technique is a good alternative method to study polymer swelling *in situ*. The hypothesis that the diffusion of the Henry's law population is responsible for swelling upon sorption was validated by accurately predicting the behavior using both the classical dual mode and Kamiya models. However, the mechanism for polymer deswelling is more complicated than that for swelling. The results for predicting deswelling strongly suggest a more complex mechanism and this should be an area for further study.

Chapter 7

Conclusions

7.1 Key Concepts

In this study, the diffusion of acetonitrile in cellulose acetate (CA) during transient sorption/desorption and the penetrant-induced swelling/deswelling in this system were studied using time-resolved FTIR-ATR spectroscopy combined with a conventional gravimetric method. Based on the gravimetric measurements for sorption, it was demonstrated that the diffusion of acetonitrile in CA was inherently Fickian. However, the time-resolved FTIR-ATR absorbance data could not be captured by the simple Fickian model. This suggested that there was another mechanism being masked by the conventional gravimetric measurement. To describe the observed behavior, a dual mode transport model with local equilibrium relaxation was proposed, which was used successfully to interpret the FTIR-ATR absorbance data. The hole-filling and hole-emptying rate constants must be taken into account to correctly describe the diffusion behavior of acetonitrile in CA. Obtaining the ratio of these rate constants from the dual mode sorption isotherm, the rate constant for hole-emptying was used as a second adjustable parameter, in addition to the diffusion coefficient. To the best knowledge of the author, this is the first investigation to uncover the limitations imposed by the local equilibrium assumption in describing dual mode transport in glassy polymers.

The dual mode transport model with local equilibrium relaxation was not able to capture the FTIR-ATR absorbance data at higher activities, specifically 0.4 and 0.5. Based on the magnitude of the diffusion coefficients of acetonitrile at these activities from the gravimetric results, a hypothesis was proposed that a penetrant-induced glass transition was occurring near activity 0.3 during sorption. This hypothesis was tested by measuring the desorption isotherm starting at activity 0.4, and indeed, a glass transition concentration was evident between activities 0.25 and 0.3. A moving boundary model was proposed to address diffusion in a penetrant-polymer system undergoing such a transition. In front of the boundary, the polymer is glassy and diffusion is governed by the dual mode transport model with local equilibrium relaxation. Behind the moving boundary, the polymer is rubbery and diffusion is governed by the simple Fickian model. This moving boundary model successfully captured the FTIR-ATR absorbance data at the higher activities, with rubbery diffusion coefficients consistent in magnitude with those in other systems above a glass transition.

The dual mode transport model with local equilibrium relaxation was also used to interpret the diffusion behavior of acetonitrile in CA below the glassy transition concentration during transient desorption. Desorption isotherms were measured at each activity from which the desorption experiments were conducted. In order to describe the kinetics of desorption, the two adjustable parameters, the diffusion coefficient and the hole-emptying rate constant, had to be increased an order of magnitude and decreased an order of magnitude, respectively, to fit the data.

Although the direction of these changes could be rationalized mechanistically, the actual magnitude of the desorption diffusion coefficients was not physically realistic owing to the excessive redistribution in favor of the Langmuir population.

In order to investigate whether a different physical interpretation can improve the description of the desorption behavior of acetonitrile in CA, a dual mode transport model based on Kamiya's sorption model was proposed. The Kamiya model takes into account the plasticization induced by penetrant molecules and the resulting loss of pre-existing holes as sorption sites. The dual mode transport model based on Kamiya sorption was used to interpret the diffusion of acetonitrile in CA for both sorption and desorption kinetics. The diffusion coefficients and hole-emptying rate constants for both sorption and desorption were obtained, and were compared to the corresponding parameters obtained by the classical dual mode model. The result of this comparison showed that two models gave similar results for sorption. For desorption, the diffusion coefficients from the Kamiya model were physically more realistic than those obtained from the classical dual mode model.

In order to study volumetric changes, the penetrant-induced swelling/deswelling of CA by acetonitrile was studied using the FTIR-ATR data for the polymer. The FTIR-ATR swelling data were compared to direct measurements of film elongation, and the good agreement between the two suggested that FTIR-ATR spectroscopy is an excellent technique for studying polymer swelling. The classical dual mode and Kamiya models were used to predict the swelling and deswelling kinetics. Both

models were excellent in predicting swelling kinetics in the acetonitrile/CA system. Both models were consistent with the assumption that the Henry's law species is the only population contributing to polymer swelling with the Langmuir species residing in the pre-existing holes and not contributing to the swelling. The deswelling mechanism, however, was more complicated, with neither model able to predict the behavior well. However, the Kamiya framework is somewhat better than the classical dual mode model, which was expected given the more even redistribution between populations in the former.

In summary, time-resolved FTIR-ATR spectroscopy was proven in this study to be an excellent technique to investigate the diffusion of small molecules in glassy polymers and their swelling behavior. A significant advantage of the FTIR-ATR spectroscopy is its ability to study the kinetics of diffusion and penetrant-induced swelling *in situ* and simultaneously. The most significant outcome of this study is that the local equilibrium assumption in the dual mode model must be relaxed to describe the acetonitrile/cellulose acetate system. It is expected that other glassy polymer-penetrant systems will exhibit similar behavior and local equilibrium relaxation will be necessary to fully describe the systems. The additional mechanism associated with hole-filling/hole-emptying was masked by the integral gravimetric method and was revealed by the unique capability of FTIR-ATR spectroscopy to monitor the local penetrant concentration at an interface.

7.2 Recommendations

The inability to predict deswelling kinetics was the only limitation found thusfar in the application of the dual mode transport model with local equilibrium relaxation to diffusion in glassy polymers. One constraint in the investigation of deswelling in the present study is that there was no equilibrium volume (elongation) measurement for deswelling, directly or spectroscopically. Parameters such as the partial molar volume of acetonitrile and f were obtained from swelling. It will be of interest in the future to obtain deswelling volume measurements and further investigate the deswelling behavior.

The desorption and swelling/deswelling behavior of acetonitrile in cellulose acetate above the glass transition were not studied in the present work. It will be interesting to discover if the moving boundary model for sorption applies to desorption, as well as for swelling and deswelling.

The dual mode transport model with local equilibrium relaxation may find application in the development of polymer-based FTIR-ATR sensors. Taken together, the diffusion coefficient and the hole-emptying rate constant for a penetrant in a glassy polymer may provide a unique signature based on molecular size and shape. Hence, the ability to detect and identify specific molecules would expand the use of such sensors. In addition to conventional glassy polymers as the sensor polymer, molecular imprinted polymers have been suggested as the selective material. Synthesizing

highly cross-linked polymeric materials around template molecules will result in materials that can also be physically modeled in terms of pre-existing holes with transient behaviors likely to be influenced by both a matrix diffusion coefficient and hole-emptying rate constant. Future work is recommended in applying the models developed here to this application.

Appendix A. Individual Experimental Diffusion Coefficient Results

A.1 Individual diffusion coefficient results from Table 2.1

A.2 Individual diffusion coefficient results from Table 2.2

A.3 Individual diffusion coefficient results from Table 3.1

A.4 Individual diffusion coefficient results from Table 4.3

A.5 Individual diffusion coefficient results from Table 5.2

A.6 Individual diffusion coefficient results from Table 5.4

Appendix A.1

Individual diffusion coefficient results from Table 2.1

Diffusion Coefficients of Acetonitrile in CA Obtained from Mass Uptake Measurements

Activity	Thickness (μm)	$D \times 10^{10}\ cm^2/s$
0.06	30.2	2.3
	62.0	2.1
	33.5	1.8
0.1	28.6	3.1
	33.3	3.7
	39.5	2.9
0.2	44.6	6.6
	48.0	6.9
	50.4	6.1
0.3	46.1	10.4
	51.2	10.0
	48.2	9.1
0.4	78.6	28.5
	64.2	25.4
	79.4	26.5
0.5	37.0	52.0
	60.7	49.0
	70.8	56.8
	89.8	57.9

Appendix A.2

Individual diffusion coefficient results from Table 2.2

Diffusion Coefficients of Acetonitrile in CA Obtained from Dual Mode Transport Model with Local Equilibrium Relaxation

Activity	Thickness (μm)	$D_D \times 10^{10}\ cm^2/s$
0.06	37.8	1.92
	39.1	1.88
	30.8	1.92
	15.2	1.75
0.1	29.8	2.95
	33.6	2.97
	36.8	2.94
0.15	38.4	4.65
	38.3	4.67
	38.7	4.65
	29.2	4.80
0.2	49.2	6.34
	34.2	6.37
	44.0	6.42
0.25	30.4	6.96
	58.4	7.31
	60.8	7.66
	71.6	6.92
0.3	57.8	8.18
	39.4	8.05
	48.3	8.09
	49.4	8.05
0.4	42.7	18.1
	60.7	18.6
	58.4	17.8
	59.8	17.8
0.5	76.2	50.4
	47.3	54.6
	94.0	52.8
	55.2	52.7

Appendix A.3

Individual diffusion coefficient results from Table 3.1

Diffusion Coefficients of Acetonitrile in Rubbery Region Obtained from Moving Boundary Model

Activity	Thickness (μm)	$D_r \times 10^{10}\ cm^2/s$
0.3	57.8	8.0
	39.4	8.2
	48.3	8.1
	49.4	8.4
0.4	42.7	30
	60.7	29
	58.4	33
	59.8	30
0.5	76.2	87
	47.3	89
	94.0	86
	55.2	85

Appendix A.4

Individual diffusion coefficient results from Table 4.3

Desorption Diffusion Coefficients of Acetonitrile in CA Obtained from Dual Mode Transport Model with Local Equilibrium Relaxation

Activity	Thickness (μm)	$D_D \times 10^9\ cm^2/s$
0.06	37.8	0.74
	30.8	0.8
	15.2	0.81
0.1	29.8	1.73
	33.6	1.28
	36.8	1.68
0.15	38.4	3.24
	38.7	3.18
	29.2	3.30
0.2	49.2	5.54
	34.2	7.56
	44.0	6.50
0.25	30.4	15.1
	58.4	13.1
	60.8	11.0

Appendix A.5

Individual diffusion coefficient results from Table 5.2

Diffusion Coefficients Obtained from Modified Dual Mode Transport Model Accounting for Plasticization with Local Equilibrium Relaxation

Activity	Thickness (μm)	$D_D \times 10^{10}\ cm^2/s$
0.06	37.8	1.43
	39.1	1.53
	30.8	1.41
	15.2	1.35
0.1	29.8	2.16
	33.6	2.16
	36.8	2.27
0.15	38.4	3.62
	38.3	3.62
	38.7	3.21
	29.2	3.43
0.2	49.2	4.91
	34.2	4.64
	44.0	4.73
0.25	30.4	5.14
	58.4	6.20
	60.8	5.81
0.3	71.6	5.39
	57.8	6.40
	39.4	6.49
	48.3	6.25
	49.4	6.07
0.4	42.7	15.2
	60.7	14.8
	58.4	16.7
	59.8	14.1
0.5	76.2	36.1
	47.3	38.2
	94.0	34.7
	55.2	31.8

Appendix A.6

Individual diffusion coefficient results from Table 5.4

Desorption Diffusion Coefficients Obtained from Modified Dual Mode Transport Model Accounting for Plasticization with Local Equilibrium Relaxation

Activity	Thickness (μm)	$D_D \times 10^9\ cm^2/s$
0.15	38.4	1.4
	38.7	1.4
	29.2	1.4
0.2	49.2	1.3
	34.2	1.6
	44.0	1.5
0.25	30.4	1.8
	58.4	1.9
	60.8	1.8

Appendix B. Matlab Programs

Appendix B.1

Program to fit mass uptake data by the simple Fickian model, Equation (2.3)

```
% Juchen Guo
% Fitting mass uptake data to obtain diffusion coefficient
% Before running program, first import mass uptake data file, and save it
% as ".mat" file.
clear
clf

actualL=5.04e-3;% actual film thickness in mass uptake experiments
L=actualL/2;% thickness used in Equation (2.3)
load m2b.mat;% load data to work space
t=m2b(:,1);% generate time array
Nt=length(t);

n=50;% number of terms in the infinite series of Equation (2.3)
D(1)=5.3e-10;% initial guess of diffusion coefficient
D_inc=1e-11;% interval
iteration=100;% number of repeating steps

% non-linear regression
for k=1:iteration
   % diffusion coefficient fitting loop
   for i=1:Nt
      % time loop
      for j=0:n
         h(j+1)=8/((2*j+1)^2*pi^2)*exp(-D(k)*(2*j+1)^2*pi^2*t(i)/(4*L^2));
      end
      M_ana(i)=1-sum(h);
      M_exp=m2b(:,5)';% actual experimental mass uptake data
      error(i)=M_ana(i)-M_exp(i);
      se(i)=error(i)^2;
   end
   D(k+1)=D(k)+D_inc;
   sse(k)=sum(se);
end
[sse_min,k_min]=min(sse);
D_min=D(k_min);% diffusion coefficient

% Generating the analytical solution from the best diffusion coefficient
t_ana=0:t(Nt)/60:t(Nt);
Nt_ana=length(t_ana);
```

```
for i=1:Nt_ana

      for j=0:n
         h_ana(j+1)=8/((2*j+1)^2*pi^2)*exp(-
D_min*(2*j+1)^2*pi^2*t_ana(i)/(4*L^2));
      end
      M_ana(i)=1-sum(h_ana);
end

sse_min
D_min
plot(t,M_exp,'*',t_ana,M_ana)
```

Appendix B.2

Program to fit ATR absorbance data by the simple Fickian model, Equation (2.4)

```
%Juchen Guo
% Fitting ATR diffusion data using simple Fickian model
% Before running program, first import corresponding data Excel file, and
% save it as .mat file.
clear
clf

load CA2BP.mat;% load data file to work space
L=4.92e-3;% thickness of polymer film [cm]
total_t=885.15*60;% total experimental time [s]
delta_t=total_t/1905;% experimental time interval [s]
t=[0:delta_t:total_t];
Nt=length(t);

n=50;% number of terms in the infinite series of Fickian analytical solution
n1=1.475;% refractive index of polymer
n2=2.43;% refractive index of ATR crystal
theta=pi/4;% incidence angle
wavenumber=2275;% peak of carbonyl group
lambda=1/wavenumber;% wave length
gamma=(2*n2*pi*sqrt((sin(theta)^2-(n1/n2)^2)))/lambda;% decay coefficient

D(1)=4.7e-10;% initial guess of diffusion coefficient
D_inc=1e-11;% step interval
iteration=50;% number of repeating steps

%Nonlinear regression
for k=1:iteration
   % diffusion coefficient fitting loop
   for i=1:Nt
      % time loop
      for j=0:n
         %numerical solution for infinite series
         f(j+1)=((2*j+1)*pi)/(2*L);
         g(j+1)=(-D(k)*(2*j+1)^2*pi^2*t(i))/(4*L^2);
         h(j+1)=(exp(g(j+1))*(f(j+1)*exp(-2*gamma*L)+(-1)^j*(2*gamma)))/...
            ((2*j+1)*(4*gamma^2+f(j+1)^2));
      end
```

```
        A_ana(i)=1-8*gamma/(pi*(1-exp(-2*gamma*L)))*sum(h);% analytical solution
        A_exp=CA2BP(:,2)';% experimental data
        error(i)=A_ana(i)-A_exp(i);
        se(i)=error(i)^2;
    end
    D(k+1)=D(k)+D_inc;
    sse(k)=sum(se);
end
[sse_min,k_min]=min(sse);
D_min=D(k_min);

% Generating the analytical solution from the best diffusion coefficient
for i=1:Nt

        for j=0:n
            f(j+1)=((2*j+1)*pi)/(2*L);
            g(j+1)=(-D_min*(2*j+1)^2*pi^2*t(i))/(4*L^2);
            h(j+1)=(exp(g(j+1))*(f(j+1)*exp(-2*gamma*L)+(-1)^j*(2*gamma)))/...
                ((2*j+1)*(4*gamma^2+f(j+1)^2));
        end
        A_ana(i)=1-8*gamma/(pi*(1-exp(-2*gamma*L)))*sum(h);
end

%Diffusion coefficient from the best fit
sse_min
D_min
plot(t,A_exp,t,A_ana)
```

Appendix B.3

Program to fit ATR absorbance data by the dual mode transport model with local equilibrium assumption, Equation (2.21)

```
% Juchen Guo
% Fitting ATR diffusion data to dual mode transport model with local
% equilibrium assumption, Equation (2.21)
% Before running program, first import ATR diffusion data, and save it as
% ".mat" file
clear all;
close all;
clf

L=6.08e-3;% thickness of film
delta_l=L/100;
l=[0:L/100:L];% thickness array
Nl=length(l);
load CA25CP.mat;% load ATR data to work space
total_t=1591.99*60;% experiment time
N=3365;% number of experimental data points
delta_t=total_t/(N-1);
t=[0:delta_t:total_t];% time array
Nt=length(t);

n1=1.475;% refractive index of polymer film
n2=2.43;% refractive index of ATR crystal
theta=pi/4;% incidence angle
wavenumber=2275;% peak of nitrile group
b=38.08;% Langmuir affinity constant
kd=0.2815;% Henry's law constant
CH=0.03;% hole saturation constant
CT=0.0977;% equilibrium concentration
activity=0.25;% experimental activity
alpha=b/kd;
kappa=CH*alpha;

D_d(1)=3.02e-9;% initial diffusion coefficient guess
D_inc=1e-11;% interval
iteration=50;% number of repeating steps

% Initial condition
for i=1:Nl
```

```
   c_d(i,1)=0;
end
% Boundary condition at upper surface
for j=2:Nt
   c_d(Nl,j)=CT-CH*b*activity/(1+b*activity);
end

%Nonlinear regression
for k=1:iteration
% Calculation of concentration of diffusion population.....................
   beta(k)=delta_t/(delta_l)^2*D_d(k);
   A=zeros((Nl-2),(Nl-2));
   for m=2:Nl-3

         A(m,m)=1+2*beta(k)*(1+alpha*c_d(m+1,1:Nt)).^2/((1+alpha*c_d(m+1,1:Nt)
         ).^2+kappa);
      A(m,m+1)=-
         beta(k)*(1+alpha*c_d(m+1,1:Nt)).^2/((1+alpha*c_d(m+1,1:Nt)).^2+kappa);
      A(m,m-1)=-
         beta(k)*(1+alpha*c_d(m+1,1:Nt)).^2/((1+alpha*c_d(m+1,1:Nt)).^2+kappa);
   end
   A(1,1)=1+beta(k)*(1+alpha*c_d(2,1:Nt)).^2/((1+alpha*c_d(2,1:Nt)).^2+kappa);
   A(1,2)=-beta(k)*(1+alpha*c_d(2,1:Nt)).^2/((1+alpha*c_d(2,1:Nt)).^2+kappa);
   A(Nl-2,Nl-2)=1+2*beta(k)*(1+alpha*c_d(Nl-1,1:Nt)).^2/((1+alpha*c_d(Nl-
         1,1:Nt)).^2+kappa);
   A(Nl-2,Nl-3)=-beta(k)*(1+alpha*c_d(Nl-1,1:Nt)).^2/((1+alpha*c_d(Nl-
         1,1:Nt)).^2+kappa);
   G=zeros((Nl-2),1);
   for j=1:Nt-1
      G((Nl-2),1)=c_d(Nl,Nt)*beta(k)*(1+alpha*c_d(Nl-1,j)).^2/((1+alpha*c_d(Nl-
         1,j)).^2+kappa);
      F=c_d(2:Nl-1,j);
      K=F+G;
      c_d(2:Nl-1,j+1)=A\K;
   end
   c_d(1,2:Nt)=c_d(2,2:Nt);% boundary condition at lower surface
%-------------------------------------------------------------------------------------

% conversion of concentration to absorbance-----------------------------------------
   lambda=1/wavenumber;
   r=(2*n2*pi*sqrt((sin(theta)^2-(n1/n2)^2)))/lambda;
   for i=1:Nt
      A_ana(i)=trapz(l,c_d(:,i)'.*exp(-2*r*l))/trapz(l,c_d(:,Nt)'.*exp(-2*r*l));
%-------------------------------------------------------------------------------------
      A_exp=CA25CP(:,4)';% actual experimental ATR data
      error(i)=A_ana(i)-A_exp(i);
```

```
        se(i)=error(i)^2;
    end
    D_d(k+1)=D_d(k)+D_inc;
    sse(k)=sum(se);
end
[sse_min,k_min]=min(sse);
D_min=D_d(k_min);% diffusion coefficient

% Generating the analytical solution from the best diffusion coefficient
beta_m=delta_t/(delta_l)^2*D_min;
for i=1:Nl
    c_d(i,1)=0;
end
for j=2:Nt
    c_d(Nl,j)=CT-CH*b*activity/(1+b*activity);
end

A=zeros((Nl-2),(Nl-2));
for m=2:Nl-3

        A(m,m)=1+2*beta_m*(1+alpha*c_d(m+1,1:Nt)).^2/((1+alpha*c_d(m+1,1:Nt
        )).^2+kappa);
    A(m,m+1)=-
        beta_m*(1+alpha*c_d(m+1,1:Nt)).^2/((1+alpha*c_d(m+1,1:Nt)).^2+kappa);
    A(m,m-1)=-
        beta_m*(1+alpha*c_d(m+1,1:Nt)).^2/((1+alpha*c_d(m+1,1:Nt)).^2+kappa);
end
A(1,1)=1+beta_m*(1+alpha*c_d(2,1:Nt)).^2/((1+alpha*c_d(2,1:Nt)).^2+kappa);
A(1,2)=-beta_m*(1+alpha*c_d(2,1:Nt)).^2/((1+alpha*c_d(2,1:Nt)).^2+kappa);
A(Nl-2,Nl-2)=1+2*beta_m*(1+alpha*c_d(Nl-1,1:Nt)).^2/((1+alpha*c_d(Nl-
        1,1:Nt)).^2+kappa);
A(Nl-2,Nl-3)=-beta_m*(1+alpha*c_d(Nl-1,1:Nt)).^2/((1+alpha*c_d(Nl-
        1,1:Nt)).^2+kappa);


G=zeros((Nl-2),1);
for j=1:Nt-1
    G((Nl-2),1)=c_d(Nl,Nt)*beta_m*(1+alpha*c_d(Nl-1,j)).^2/((1+alpha*c_d(Nl-
        1,j)).^2+kappa);
    F=c_d(2:Nl-1,j);
    K=F+G;
    c_d(2:Nl-1,j+1)=A\K;
end
c_d(1,2:Nt)=c_d(2,2:Nt);

for i=1:Nt
```

```
   A_ana(i)=trapz(l,c_d(:,i)'.*exp(-2*r*l));
end
A_ana=A_ana/A_ana(Nt);

D_min
sse_min
plot(t,A_ana,t,A_exp)
xlabel('Time (sec.)')
ylabel('A_D/A_D_e_q_.')
title('Activity=0.25')
```

Appendix B.4

Program to fit ATR absorbance data by the dual mode transport model with local equilibrium relaxation, Equations (2.22) and (2.23)

```
% Juchen Guo
% Fitting ATR diffusion to dual mode transport model with local equilibrium
% assumption relaxed
% before running program, first import ATR diffusion data, and save it as
% ".mat" file
clear all
close all
clf

function main()
global z
z=0
x0=[1.95e-5, 4.0e-3];% initial guesses
lb=[1e-5, 1e-3];% lower boundary
ub=[1e-4, 1e-2];* upper Boundary
options=optimset('LargeScale','off','Display','on','MaxFunEvals',15000,'MaxIter',1500
0);
x = fmincon(@objfun,x0,[],[],[],[],lb,ub,[],options);

function obj=objfun(x)

global z;
z=z+1
m = 0;
sigma=x(1);% dimensionless factor sqrt(D/kr)
kr=x(2);

L=7.62e-3;
delta_l=L/100;
l=[0:delta_l:L];
xi=l/sqrt(sigma);% dimensionless length array
total_t=351.1*60;
N=761;
delta_t=total_t/(N-1);
t=[0:delta_t:total_t];
tau=t*kr;% dimensionless time array
Ntau=length(tau);
```

```
sol = pdepe(m,@pdex4pde,@pdex4ic,@pdex4bc,xi,tau);
theta_d = sol(:,:,1);
theta_h = sol(:,:,2);
theta_t=theta_d+theta_h;
n1=1.475;
n2=2.43;
theta=pi/4;
wavenumber=2275;
lambda=1/wavenumber;
r=(2*n2*pi*sqrt((sin(theta)^2-(n1/n2)^2)))/lambda;
for i=1:Ntau
   % conversion of concentration to absorbance
   A_i(i)=trapz(l,theta_t(i,:).*exp(-2*r*l));
end
A_i=A_i/A_i(Ntau);
load CAATY.mat;% load ATR data to work space
A_m=CAATY(:,6)';% actual ATR data
obj=sum((A_i-A_m).^2)
x
% --------------------------------------------------------------------------
function [c,f,s] = pdex4pde(xi,tau,u,DuDx)
CT=0.1689;% total concentration
b=38.08;% Langmuir affinity constant
kd=0.2815;% Henry's law constant
alpha=b/kd*CT;
CH=0.03;% hole saturation constant
thetaH=CH/CT;
c = [1; 1];
f = [1; 1e-50] .* DuDx;
F = alpha*u(1)*(thetaH-u(2))-u(2);
s = [-F; F];
% Initial condition----------------------------------------------------------
function u0 = pdex4ic(xi);
u0 = [0; 0];
% Boundary conditions --------------------------------------------------------
function [pl,ql,pr,qr] = pdex4bc(xl,ul,xr,ur,tau)
CT=0.1689;
CH=0.03;
thetaH=CH/CT;
b=38.08;
a=0.5;% activity
pl = [0; 0];
ql = [1; 1];
pr = [ur(1)-1+thetaH*(b*a/(1+b*a)); ur(2)-thetaH*(b*a/(1+b*a))];
qr = [0; 0];
```

Appendix B.5

Program to predict mass uptake data by the dual mode transport model with local equilibrium relaxation

```
% Juchen Guo
% Simulate mass uptake data from Dual mode transport model with local
% equilibrium assumption relaxed

function pdex4

m = 0;
D_d=8.06e-10;% diffusion coefficient
kr=4.88e-3;% hole-emptying rate constant
sigma=D_d/kr;
L=2.41e-3;% half of film thickness used in mass uptake experiment
delta_l=L/100;
l=[0:delta_l:L];
xi=l/sqrt(sigma);
total_t=862.53*60;% experimental time
N=1859;% number of data points
delta_t=total_t/(N-1);
t=[0:delta_t:total_t];
tau=t*kr;
Ntau=length(tau);

sol = pdepe(m,@pdex4pde,@pdex4ic,@pdex4bc,xi,tau);
theta_d = sol(:,:,1);
theta_h = sol(:,:,2);
theta_t=theta_d+theta_h;
n1=1.475;
n2=2.43;
theta=pi/4;
wavenumber=2275;
lambda=1/wavenumber;
r=(2*n2*pi*sqrt((sin(theta)^2-(n1/n2)^2)))/lambda;

for i=1:Ntau
   M_i(i)=trapz(l,theta_d(i,:));
end
M_i=M_i/M_i(Ntau)

%-------------------------------------------------------------
```

```
function [c,f,s] = pdex4pde(xi,tau,u,DuDx)
CT=0.1122;
b=38.08;
kd=0.2815;
alpha=b/kd*CT;
CH=0.03;
thetaH=CH/CT;
c = [1; 1];
f = [1; 1e-50] .* DuDx;
F = alpha*u(1)*(thetaH-u(2))-u(2);
s = [-F; F];
% --------------------------------------------------------------
function u0 = pdex4ic(xi);
u0 = [0; 0];
% --------------------------------------------------------------
function [pl,ql,pr,qr] = pdex4bc(xl,ul,xr,ur,tau)
CT=0.1122;
CH=0.03;
thetaH=CH/CT;
b=38.08;
a=0.3;
pl = [0; 0];
ql = [1; 1];
pr = [ur(1)-1+thetaH*(b*a/(1+b*a)); ur(2)-thetaH*(b*a/(1+b*a))];
qr = [0; 0];
```

Appendix B.6

Program to fit ATR absorbance data by the moving boundary model

```
% Juchen Guo
% Fitting ATR diffusion data to moving boundary model
% before running program, first import ATR diffusion data and save it as
% ".mat" file

clear all;
close all;
clf


D_1(1)=8.3e-9;% initial guess of diffusion coefficient in glassy region
D_2=7.04e-10;% diffusion coefficient in rubbery region
D_inc=1e-10;% interval of D
k(1)=7e-5;% initial guess of k
k_inc=1e-6;% interval of k
iteration=50;

load CAATY.mat;% load ATR data to work space
total_time=351.1*60;
total_n=761;
L=7.62e-3;
Cx=0.0977;% moving boundary concentration
Cl=0.1689;% equilibrium concentration
n1=1.475;
n2=2.43;
theta=pi/4;
wavenumber=2275;
lambda=1/wavenumber;
r=(2*n2*pi*sqrt((sin(theta)^2-(n1/n2)^2)))/lambda;
l_k=[0:L/100:L];

for n=1:iteration
 % determine value of k----------------------------------------------------
for i=1:iteration
    A_coeff=(Cx-Cl)/erf(k(i)/(2*sqrt(D_1(n))));
    Abs_k=1+(Cx/Cl-1)*(1-exp(-2*r*L))^-1-A_coeff*k(i)*(exp(2*r*L)-1)...
        ^-1/(Cl*L*sqrt(pi*D_1(n)))*trapz(l_k,exp(-
k(i)^2*l_k.^2/(4*L^2*D_1(n))+2*r*l_k));
    t_k=L^2/k(i)^2/60;
```

```
    error=(CAATY(:,1)'-t_k).^2;
    [err_min, t_row]=min(error);
    Abs_err(i)=(CAATY(t_row,6)-Abs_k)^2;
    k(i+1)=k(i)+k_inc;
end

[Abs_err_min,k_min]=min(Abs_err);
k=k(k_min);
A_coeff=(Cx-Cl)/erf(k/(2*sqrt(D_1(n))));
%--------------------------------------------------------------------------
delta_t=total_time/(total_n-1);
delta_l=k^2*delta_t/L;
l=[0:delta_l:L];
Nl=length(l);
t=[0:delta_t:total_time];
Nt=length(t);
b=38.08;% Langmuir affinity constant
kd=0.2815;% Henry's law constant
kr=4.85e-3;% hole-emptying rate constant
kf=kr*b/kd;% hole-filling rate constant
beta=delta_t/(delta_l)^2*D_2;
gamma=delta_t*kf;
phi=kr*delta_t;
CH=0.03;% hole saturation constant

c_rubbery=zeros(Nl,Nt);
c_d=zeros(Nl,Nt);
c_h=zeros(Nl,Nt);
A_pre=zeros(1,Nt);

for j=2:Nl
    B_t=A_coeff*sqrt(D_1(n)/(pi*t(j)))*exp(-k^2/(4*D_1(n)))/D_2;
    l_rubbery=k*sqrt((j-1)*delta_t);% length of rubbery region
    Nrubbery=l_rubbery/delta_l;
    n_rubbery=round(Nrubbery);
    z_rubbery=[0:delta_l:delta_l*n_rubbery];
    m=length(z_rubbery);
    c_rubbery(1:m,j)=Cl+A_coeff*erf(z_rubbery./(2*sqrt(D_1(n)*(j-1)*delta_t)));
    c_d(m,j)=Cx-c_h(m,j);% condition on moving boundary
    if m+1<Nl
    A=zeros((Nl-m),(Nl-m));
    B=ones(1,(Nl-m));
    C=ones(1,(Nl-(m+1)));
    D=-beta*C;
    E=(1+2*beta)*B;
    Matrix=A+diag(D,-1)+diag(D,1)+diag(E);
```

```
    Matrix(1,1)=1+beta;
    Matrix(Nl-m,Nl-m)=1+beta;
    G=zeros((Nl-m),1);
    G(1,1)=-B_t*beta*delta_l;
    F=c_d(m:Nl-1,j-1).*(1-gamma*(CH-c_h(m:Nl-1,j-1)))+phi*...
        c_h(m:Nl-1,j-1);
    K=F+G;
    c_d(m:Nl-1,j)=Matrix\K;
    c_h(m,j)=Cx-c_d(m,j);
    c_h(m+1:Nl-1,j)=gamma*c_d(m+1:Nl-1,j-1).*(CH-c_h(m+1:Nl-1,j-1))+...
        c_h(m+1:Nl-1,j-1)*(1-phi);% condition on moving boundary
    end
end

c_d(Nl,2:Nl)=c_d(Nl-1,2:Nl);
c_h(Nl,2:Nl)=c_h(Nl-1,2:Nl);
c_glassy=c_d+c_h;
c_total=c_rubbery+c_glassy;

for i=1:Nl
    A_pre(i)=trapz(l,c_total(:,i)'.*exp(-2*r*(L-l)));
end

for i=Nl+1:Nt
        for s=1:70
            g(s)=(2*s-1)*pi/(2*L);
            P(s)=trapz(l,erf(k*l/(2*L*sqrt(D_1(n))))).*sin(g(s)*l));
            Q(s)=exp(-g(s)^2*D_1(n)*(t(i)-(L/k)^2));
            O(s)=(2*r*(-1)^(s+1)+exp(-2*r*L)+g(s))/(g(s)^2+4*r^2);
            R(s)=P(s)*O(s)*Q(s);
        end
        A_post(i)=Cl*(1-exp(-2*r*L))/(2*r)+2*A_coeff*sum(R)/L;
end

A_i=A_pre+A_post;
A_i=A_i/A_i(Nt);
A_m=CAATY(:,6)';
sse(n)=sum((A_i-A_m).^2);
D_1(n+1)=D_1(n)+D_inc;
end
[sse_min,k_min]=min(sse)
D_min=D(k_min)
```

Appendix B.7

Program to fit desorption ATR absorbance data by the simple Fickian model, Equation (4.3)

```
% Juchen Guo
% Fitting ATR desorption diffusion data to simple Fickian model
% Before running program, first import ATR desorption diffusion data and
% save it as ".mat" file
clear
clf

L=4.4e-3;
delta_l=L/100;
l=[0:L/100:L];
Nl=length(l);
load CA2EN.mat;
total_t=309.1*60;
N=665;
delta_t=total_t/(N-1);
t=[0:delta_t:total_t];
Nt=length(t);

n=50;
n1=1.475;
n2=2.43;
theta=pi/4;
wavenumber=2275;
lambda=1/wavenumber;
gamma=(2*n2*pi*sqrt((sin(theta)^2-(n1/n2)^2)))/lambda;

D(1)=3.7e-10;
D_inc=1e-11;
iteration=50;

for k=1:iteration

   for i=1:Nt

      for j=0:n
         f(j+1)=((2*j+1)*pi)/(2*L);
         g(j+1)=(-D(k)*(2*j+1)^2*pi^2*t(i))/(4*L^2);
         h(j+1)=(exp(-2*gamma*L)*f(j+1)*(-1)^j+2*gamma)/(4*gamma^2+f(j+1)^2);
```

```
        m(j+1)=4*(-1)^j*2*gamma/((1-exp(-2*gamma*L))*pi*(2*j+1));
        o(j+1)=exp(g(j+1))*h(j+1)*m(j+1);
      end
      A_ana(i)=sum(o);
      A_exp=CA2EN(:,5)';
      error(i)=A_ana(i)-A_exp(i);
      se(i)=error(i)^2;
   end
   D(k+1)=D(k)+D_inc;
   sse(k)=sum(se);
end
[sse_min,k_min]=min(sse);
D_min=D(k_min);

for i=1:Nt

      for j=0:n
        f(j+1)=((2*j+1)*pi)/(2*L);
        g(j+1)=(-D_min*(2*j+1)^2*pi^2*t(i))/(4*L^2);
        h(j+1)=(exp(-2*gamma*L)*f(j+1)*(-1)^j+2*gamma)/(4*gamma^2+f(j+1)^2);
        m(j+1)=4*(-1)^j*2*gamma/((1-exp(-2*gamma*L))*pi*(2*j+1));
        o(j+1)=exp(g(j+1))*h(j+1)*m(j+1);
      end
      A_ana(i)=sum(o);
end

sse_min
D_min

plot(t,A_exp,t,A_ana)
```

Appendix B.8

Program to fit desorption ATR absorbance data by the dual mode transport model with local equilibrium relaxation, Equations (4.7) and (4.8)

```
% Juchen Guo
% Fitting ATR desorption diffusion data to dual mode transport model with
% local equilibrium assumption relaxed
% Before running program, first import ATR desorption diffusion data and
% save it as ".mat" file.

function main()
global z
z=0
x0=[2.0e-5, 5.4e-4];
lb=[1e-5, 1e-4];
ub=[2e-4, 1e-3];
options=optimset('LargeScale','off','Display','on','MaxFunEvals',15000,'MaxIter',1500
0);
x = fmincon(@objfun,x0,[],[],[],[],lb,ub,[],options);

function obj=objfun(x)
global z;
z=z+1
m = 0;

sigma=x(1);
kr=x(2);
L=6.08e-3;
delta_l=L/100;
l=[0:delta_l:L];
xi=l/sqrt(sigma);
delta_t=593.64/1170*60;
t=[0:delta_t:593.64*60];
tau=t*kr;
Ntau=length(tau);

sol = pdepe(m,@pdex4pde,@pdex4ic,@pdex4bc,xi,tau);
theta_d = sol(:,:,1);
theta_h = sol(:,:,2);
theta_t=theta_d+theta_h;
n1=1.475;
n2=2.43;
```

```
theta=pi/4;
wavenumber=2275;
lambda=1/wavenumber;
r=(2*n2*pi*sqrt((sin(theta)^2-(n1/n2)^2)))/lambda;
for i=1:Ntau
    A_i(i)=trapz(l,theta_t(i,:).*exp(-2*r*l));
end
A_i=A_i/A_i(1);
load CA25CN.mat;
A_m=CA25CN(:,5)';
obj=sum((A_i-A_m).^2)
x
% --------------------------------------------------------------
function [c,f,s] = pdex4pde(xi,tau,u,DuDx)
CT=0.0977;
CH=0.094;
b=38.08;
kd=0.05928;
alpha=b/kd*CT;
thetaH=CH/CT;
c = [1; 1];
f = [1; 1e-50] .* DuDx;
F = alpha*u(1)*(thetaH-u(2))-u(2);
s = [-F; F];
% --------------------------------------------------------------
function u0 = pdex4ic(xi);
CT=0.0977;
CH=0.094;
b=38.08;
thetaH=CH/CT;
a=0.25;
u0 = [1-thetaH*(b*a/(1+b*a)); thetaH*(b*a/(1+b*a))];
% --------------------------------------------------------------
function [pl,ql,pr,qr] = pdex4bc(xl,ul,xr,ur,tau)
pl = [0; 0];
ql = [1; 1];
pr = [ur(1); ur(2)];
qr = [0; 0];
```

Appendix B.9

Program to fit ATR absorbance data by the modified dual mode transport model taking into account plasticization, Equations (5.9) and (5.10)

```
% Juchen Guo
% Fitting ATR diffusion to Modified dual mode transprot model accounting
% for plasticization effect
% before running program, first import ATR diffusion data, and save it as
% ".mat" file

function main()
global z
z=0
x0=[2.3e-10, 4e-4];% initial guesses
lb=[1e-10, 1e-5];% lower boundary
ub=[2e-8, 1e-3];% upper Boundary
options=optimset('LargeScale','off','Display','on','MaxFunEvals',15000,'MaxIter',1500
0);
x = fmincon(@objfun,x0,[],[],[],[],lb,ub,[],options);

function obj=objfun(x)

global z D kr;
z=z+1
m = 0;
D=x(1);% dimensionless factor (D/kr)
kr=x(2);

L=1.43e-3;
delta_l=L/100;
l=[0:delta_l:L];
delta_t=767/1655*60;
t=[0:delta_t:767*60];
Nt=length(t);

sol = pdepe(m,@pdex4pde,@pdex4ic,@pdex4bc,l,t);
cd = sol(:,:,1);
ch = sol(:,:,2);
ct=cd+ch;
n1=1.475;
n2=2.43;
theta=pi/4;
wavenumber=2275;
```

```
lambda=1/wavenumber;
r=(2*n2*pi*sqrt((sin(theta)^2-(n1/n2)^2)))/lambda;
for i=1:Nt
    A_i(i)=trapz(l,ct(i,:).*exp(-2*r*l));
end
A_i=A_i/A_i(Nt);
% A_i'
load CA1GP.mat;
A_m=CA1GP(:,4)';
obj=sum((A_i-A_m).^2)
x
% --------------------------------------------------------------------
function [c,f,s] = pdex4pde(l,t,u,DuDx)
global kr D
phi=0;
b=40.17;
kd=0.3754;
kf=kr*b/kd;
CH=0.02833;
CG=0.0523;
c = [1; 1];
f = [D; 1e-50] .* DuDx;
F = kf*u(1)*(CH*(1-(u(1)+phi*u(2))/CG)-u(2))-kr*u(2);
s = [-F; F];
% --------------------------------------------------------------
function u0 = pdex4ic(l);
u0 = [0; 0];
% --------------------------------------------------------------
function [pl,ql,pr,qr] = pdex4bc(xl,ul,xr,ur,t)
CT=0.0523;
kd=0.3754;
a=0.1;
pl = [0; 0];
ql = [1; 1];
pr = [ur(1)-kd*a; ur(2)-CT+kd*a];
qr = [0; 0];
```

Appendix B.10

Program to predict mass uptake data by the modified dual mode transport model taking into account plasticization

```
% Juchen Guo
% Simulate mass uptake data from modified dual mode transport model
% accounting plasticization effect

function pdex4
m = 0;
L=1.43e-3;
delta_l=L/100;
x=[0:delta_l:L];
total_t=767*60;
N=1656;
delta_t=total_t/(N-1);
t=[0:delta_t:total_t];
Nt=length(t);

sol = pdepe(m,@pdex4pde,@pdex4ic,@pdex4bc,x,t);
cd = sol(:,:,1);
ch = sol(:,:,2);
ct=cd+ch;
n1=1.475;
n2=2.43;
theta=pi/4;
wavenumber=2275;
lambda=1/wavenumber;
r=(2*n2*pi*sqrt((sin(theta)^2-(n1/n2)^2)))/lambda;

for i=1:Nt
    M_i(i)=trapz(x,ct(i,:));
end
M_i=M_i/M_i(Nt);
M_i'

function [c,f,s] = pdex4pde(x,t,u,DuDx)
D=2.3e-10;
phi=0;
kr=4.74e-3;
b=40.17;
kd=0.3754;
kf=kr*b/kd;
```

```
CH=0.02833;
CG=0.0523;
c = [1; 1];
f = [D; 1e-50] .* DuDx;
F = kf*u(1)*(CH*(1-(u(1)+phi*u(2))/CG)-u(2))-kr*u(2);
s = [-F; F];
% --------------------------------------------------------------
function u0 = pdex4ic(x);
u0 = [0; 0];
% --------------------------------------------------------------
function [pl,ql,pr,qr] = pdex4bc(xl,ul,xr,ur,t)
CT=0.0523;
kd=0.3754;
a=0.1;
pl = [0; 0];
ql = [1; 1];
pr = [ur(1)-kd*a; ur(2)-CT+kd*a];
qr = [0; 0];
```

Bibliography

1. Crank, J and Park, G. S. *Diffusion in Polymers*, Academic Press, London and New York, 1968.
2. Crank, J. *The Mathematics of Diffusion*, Clarendon Press, Oxford, 1975.
3. Alfrey, T. Jr, Gurnee, E. F. and Lloyd, W. G. *Journal of polymer Science: Part C* 1966, 12, 249.
4. Peterlin, A. *Journal of polymer Science: Part C, Polymer Letters* 1965, 3, 1083.
5. Peterlin, A. *Die Makromolekulare Chemie* 1969, 1245, 136.
6. Frisch, H. L. *Polymer Engineering and Science* 1980, 20, 1, 2.
7. Kwei, T. K., Zupko, H. M. *Journal of polymer Science: Part A-2* 1969, 7, 867.
8. Frisch, H. L. *Journal of polymer Science: Part A-2* 1969, 7, 879.
9. Wang, T. T., Kwei, T. K. *Journal of polymer Science: Part A-2* 1969, 7, 2019.
10. Kishimoto, A., Fujita, H., Odani, H., Kurata, M. and Tamura, M. *Journal of Physical Chemistry* 1960, 64, 594.
11. Neogi, P., Kim, M. and Yang, Y. *AIChE Iournal* 1986, 32, 7, 1146.
12. Ocone, R. and Astarita, G. *AIChE Iournal* 1987, 33, 3, 423.
13. Camera-Roda, G. and Sarti, G. C. *AIChE Iournal* 1990, 36, 6, 851.
14. Kalospiros, N. S., Ocone, R., Astarita, G. and Meldon, J. H. *Ind. Eng. Chem. Res.* 1991, 30, 851.

15. Kwei, T. K., Wang, T. T. and Zupko, H. M. *Macromolecules* 1972, 5, 5, 645.

16. Wang, T. T., Kwei, T. K. *Macromolecules* 1973, 6, 6, 919.

17. Barrer, R. M., Diffusion in and through Solids, Cambridge University Press, London, 1951.

18. Fujita, H. *Fortschr. Hochpolym.-Forsch.* 1961, 3, 1.

19. Vrentas, J. S. and Duda, J. L. *Journal of Polymer Science: Polymer Physics Edition* 1977, 15, 403.

20. Vrentas, J. S. and Duda, J. L. *Journal of Polymer Science: Polymer Physics Edition* 1977, 15, 417.

21. Meares, P., *J. Am. Chem. Soc.* 1954, 76, 3415.

22. Michaels, A. S., Vieth, W. R. and Barrie, J. A. *Journal of Applied Physics* 1963, 34, 1, 1.

23. Michaels, A. S., Vieth, W. R. and Barrie, J. A. *Journal of Applied Physics* 1963, 34, 1, 13.

24. Vieth, W. R., Alcalay, H. H. and Frabetti, A. J. *Journal of Applied Polymer Science* 1964, 8, 2125.

25. Vieth, W. R. and Sladek, K. J. *Journal of Colloid Science* 1965, 20, 1014.

26. Vieth, W. R. *Diffusion In and Through Polymers Principles and Applications,* Hanser Publishers, Munich Vienna New York Barcelona, 1991.

27. Paul. D. R. *Journal of Polymer Science: Part A*-2 1969, 7, 1811.

28. Petropoulos, J. H. *Journal of Polymer Science: Part A*-2 1970, 8, 1797.

29. Paul, D. R. and Koros, W. J. *Journal of Polymer Science: Polymer Physics Edition* 1976, 14, 675.

30. Koros, W. J., Paul, D. R. and Rocha, A. A. *Journal of Polymer Science: Polymer Physics Edition* 1976, 14, 687.

31. Tshudy, J. A. and Von Frankenberg, C. *Journal of Polymer Science: Polymer Physics Edition* 1973, 11, 2027.

32. Mauze, G. R. and Stern, S. A., *Journal of Polymer Science* 1982, 12, 51.

33. Mauze, G. R. and Stern, S. A., *Polym. Eng. Sci.* 1983, 23, 548.

34. Kamiya, Y., Hirose, T., Mizoguchi, K., and Naito, Y. *Journal of Polymer Science: Part B: Polymer Physics* 1986, 24, 1525.

35. Elabd, Y. A., Baschetti, M. G. and Barbari, T. A., *Journal of Polymer Science: Part B: Polymer Physics* 2003, 41, 22, 2794.

36. Tong, H. M., Saenger, K. L. and Durning, C. J., *Journal of Polymer Science: Part B: Polymer Physics* 1989, 27, 689.

37. Hassan, M. M. and Durning, C. J., *Journal of Polymer Science: Part B: Polymer Physics* 1999, 37, 22, 3171.

38. Roger, P., Mattisson, C., Axelsson, A. and Zacchi, G., *Biotechnology and Bioengineering* 2000, 69, 9, 654.

39. Mattisson, C., Karlsson, D., Pettersson, S. G., Zacchi, G. and Axelsson, A., *Journal of Physics D: Applied Physics* 2001, 34, 20, 3088.

40. Schottler, N. E. and Furland, P. Y., *Polymer* 1992, 33, 3323.

41. Filippov, L. K., *Chemical Engineering Science* 1993, 48, 19, 3391.

42. Wind, J. D., Sirard, S. M., Paul, D. R., Green, P. F., Johnston, K. P. and Koros, W. J., *Macromolecules* 2003, 36, 17, 6433.

43. Wind, J. D., Sirard, S. M., Paul, D. R., Green, P. F., Johnston, K. P. and Koros, W. J., *Macromolecules* 2003, 36, 17, 6442.

44. Pawlisch, C. A., Macris, A. and Laurence, R. L., *Macromolecules* 1987, 20, 1564.

45. Pawlisch, C. A., Bric, J. R. and Laurence, R. L., *Macromolecules* 1988, 21, 1685.

46. Bonifaci, L., Carnell, Lino. And Cori, L., *Journal of Applied Polymer Science* 1994, 51, 11, 1923.

47. Xie, L. Q., *Polymer* 1993, 34, 21, 4579.

48. Cai, W. D., Ramesh, N., Tihminlioglu, F., Danner, R. P., Duda, J. L. and De Haan, A., *Journal of Polymer Science: Part B: Polymer Physics* 2002, 40, 10, 1046.

49. Kosmeyer, R. W., Mierwan, V. E. and Peppas N. A., *Journal of Polymer Science: Part B: Polymer Physics* 1986, 24, 409.

50. Hui, C. Y., Wu, K. C., Laskey, R. C. and Kramer, E. J., *Applied Physics* 1987, 61, 5137.

51. Mills, P. J., Palmstrom, C. J. and Kramer, E. J., *Journal of Materials Science* 1986, 21, 5, 1479.

52. Romanelli, J. F., Mayer, J. W., Kramer, E. J. and Russell, T. P., *Journal of Polymer Science, Polymer Physics Edition* 1986, 24, 2, 263.

53. Laskey, R. C., Kramer, E. J. and Hui, C. Y., *Polymer* 1988, 29, 4, 673.

54. Laskey, R. C., Kramer, E. J. and Hui, C. Y., *Polymer* 1988, 29, 6, 1131.

55. Gall, T. P., Laskey, R. C. and Kramer, E. J., *Polymer* 1990, 31, 8, 1491.

56. Trifonov, A., Nikolov, P., Kolev, D and Tsenov, I. *Phys Status solidi A* 1975, 27, 135.

57. Lavrent'ev, V. V., Popov, V. Y. and Vasenin, R. M. *Vysokomol Soedin A* 1975, 17, 1621.

58. Lavrent'ev, V. V., Popov, V. Y. and Vasenin, R. M. *Zh Fiz Khim* 1975, 49, 2652.

59. Popov, V. Y., Remizov, N. A., and Lavrent'ev V. V. *Kolloidn Zh* 1976, 37, 1212.

60. Popov, V. Y., Tarasevich, B. N. and Momotenko, V. A. *Proc Moscow Univ Chem* 1976, 17, 721.

61. Popov, V. Y. and Lavrent'ev V. V. *J Appl Spectrosc* 1980, 32, 193.

62. Popov, V. Y. and Lavrent'ev V. V. *Zh Prikl Spektrosk* 1980, 32, 336.

63. Remizov, N. A., Chalykh, A. Y., Popov, V. Y. and lavrent'ev V. V. *Vysokomol Soedin A* 1982, 24, 1853.

64. Brandt, V. H. and Riegger, P. *Exp Tech Phys* 1984, 32, 413.

65. Hemmelman, K. and Brandt, V. H. *Exp Tech Phys* 1986, 34, 439.

66. Brandt, V. H. and Hemmelman, K. *Exp Tech Phys* 1987, 35, 349.

67. Hemmelman, K. and Brandt, V. H. *Exp Tech Phys* 1989, 37, 495.

68. Xu, J. R. and Balik, C. M. *Appl Spectrosc* 1988, 42, 1543.

69. Xu, J. R. and Balik, C. M. *Appl Polym Sci* 1989, 38, 173.

70. Balik, C. M. and Xu, J. R. *Appl Polym Sci* 1994, 52, 975.

71. Fieldson, G. T., Barbari, T. A. *Polymer*, 1993, 34, 6, 1146.

72. Fieldson, G. T., Barbari, T. A. *AIChE Journal* 1995, 41, 4, 795.

73. Barbari, T. A., Kasargod, S. S. and Fieldson, G. T. *Ind. Eng. Chem. Res.* 1996, 35, 1188.

74. Hong, S. U., Barbari, T. A. and Sloan, J. M. *Journal of Polymer Science, Part B: Polymer Physics* 1997, v 35, n 8, 1261.

75. Hong, S. U., Barbari, T. A. and Sloan, J. M. *Journal of Polymer Science, Part B: Polymer Physics* 1998, v 36, n 2, 337.

76. Hong, S. U., Barbari, T. A. *Journal of Polymer Science, Part B: Polymer Physics* 2001, v 39, n 9, 908.

77. Elabd Y.A. *Ph.D Thesis*, Johns Hopkins University, 2000.

78. Elabd, Y. A., Sloan, J. M. and Barbari, T. A. *Polymer* 2000, 41, 2203.

79. Elabd, Y. A., Barbari, T. A. *AIChE Journal* 2001, 47, 6, 1255.

80. Elabd, Y. A., Barbari, T. A. *Industrial & Engineering Chemistry Research* 2001, 40, 14, 3076.

81. Elabd, Y. A., Sloan, J. M., Tan, N. B. and Barbari, T. A. *Macromolecules* 2001, 34, 6268.

82. Elabd, Y. A., Barbari, T. A. *AIChE Journal* 2002, 48, 8, 1610.

83. Pereira, M. R., Yarwood, J. *J. Chem. Soc., Faraday Trans*. 1996, 92, 2731.

84. Pereira, M. R., Yarwood, J. *J. Chem. Soc., Faraday Trans.* 1996, 92, 2737.

85. Sammon, C., Everall, N. and Yarwood, J. *Macromol. Symp*. 1997, 119, 189.

86. Hajatdoost, S., Yarwood, J. *J. Chem. Soc., Faraday Trans.* 1997, 93, 1613.

87. Sammon, C., Mura, C., Yarwood, J., Everall, N., Swart, R. and Hodge, D. *J. Phys. Chem. B* 1998, 102, 3402.

88. Yarwood, J., Sammon, C., Mura, C. and Pereira, M. *Journal of Molecular Liquids* 1999, 80, 93.

89. Sammon, C., Yarwood, J. and Everall, N. *Polymer* 2000, 41, 2521.

90. Eaton, P., Holmees, P. and Yarwood, J. *Appl Spectrosc* 2000, 54, 508.

91. Mura, C., Yarwood, J., Swart, R. and Hodge, D. *Polymer* 2001, 42, 4141.

92. Eaton, P., Holmes, P. and Yarwood, J. *J Appl Polym Sci* 2001, 82, 2016.

93. Sammon, C., Mura, C., Hajatdoost, S. and Yarwood, J. *Journal of Molecular Liquids* 2002, 96-97, 305.

94. Sammon, C., Deng, C. S., Mura, C. and Yarwood, J. *Journal of Molecular Liquids* 2002, 101, 35.

95. Hajatdoost, S., Sammon, C. and Yarwood, J. *Polymer* 2002, 43, 1821.

96. Deng, C., Sammon, C. and Yarwood, J. *Polymer* 2003, 44, 2057.

97. Philippe, L., Sammon, C., Lyon, S. B. and Yarwood, J., *Progress in Organic Coating* 2004, 49, 315.

98. Doppers, L.-M., Sammon, C., Breen, C. and Yarwood, J., *Polymer* 2006, 47, 2714.

99. Dobbyn, V., Howley, R., Kirwan, P. and McLoughlin, P., *Intern. J. Environ. Anal. Chem*. 2003, 83, 7-8, 643.

100. Murphy, B. and McLoughlin, P., *Intern. J. Environ. Anal. Chem*. 2003, 83, 7-8, 653.

101. Murphy, B., Kirwan, P. and McLoughlin, P., *Anal. Bioanal. Chem*. 2003, 377, 195.

102. Flavin, K., Hughes, H., Dobbyn, V., Kirwan, P., Murphy, K., Steiner, H., Mizaikoff, B. and McLoughlin, P., *Intern. J. Environ. Anal. Chem*. 2006, 86, 6, 401.

103. Fried, J. R., Li, W. *Journal of Applied Polymer Science* 1990, 41, 1123.

104. Schlotter, N. E. and Furlan, P. Y. *Vib Spectrosc* 1992, 3, 147.

105. van Alsten, J. G. and Coburn, J. C. *Macromolecules* 1994, 27, 3746.

106. Farinas, K. C., Doh, L., Venkatraman, S. and Potts, R. O. *Macromolecules* 1994, 27, 5220.

107. Flichy, N. M. B., Kasarian, S. G., Lawrence, C. J. and Briscoe, B. J. *J Phys Chem B* 2002, 106, 754.

108. Baschetti M. G., Piccinini E, Barbari T. A. and Sarti G. C. *Macromolecules* 2003, 36, 25, 9574.

109. Mizaikoff, B., *Meas. Sci. Technol*. 1999, 10, 1185.

110. Kraft, M., Jakusch, M., Karlowatz, M., Katzir, A. and Mizaikoff, B., *Applied Spectroscopy* 2003, 57, 6, 591.

111. Moon, S.-M., Bock, C. and MacDougall, B. J. *Electroanalytical Chemistry* 2004, 568, 225.

112. Gupper, A., Andrew Chan, K. L. and Kazarain, S. G., *Macromolecules* 2004, 37, 6498.

113. Li, W. and Wu, P., *Macromolecular Chemistry and Physics* 2004, 205, 1338.

114. Musto, P., Mascia, L., Mensitieri, G. and Ragosta, G., *Polymer* 2005, 46, 4492.

115. Cotugno, S., Mensitieri, G., Musto, P. and Sanguigno, L., *Macromolecules* 2005, 38, 801.

116. Bodzenta, J., Kazmierczak, A., Hanh, B. D., Neubert, R. H.H. and Wartewig, S., *Instrumentation Science and Technology* 2006, 34, 107.

117. Salgin, S., Takac, S. and Ozdamar, T. H., *Journal of Colloid and Interface Science* 2006, 299, 806.

118. Smith, B. C. *Fundamentals of Fourier Transform infrared Spectroscopy*, CRC Press, c1996.

119. Tomkins, H. G. T. *Applied Spectroscopy* 1970, 24, 335.

120. Mirabella, Jr., F. M. *Internal Reflection Spectroscopy*, Marcel Dekker Inc., New York, 1993.

121. Huang, C. *Master Thesis*, University of Maryland, 2001.

122. Poling, B. E., Prausnitz, J. M. and O'Connell, J. P. *The Properties of Gases and Liquids, 5th Ed*., Mcgraw-Hill, New York, 2001.

123. Smith, J. M. and van Ness, H. C., *Introduction to Chemical Engineering Thermodynamics*, Thrid Edition, McGraw-Hill Book Company.

124. Fredrickson, G. H., Helfand, E. *Macromolecules*, 1985, 18, 11, 2201.

125. Paul, D. R., Yampol'skii, Yu. P. *Polymeric Gas Separation Membranes*, CRC Press, 2000.

126. Vasenin, R. M., Chalykh, A. Ye. and Korobko, V. I. *Vysokomol. Soyed*., 1965, 7, 4, 593.

127. Thomas, N. L. and Windle A. H. *Journal of Membrane Science*, 1978, 3, 337.

128. Thomas, N. L. and Windle A. H. *Polymer*, 1978, 19, 255.

129. Thomas, N. L. and Windle A. H. *Polymer*, 1980, 21, 613.

130. Thomas, N. L. and Windle A. H. *Polymer*, 1982, 23, 529.

131. Astarita, G. and Sarti, G. C. *Polymer Engineering and Science*, 1978 18, 5, 388.

132. Gostoli, C. and Sarti, G. C. *Polymer Engineering and Science*, 1982 22, 16, 1018

133. Peppas, N. A. and Sinclair, J. L. *Colloid Polymer Science*, 1983, 261, 404.

134. Korsmeyer, R. W., Lustig, S. R. and Peppas, N. A. *Journal of Polymer Science: Polymer Physics Edition*, 1986, 24, 395.

135. Singh, S. K. and Fan L. T. *Mathematical and Computer Modelling*, 1989, 12, 8, 947.

136. Cox, R. W. and Cohen, D. S. *Journal of Polymer Science B: Polymer Physics*, 1989, 27, 589.

137. Cohen, D. S. and White, A. B. *Journal of Polymer Science B: Polymer Physics*, 1989, 27, 1731.

138. Cohen, D. S. and White, A. B. *SIAM Journal on Applied Mathematics*, 1991, 51, 472.

139. Hayes, C. K. and Cohen, D. S. *Journal of Polymer Science B: Polymer Physics*, 1992, 30, 145.

140. Edwards, D. A. and Cohen, D. S. *SIAM Journal on Applied Mathematics*, 1995, 55, 662.

141. Fleming, G. K. and Koros, W. J. *Macromolecules*, 1986, 19, 2285.

142. Jordan, S. M., Koros, W. J. and Fleming, G. K. *Journal of Membrane Science,* 1987, 30, 191.

143. Berens, A. R. and Hopfenberg, H. B. *Journal of Polymer Science, Polymer Physics Edition*, 1979, 17, 1757.

144. Berens, A. R. and Hopfenberg, H. B. Polymer, 1978, 19, 489.

145. Fleming, G. K. and Koros, W. J. *Journal of polymer Science: part B: Polymer Physics*, 1990, 28, 1137.

146. Fleming, G. K. and Koros, W. J. *Macromolecules*, 1990, 23, 1353.

147. Stannett, V., Haider, M., Koros, W. J. and Hopfenberg, H. B. *Polymer Engineering and Science* 1980, 20, 300.

148. Mauze. G. R. and Stern, S. A. *Journal of Membrane Science* 1984, 18, 99.

149. Pace R. J. and Datyner, A. *Journal of Polymer Science: Polymer Physics Edition* 1981, 19, 1657.

150. Petropoulos, J. H. *Advances in Polymer Science* 1985, 64, 93.

151. Kamiya, Y., Mizoguchi, K., Hirose, T. and Naito, Y. *Journal of Polymer Science: Part B: Polymer Physics*, 1989, 27, 879.

152. Kamiya, Y., Mizoguchi, K., Terada, K., Fujiwara, Y. and Wang, J. *Macromolecules*, 1998, 31, 472.

153. Kamiya, Y., Mizoguchi, K., Naito, Y. and Hirose, T. *Journal of Polymer Science: Part B: Polymer Physics* 1986, 24, 535.

154. Hirose, T., Mizoguchi, K., and Kamiya, Y. *Journal of Polymer Science: Part B: Polymer Physics* 1986, 24, 2107.

155. Kamiya, Y., Hirose, T., Naito, Y. and Mizoguchi, K. *Journal of Polymer Science: Part B: Polymer Physics* 1988, 26, 159.

156. Kamiya, Y., Hirose, T., Mizoguchi, K. and Terada, K. *Journal of Polymer Science: Part B: Polymer Physics* 1988, 26, 1409.

157. Kamiya, Y., Bourbon, D., Mizoguchi, K. and Naito, Y. *Polymer Journal* 1992, 24, 5, 443.

158. Bondar, V. I., Kamiya, Y. and Yampol'skii, Y. P. *Journal of Polymer Science: Part B: Polymer Physics* 1996, 34, 369.

159. Koros, W. J. and Paul, D. R. *Journal of Polymer Science: Polymer Physics Edition* 1978, 16, 1947.

160. Chan, A. H. and Paul, D. R. *Polymer Engineering and Science* 1980, 20, 87.

161. Bohning, M. and Springer, J. *Polymer* 1998, 39, 21, 5183.

162. Fleming G. K. *Ph.D Thesis*, The University of Texas at Austin, 1988

163. Puleo, A. C. and Paul, D. R. *Journal of Membrane Science* 1989, 47, 301.

164. Seitz, J. T. *Journal of Applied Polymer Science* 1993, 49, 1331.

165. Van Krevelen, D. W. and Hoftyzer, P. J. *Properties of Polymers-Their Estimation and Correlation with Chemical Structure*, Elsevier Scientific Publishing Company, Amsterdam, Oxford and New York, 1976.

166. Carlton, Jr. T. A. and Aramayo, G. A. "*Stability of Small Plastic Cylinders Subjected to Internal Pressure and Axial Compression*", Technical Report

submitted to George E. Marshall Space Flight Center, NASA, Accession No. N65-34391, University of Alabama, 1965.

167. Barbari, T. A. *Journal of Polymer Science, Part B: polymer Physics* 1993, 31, 501.